Modelling and Analysis of the Control Mechanisms of Bacterial Growth

Mohammad Daoud Omar Abbadi

A dissertation submitted in partial fulfillment

of the requirements for the degree of

Doctor of Philosophy

of

University College London.

Department of Electronic and Electrical Engineering

University College London

April 8, 2020

Abstract

This thesis concerns the control mechanisms of bacterial growth. Mathematical and experimental work has shown the control of bacterial growth behaves as a switch. It is known that the vitamin B_{12} riboswitch plays a role in this switching mechanism. These facts motivate considering variable structure control techniques to investigate the control mechanism and the robustness of the riboswitch. Whilst the existence and importance of switches are widely acknowledged within the biological literature, many life scientists do not deal explicitly with the switching behaviour. Frequently, steady-state behaviour before and after switching is the primary focus. The main objective of this thesis is to study the control mechanisms of the vitamin B_{12} riboswitch on bacterial growth at both a cellular and population level. The results using different bacterial strains show that changing the concentration of vitamin B_{12} affects the growth until saturation level is reached. The thesis then studies the control mechanism in algal and bacterial co-culture. A model has been developed using data from an *in vivo* experimental two-species system where the bacterium $Mesorhizobium\ loti$ $(M.loti)$ supplies the vitamin B_{12} required for growth to the freshwater green alga *Lobomonas rostrata* $(L.rostrata)$ and where the action of the B_{12} riboswitch is known to be a determinant of system behaviour. The reachability analysis from sliding mode control is used to find the algal and bacterial saturation level and study the robustness of the system. Using the validated riboswitch model, an observer design method from the domain of control engineering is used to estimate the vitamin B_{12} transporter *BtuB* given measurements of the concentration of vitamin B_{12}. Validation of the estimates of *BtuB* has been undertaken by comparing the relationship between the *BtuB* and vitamin B_{12} concentrations estimated from

the observer with the relationship between green fluorescent protein production and the concentration of vitamin B_{12} obtained experimentally.

Impact Statement

This thesis has an impact across several fields: academia, biology and clinical medicine. Firstly, the thesis presents a new method of determining bacterial growth using information from the control mechanisms of the vitamin B_{12} riboswitch. The method provides a straightforward estimate of bacterial growth by linking the dynamics of bacterial growth together with the concentration of vitamin B_{12}. The dynamics of bacterial growth can be established based on knowledge of the bacterial strain and the growth rate. The thesis also provides a significant contribution to finding the saturation level of algal and bacterial growth using paradigms from control engineering. These findings contribute to finding the maximum active concentration of vitamin B_{12} using the minimum nutrients. In extensive surveys, 3.2% of adults over age 50, and 6% of those aged more than 60 have a vitamin B_{12} deficiency, and around 20% have a marginal vitamin B_{12} deficiency [1] [2]. The models developed in the thesis provide mechanisms to reduce the production costs of vitamin B_{12} as well as to provide insight into specific medical complaints where the uptake of vitamin B_{12} is known to be problematic for patients, for example, Crohns Disease. Models of the saturation level of algal growth are famous in ecology and can contribute to the management of global warming. Calculations linking minimum nutrient levels for maximum growth are essential in this regard. The theoretical impact of this thesis is as an interdisciplinary study showing how variable structure control methods can be used in biomedical applications. The thesis provides examples on how to check the robustness of biological systems using control methods and how to ensure desired outcomes are achieved by considering stability analysis from the control domain. A particular contribution is the use of

observation methods such as the sliding mode observer and Luenburger observer to develop a soft sensor to measure difficult to measure states of the vitamin B_{12} riboswitch. The observation analysis can be used as a basis to use the same technique in other biomedical applications that exhibit the same or similar switching mechanisms such as muscles. In this thesis, the analysis was used to observe the concentration of *BtuB*; the same analysis can be used to find *btub* and other concentrations that are hard to be estimated experimentally. A comparison was made between different types of observers, and it is proven using experimental validation that sliding mode observers give the best estimate.

Acknowledgements

I would like to thank GOD for giving me the strength and the ability to complete this thesis. I also can not forget Professor Sarah K. Spurgeon for her supervision, this thesis and all of the PhD journey would not be achieved without her generous support and help.

I also would like to thank everyone from the Electronics and Electrical Engineering department at UCL for their support during my doctoral research.

My family, I will always remember and never forget your continued support during my university journey, it was a ten-year journey, and I always felt the support from you, financially and emotionally and believe me, without it I would not be able to continue it. My Dad, Daoud Omar Abbadi, you are the main reason I am able to complete my studies, you always supported me financially without me asking and this was one of the keys for me to stay active and focus on my studies. My Mum, Khawala Mouwafaq Abu-Libdeh, thank you for your tremendous emotional support, I know it is not easy to take care about my siblings and me at all time, so your support is much appreciated. Ahmad, Yazan and Omar, you were always there for me when I needed you and me seriously proud of you all. My sister, Doaa, thank you for your help that you always give when I asked for, your support was excellent, and I will never forget it.

I would also like to thank University College London for giving me a studentship and make support in a portion of my tuition fees, this was a generous move from the university, and I cannot express my appreciation.

The support of Professor Martin Warren, Naziyat Khan (University of Kent, UK), Professor Alison Smith (University of Cambridge, UK) and Bernhard Krut-

ler (Institute of Organic Chemistry & Center of Molecular Biosciences (CMBI), University of Innsbruck) by providing experimental data for this work is gratefully acknowledged.

Special thanks to Asif Chalanga for his help and sharing his experience with me, your support helped me understand aspects of control engineering.

My friends that I made in the United Kingdom, thanks to you all for everything, you all were brilliant.

Thanks to London, thanks to Canterbury, I had great time in those two cities.

Contents

List of Figures

List of Tables

List of Acronyms

VSC Variable Structure Control

SMC Sliding Mode Control

DNA Deoxyribonucleic Acid

RNA Ribonucleic Acid

mRNA Messenger Ribonucleic Acid

GRN Gene Regulatory Network

E. coli Escherichia coli

S. enterica Salmonella enterica

L. rostrata Limonia rostrata

M. loti Mesorhizobium loti

SMO Sliding Mode Observer

TPP Thiamine Pyrophosphate

UTR Untranslated Region

RBS Ribosome Binding Site

AUG START codon

UAA Stop Codon

OD600 Optical Density Measured at a Wavelength of 600 nm

DOC Dissolved organic carbon

GFP Green Fluorescent Protein

Chapter 1

Introductory Material

1.1 Overview

This thesis presents interdisciplinary research between control engineering and mathematical biology. The variable structure control (VSC) paradigm is applied to study the control mechanisms of bacterial growth. One of the mechanisms that control bacterial growth is the vitamin B_{12} riboswitch [6] [7] [8]. Riboswitches are naturally occurring RNA-based regulatory components that essentially function by first sensing specific metabolites such as cofactors, amino acids and nucleotides and then regulating the expression level of proteins in the corresponding metabolic pathways [9]. The switches undergo a conformational change in response to a small-molecule ligand whereby increasing ligand concentrations either increase or decrease gene expression. To understand the control mechanisms of the vitamin B_{12} riboswitch, a study of the gene regulatory network (GRN), which is a collection of molecular regulators that interact with one to the other and with substances in the cell to govern the gene expression [5] [10] is required. Models of GRN provide significant insights into the underlying molecular mechanisms, which can lead to important biotechnological applications [11]. These models allow researchers to investigate the role of components of a given system, and to give precise definitions of the functions exerted by system components and their interactions. Also, the models can be easily used to perform system simulations to test different scenarios that are not readily accessible by experimental work. The vitamin B_{12} riboswitch

will exhibit switching behaviour between high (ON) and low (OFF) and affect the overall growth. The riboswitch provides a mechanism for regulating the concentration of a metabolite by uptake or by controlling the synthesis of an enzyme involved in the synthesis. When levels of the metabolite are high, it binds to the riboswitch and alters the secondary structure of the RNA helix such that it stops additional transcription of the mRNA; when no metabolite is bound, the levels will be low, and the riboswitch adopts an alternative structure and transcription can proceed [12]. It has been discovered that riboswitches sense a variety of ligands. The steady increasing number of examples of such natural *RNA* regulators that control gene expression through diverse mechanisms in different organisms has fostered a growing interest in using *RNA* to build synthetic controllers. Both naturally occurring and synthetic riboswitches are seen to be highly tunable components capable of regulating gene expression.

Some work to model riboswitch function has taken place, and useful guidelines have been developed for tuning, but this work has been performed under steady-state operating conditions. Beisel et al. [4] modelled the kinetics of riboswitch function when it is operating under known regulatory mechanisms. They used the models to develop a generalized framework for examining quantitative aspects of riboswitch tuning, which is complicated by the integration of various regulatory mechanisms and processes such as RNA folding. To design synthetic riboswitches, Sha Gong et al. [13] studied computational methods for modelling the structure and kinetics of riboswitch aptamers. Manja et al. [14] studied the regulation levels which occur at either the level of transcription or translation in riboswitches to regulate gene expression in synthetic biology. The prior literature has also considered riboswitch modelling by linking the aptamer-ligand binding and expression platform [15], studying the structure and the dynamics in RNA [16] and by designing artificial riboswitches [17], [18]. The literature on the tuning of riboswitches also focusses primarily on the riboswitch as an individual element rather than as a component within a wider biological pathway [4]. As it is operating as a switch, a control engineering perspective can be used to model the control of the riboswitch

and to understand its dynamics. Thus, the use of VSC provides a useful view of the switching behaviour of the riboswitch. In this thesis, the importance of vitamin B_{12} concentration in different bacterial strains have been studied. As the concentration of vitamin B_{12} is easy to be measured, the measurements can be used to estimate *BtuB* concentration, the cobalamin transporter from Escherichia coli, which is hard to be measured experimentally using observer theory.

1.2 Thesis organisation

The thesis is organized as follows:

Chapter 2 provides the biological background about the control mechanisms in bacterial growth. Cell types and gene expression are discussed, and it is explained how riboswitches affect the gene regularity network. The chapter also shows the main differences between Prokaryotic and Eukaryotic cells. The chapter then shows the relation between the control mechanism in gene regulation and the bacterial growth at the cellular and population levels. This chapter motivates the use of VSC as a technique to investigate the control mechanisms of bacterial growth.

Chapter 3 provides a relevant background to the VSC paradigm. The purpose of this chapter is to introduce analytical tools from VSC theory. For simplicity, a second-order system is used to present the framework of sliding mode control (SMC). The design procedure for a SMC along with the reachability condition, which represents a condition for the sliding manifold to be attractive to the states of the system, and the concept of the equivalent control are discussed. Moreover, this chapter introduces the background to the different observers that have been used in the thesis; the sliding mode observer and the Luenburger observer.

Chapter 4 begins with an analysis of a simple model of the vitamin B_{12} riboswitch. Next, methods for the study of switched systems from control engineering are applied to the modelling and analysis of the riboswitch. The simulation results have been validated using *in vivo* experiments by checking the bacterial growth when using *Escherichia coli* and *Salmonella enterica* where the action of the vitamin B_{12} riboswitch is known to be a determinant of system behaviour. Val-

idation of the simulation results has been undertaken by linking the dynamics of the riboswitch to bacterial growth. These findings showed that the riboswitch could help develop high-yield strains by metabolic engineering.

Chapter 5 shows a control engineering perspective on the growth dynamics of algal-bacterial co-cultures. This chapter first describes a simple model of algal-bacterial growth and analysis is undertaken before and after the add-back of nutrients. The effect of system parameters and control mechanisms is quantified with both steady-state analysis and physical limitations. Motivated by the inherent switching action within the biology, a sliding mode interpretation of the control mechanisms is hypothesized based on knowledge of the maximum carrying capacities for each growth. The results of a range of experiments reported in the literature are used to validate the assertions.

Chapter 6 begins with background on the relationship between the concentration of vitamin B_{12} and the concentration of *BtuB*. Observer design methods are then used to estimate *BtuB* given measurements of the concentration of vitamin B_{12}, which is easy to be measured experimentally. Validation of the estimates of *BtuB* has been undertaken by comparing the relationship between the *BtuB* and vitamin B_{12} concentrations estimated from the observer with the relationship between green fluorescent protein production and the concentration of vitamin B_{12} obtained experimentally.

The first part of the final chapter presents the general conclusion of this thesis, and the second part suggests ideas for future work to build on the findings of the work.

1.3 Contribution

The contributions of this thesis lie within the realm of modelling and analysis of the control mechanisms of bacterial growth. The novelty of the approach resides in the fact that VSC theory is utilised to both models the control mechanism in bacterial growth as well as to observe the concentration of *BtuB* from measurements of vitamin B_{12}. The specific contributions are as follows:

After two introductory chapters on the biological background (Chapter 2) and control theory background (Chapter 3), Chapter 4 demonstrates the effect of the vitamin B_{12} riboswitch at a cellular level. A mathematical model that describes the protein synthesis that contains the concentration of gene *btub* mRNA, the concentration of the *BtuB* and the concentration of vitamin B_{12}, which was developed by Santillan et al. (2005) [6] have been analysed to determine how they affect the cells during transcription and translation. The dynamics of the vitamin B_{12} riboswitch have been incorporated in a model of *Escherichia coli (E. coli)* bacterial growth. The same analysis has been performed with different bacterial strains. The effect of changing the concentration of vitamin B_{12} in bacterium *Salmonella enterica (S. enterica)* has been tested. The simulation results obtained replicate the experimental results.

In Chapter 5, mathematical models for the growth of *Lobomonas rostrata* algae and *Mesorhizobium loti* bacteria, which was developed by Matthew et. al [19] have been analysed both before and after the add-back of nutrients. This work takes the results from the cellular level to the population level and explores how the riboswitch can affect a co-culture environment. The specific nutrients studied are vitamin B_{12} and carbon. The physical limitations on the parameters have been identified, and simulations show how the growth saturates. Linearised models have been identified and the degree to which they are useful to represent the dynamics explored. SMC analysis has been carried out to quantify the action of the control mechanisms and the system robustness explicitly. A reachability condition is formulated, and then, a natural VSC is identified which satisfies this reachability condition so that the system states lie in the vicinity of the chosen switching function.

In Chapter 6, the framework of a sliding mode observer (SMO) is seen to observe *BtuB*. The results establish that using an observer as a soft sensor is a useful approach to explore the operation of a vitamin B_{12} riboswitch if measurements of the concentration of vitamin B_{12} are available. The work also shows how a SMO can observe *BtuB* concentration using a third-order observer. The work in this thesis

has produced the following articles:

- M. Abbadi, S. Spurgeon, N. Khan, M. Warren and Bernhard Krutler "Using sliding mode observers to estimate $BtuB$ concentration from measured vitamin B_{12} concentration" submitted to IET system biology journal, 2019.

- M. Abbadi, S. Spurgeon, N. Khan and M. Warren, "Understanding the Control of a Vitamin B_{12} Riboswitch," 2018 UKACC 12th International Conference on Control (CONTROL), Sheffield, 2018, pp. 474-479. doi: 10.1109/CONTROL.2018.8516881

- M. Abbadi and S. Spurgeon, "Growth Dynamics of Algal-bacterial Cocultures: A Control Engineering Perspective," 2018 European Control Conference (ECC), Limassol, 2018, pp. 2344-2349. doi: 10.23919/ECC.2018.8550593

1.4 Conclusion

In this chapter, the main structure of the thesis and the highlight of the main contributions are presented. Next chapter presents the biological background of bacterial growth and explains in detail the work of riboswitches and how they are playing a role in the control mechanism.

Chapter 2

Biological Background of the Control Mechanisms in Bacterial Growth

In this chapter, a brief introduction of the essential concepts of molecular cell biology that are used throughout the thesis is presented. First, the main differences between cell types (prokaryotes and eukaryotes) are described. A particular focus will be gene expression, its regulation, and how protein synthesis occurs from DNA to gene production. The control mechanism is studied throughout the process; at the transcriptional level, translation level and inside the *mRNA*. This chapter will also define the riboswitch, how it evolves, the classification, the structure and function and the role played in transcription and translation levels. The importance of studying riboswitches is a key motivation.

2.1 The Cell

Everything living on this planet is made of cells. The cell meaning ”small room” from the Latin word *cella*, is the smallest unit of life and it is the basic biological, functional, and structural unit of all known living organisms [20]. Organisms may contain one cell or can be multicellular. The multicellular are normally organized into tissues, which are collections of similar cells organized to perform a particular function in addition to the usual housekeeping processes to all cells. The size of the cells varies from typically 1 to 100μm, and they are only visible under a microscope [21]. Each cell has the same genetic information as the parent organism, and

this data is passed on to the new cells produced from binary fission [22]. Modelling analysis of the control mechanism is the core focus of this thesis, so that cell differentiation, for example, is not studied. When categorizing life at a very high level, it can be categorized in terms of either eukaryotic cells or prokaryote cells [23]. Complex member-bound structures are the main distinction between eukaryote cells and prokaryote cells; the main member-bound structure is the nucleus, which has genetic information (DNA) inside it. In Prokaryote cells, the DNA is bundled up into a section of the cell, which is not the member-bound nucleus. Eukaryotes cells also have other membrane-bound structures such as mitochondria and Golgi apparatus. The nucleus is an important part of the cell as it is where the DNA is generated, and the nucleolus is where the ribosomal RNA is produced. DNA tends to be in multiple strands in Eukaryote cells, but it is circular in the prokaryote cells. Eukaryote cells include all multicellular organisms: humans, animals, plants, protists and fungi. The bacterial cell is of main concern in this thesis, and it is the most common example of Prokaryote cell. The two major types of cells are shown in Fig. 2.1. In

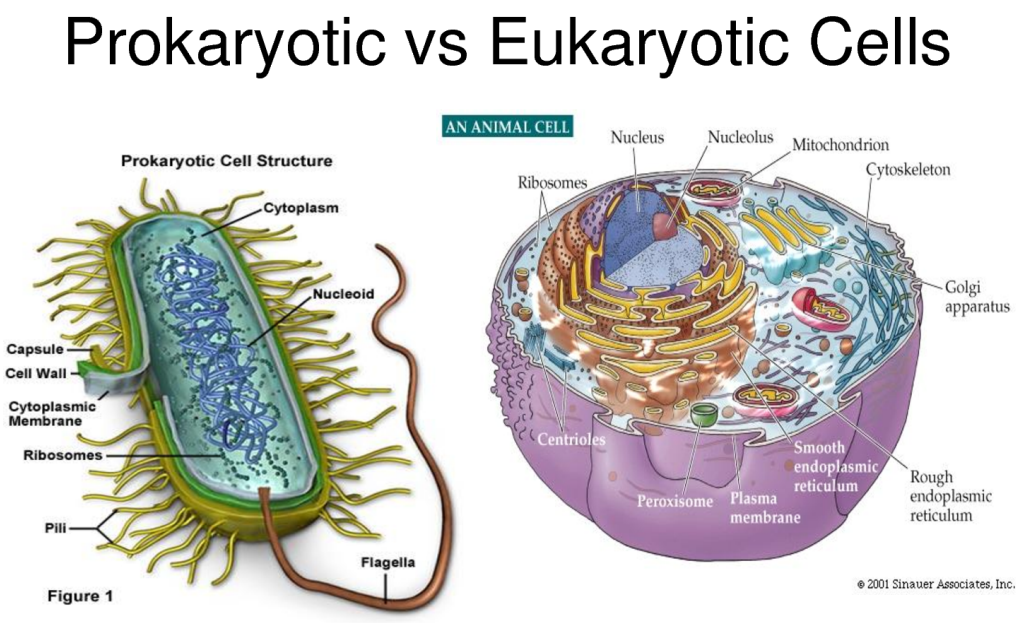

Figure 2.1: Differences between Prokaryotic and Eukaryotic cells [3]

controlling the mechanism of the cell, the metabolites have to stay at a specific state of equilibrium; this value might be affected based on some needs. The structure of the cell can maintain the metabolite concentration at the desired level by regulating gene protein-encoding through particular ”switches”, called riboswitches, which can block or activate protein synthesis. The next section will explain the control mechanisms at both transcription and translation levels in a riboswitch [7].

2.2 Riboswitches

Riboswitches are metabolite-sensing RNA elements that combine small molecules in the five prime untranslated regions (5‘ UTR). This region is also identified as a leader sequence or leader RNA [8]. These genetic regulation networks are defined as mRNA elements that bind metal, ions or metabolites as ligands. This binding process determines whether or not the associated genes are expressed. Riboswitches are also known as a controlling segment of mRNAs that bind a small molecule to regulate the change in the production of the proteins encoded by the messenger RNA. Riboswitches also regulate mRNA expression by forming different structures in response to this ligand binding. However, not all riboswitches are at the five prime untranslated regions; Breaker et al. [8] found that the thiamine pyrophosphate (TPP) riboswitch in some eukaryotic mRNA regulates splicing at the 3’ end.

Riboswitches were first discovered through an experiment on vitamin B derivatives and since then have been found to occur naturally as molecule binders. They were found in bacteria only in 2002 [9]. There are approximately twenty well-known classes of riboswitches discovered to date. The focus of this thesis will be on the vitamin B_{12} (Cobalamin) riboswitch [12], which binds the coenzyme form of vitamin B_{12} to regulate cobalamin and transport genes. Chapter 4 describes a mathematical model that presents the control mechanism in the bacterial growth based on the vitamin B_{12} riboswitch and Chapter 5 uses the same riboswitch but considers it in a co-culture environment.

Vitamin B_{12}, the cyano-derivative of cobalamin, is a water-soluble vitamin whose biological forms play vital roles in metabolism that affect the normal func-

tioning of the brain and nervous system in humans. The term B_{12} is generically used to refer to cobalamin in this thesis. B_{12} is unique among the vitamins in that it is made exclusively by only certain prokaryotes and there is significant interest in how B_{12} production is controlled within microbial communities and how the nutrient makes its way through the food chain into animals.

Wachter A [24] and Serganov A et al. [9] showed in their researches that riboswitches play a role in controlling the gene expression in eukaryotes cells. If the production of vitamin B_{12} is controlled by the riboswitches, then more vitamin B_{12} can be produced using biotechnological approaches depending on the riboswitch ON and OFF behaviour. For humans, B_{12} deficiency is most often associated with an autoimmune disorder that prevents the body from absorbing the nutrient, but people on a strictly vegetarian diet are also prone to deficiency as plants neither make nor require B_{12}. Dietary B_{12} deficiency is a severe problem in many developing countries, including the Indian subcontinent, Mexico, Central and South America and selected areas of Africa [25]. Moreover, B_{12} deficiency is also a common problem for the 115000 sufferers of Crohn's disease in the UK and millions more worldwide as the inflammation caused by the condition can affect the end of the ileum, which is the main area where B_{12} is absorbed [26] [27]. This motivates the use of modelling to understand the dynamics of vitamin B_{12} better.

2.2.1 Riboswitches Structure

The riboswitch has two main elements, the aptamer and the expression platform. Although it may seem that the aptamer and the expression platform are two separate structures because of their different functions, they are connected. They overlap each other in a space that is called the switching sequence, as shown in Fig. 2.2, where the information is passed from the aptamer to the expression platform domain, and the conformation of the expression platform is decided. [5]. Riboswitches can also be broken into two classes based on their structure: Pseudoknot fold and Multi-helical junction. Pseudoknot is formed by base pairing between a loop of RNA and outside the region. Junctional riboswitches combine several several metabolite-sensing RNAs by stacking them on top of each other and packing

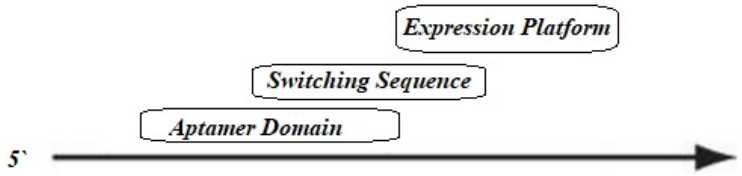

Figure 2.2: Riboswitch domains

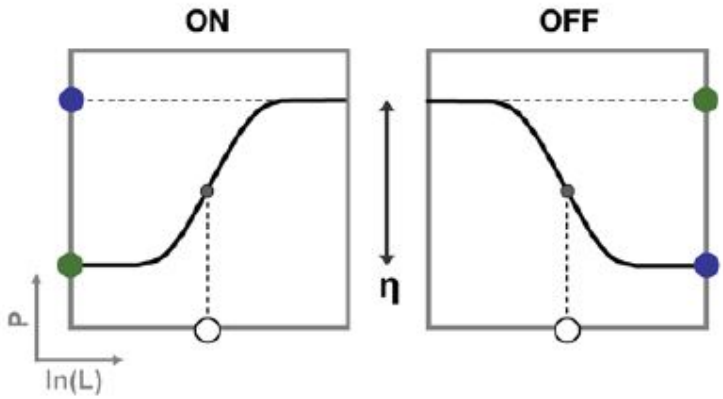

Figure 2.3: Gene expression when the riboswitch is ON and when it is OFF [4]

them side to side to make the commonly seen Y shape [28] as shown in the aptamer domain described in Fig. 2.4 . When a metabolite accesses the cell, it binds to the riboswitch, which will stop production. A riboswitch is not always a single unit; there can be two sensor domains or two riboswitches next to each other, which is present in the glycine riboswitch [29]. The aptamer is a specialised living receptor. It can range in size from 70 to 200 nucleotides and the types of compounds the aptamer binds are small pairing coenzymes amino acids and metal cations.

Each aptamer is very specific to the ligand it can bind, and a small variation of the compound may interrupt binding. The aptamer has several different ways of insuring; it only selects the correct metabolite. Most aptamers have a tight ligand-binding pocket and hold in ligand with Van der Waals forces [30]. Hydrogen bonding between Logan edges and non-paired nucleotides of RNA are used to ensure the correct orientation of the metabolites. The aptamer signals the switching sequence and expression platform to change conformation to the ON or OFF position. Figure 2.3 shows the dynamics of the gene expression when the riboswitch is ON and when it is OFF.

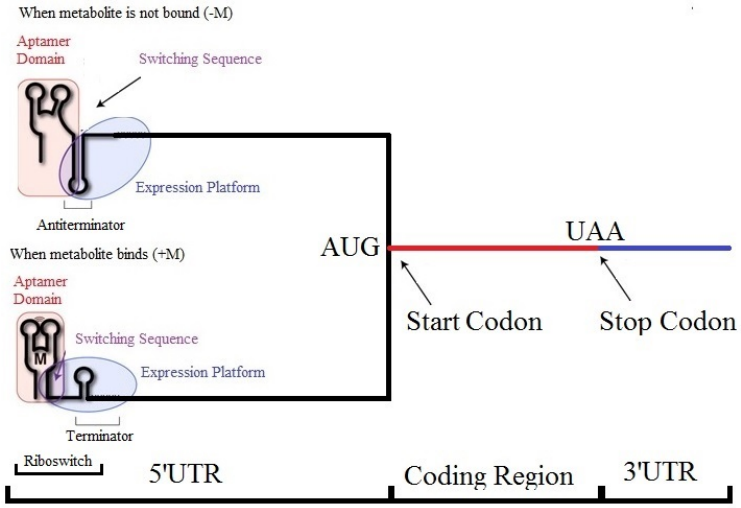

Figure 2.4: Typical bacterial mRNA transcript [5]

The expression platform is a secondary switch which dictates whether the gene expression will be turned ON or OFF. A ligand is bound to the aptamer which signals to fold in the switching sequence, and that will cause the expression platform to fold into the designated confirmation. The conformation will determine whether transcription, translation or other gene expressions are terminated or continued [5]. The confirmation of the expression platform will make the ribosome binding site available, or not, for translation, and the platform can fold into either a terminator or anti-terminator position for transcription, as shown in Fig. 2.4.

2.2.2 Riboswitches in Transcription and Translation Levels

Transcription is the process of converting DNA to RNA. This process is a crucial step to transfer genetic information to the ribosome, and each gene can be transcribed with different rates and efficiencies. RNA differs mainly from DNA in that it is single-stranded and often contains short sequences that are complementary to other sequences that allow it to fold over on itself. Riboswitches regulate gene expression almost exclusively in prokaryotes; they control gene expression by promoting innate transcription termination or by impeding translation initiation. Riboswitches can regulate the ability of RNA-dependent helicase Rho factor, which is a prokaryotic protein, to terminate transcription [31]. They promote transcription when there is no ligand present, and the anti-terminator loop is engaged. All of the

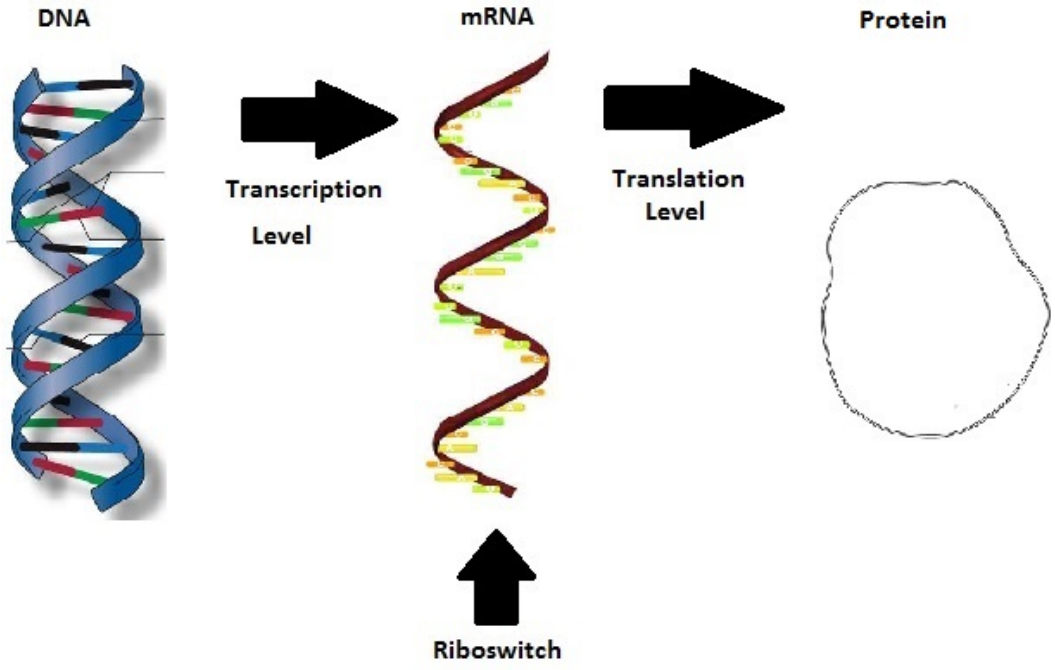

Figure 2.5: Regulatory pathway of the gene in Prokaryotes

previous steps are shown in Fig. 2.4, where AUG is the start codon and UAA is the stop codon of the coding region.

Translation is the second mechanism after transcribing DNA to a single strand of RNA. This RNA then requires a ribosome to be translated into a protein as shown in Fig. 2.5. For translation initiation which occurs in prokaryotes when a specific ligand binds to the aptamer domain, this causes a rearrangement in the structure of the expression platform side which includes the ribosome binding site. In translation termination, it stops the mRNA from producing the protein due to the adequate amount that is produced in the bacteria, in order to prevent or terminate the translation mechanism as specifically must bind to the aptamer domain and this changes the confirmation of the RNA. As a result, translation is then terminated, and the mRNA will stop producing the protein.

2.2.3 Importance and Application of Riboswitches

Riboswitches have the potential to be used as drug targets; they can distinguish between different cognate molecules as well as their existence in bacteria. The use of riboswitches within antimicrobial drug targets has many advantages over classic

antibiotics; they have lower toxicity because small metabolites control them. This makes them relatively straightforward to introduce into the system and would make them cheaper to manufacture and more natural to modify. In riboswitches, there is less chance of resistance from bacteria since there is only a single type of riboswitch with bacterial genes which makes mutation harder to stop the effect of the antibiotic. The dynamics of a vitamin B_{12} riboswitch is shown in detail in Chapter 4, and the effect of it is studied by linking it with the bacterial growth phases. The model is also used to find and estimate the concentration of *BtuB* using several observation methods as shown in details in Chapter 6.

2.3 The Dynamics of Bacterial Growth

This section will explain the dynamics and determine the mathematical equation that describes bacterial growth. Bacteria has three growth phases, as shown in Fig 2.6.

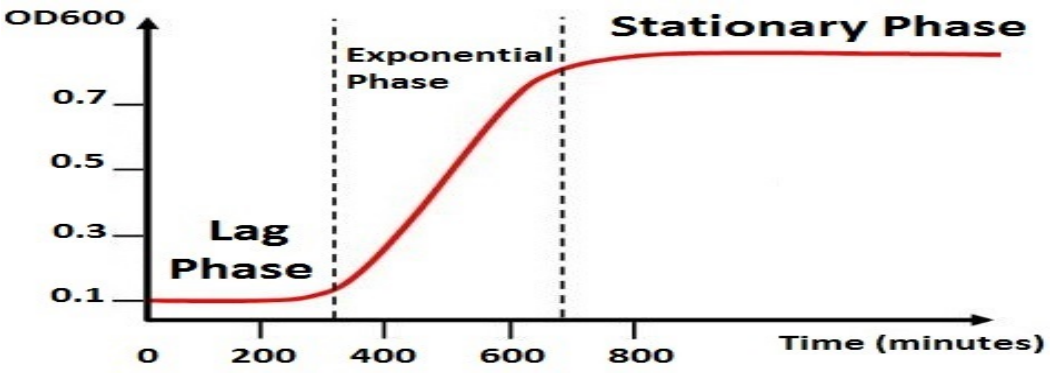

Figure 2.6: Bacterial and algal growth curve

1. **Lag phase**: When cells are transferred to fresh media, they require time to detect the environment, express specific genes, and synthesize components necessary for rapid growth. The cells do not divide at this time.

2. **Exponential (log) phase**: Binary fission occurs at a maximum rate; the cells are dividing as rapidly as possible.

3. **Stationary phase**: At this point, growth has stopped, and there is no net increase or decrease in the number of cells.

In modelling a bacterial population as a function of time, the rate of change of population with respect to time is proportional to the population itself [32], so that:

$$\dot{N(t)} = rN(t) \tag{2.1}$$

where $N(t)$ is the population and r is the growth rate. It follows that $N(t) = N_0 e^{rt}$ where N_0 is the initial population and the growth curve for freshwater green algae, for example, is as shown in Figure 2.7.

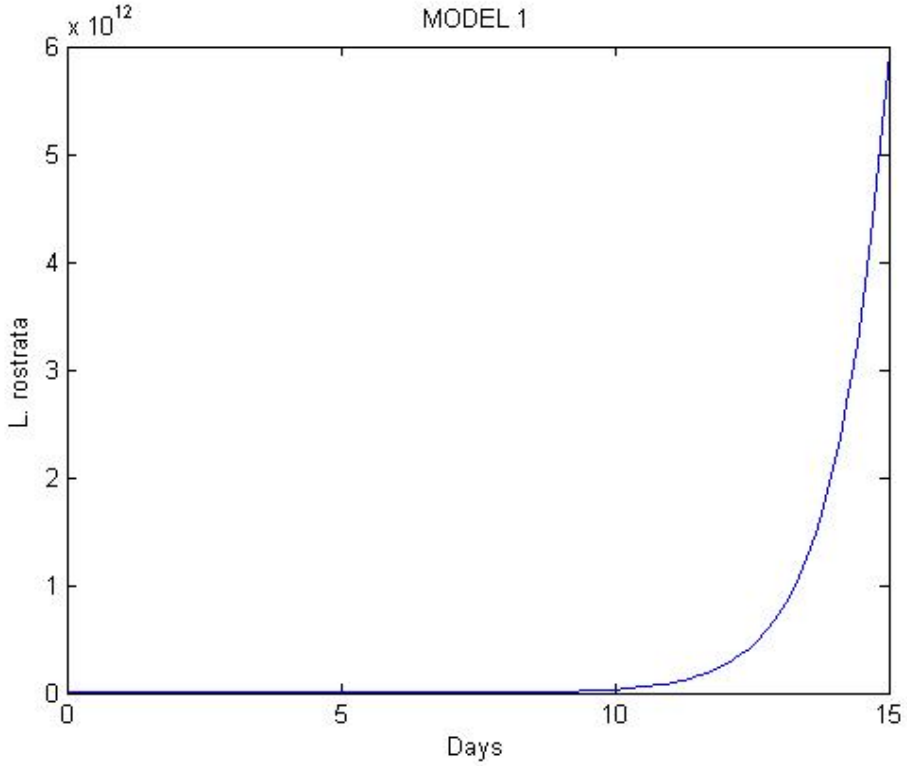

Figure 2.7: The growth curve when $N(t) = N_0 e^{rt}$

From Figure 2.7, it is seen that as time increases, the population will increase exponentially. After some time, however, the environment will not be able to support more than a specific population. This value, corresponding to saturation of growth, is given by K. One reason why the population will saturate may be that there is not enough vitamin B_{12} to support the cells. In this case, equation (2.1) is

not valid, and as shown by Verhulst [33], the model becomes:

$$\dot{N} = rN(1 - \frac{N}{K}) \tag{2.2}$$

where r is the population growth rate, and K is the carrying capacity. Equation (2.2) is called the *logistic differential equation* [34]. To study the limitation of the *logistic differential equation*, note that if the population N is equal to zero, the rate of change of population will be zero. When $N = K$, the rate of change will be zero and thus growth will only occur when $0 < N < K$. In this case, the population will grow exponentially to reach a steady-state value K. The solution of the logistic differential equation (2.2) is given by $N(t) = \frac{N_0 K}{(K-N_0)e^{-rt}+N_0}$ where N_0 is the initial population, K is the maximum carrying capacity and r is the growth rate. Riboswitch plays a role in controlling bacterial growth. When the switch is ON, the growth is in the exponential phase, and when it is OFF, it is at the saturation level. Chapter 5 shows in detail the relation between bacterial growth and algal growth; it studies the interaction between them and how the riboswitch affects growth.

2.4 Conclusions

In this chapter, types of cell in all living organisms are considered, mainly focusing on describing the differences between prokaryotic cells and eukaryotic cells. Bacterial cells are regarded as a prokaryotic cell and are the focus of this thesis. The process of the regulatory pathway is then considered. The riboswitch is seen to be the element that controls the mechanisms in the protein synthesis process, as it regulates the expression level of proteins in the corresponding metabolic pathways. This is because different regulatory activities inside the mRNA are associated with each pathway. The increase in ligand concentration either leads to an increase (ON behaviour) or a decrease (OFF behaviour) of gene expression. The riboswitch structure is then studied in both transcription and translation levels in-depth. The first part of this chapter shows how the riboswitch works at the cellular level; then, this chapter shows the relation between the riboswitch and bacterial levels. Finally, this section shows the growth levels in both bacteria and algae. This will be used in an

application in cellar level in chapter 4 and population level in chapter 5. The findings in this chapter show that switching is essential in riboswitch behaviour. VSC is one of the primary mechanisms to design switched control systems in engineering applications. This will be applied in the next chapters to analyse riboswitch behaviour. Chapter 3 will discuss the control background and VSC theory in detail.

Chapter 3

Variable Structure Control

3.1 Introduction

The field of control engineering involves the study of uncertain dynamical systems. The key paradigm introduces feedback to achieve the desired stability and performances of the system in the presence of parameter uncertainty and disturbances. VSC is a form of discontinuous non-linear control and particular sub-class of the control system. The idea developed from a study in Russia by Emel'yanov and his co-workers in 1967 [35]. The work did not appear outside Russia until 1976 when Itkis [36] and Utkin [37] respectively published work in English. A VSC changes the dynamics of a system by using a switch control mechanism [38]. Fundamentally, the feedback control law switches between conditions to achieve stability and performance. VSC concepts have been used to design robust controllers for non-linear, time-delayed and uncertain systems [39] [40] [41]. Implementing a VSC strategy yields strong robustness to a class of uncertainties [42] [43]. One of the advantages of using the switching mechanisms is that by switching between subsystems, the properties of some subsystems can be combined so that the overall system holds new dynamical behaviours that are not present in any of the subsystems individually. Systems engineers have used a VSC approach to ensure robustness to uncertainty and disturbances. VSC techniques can deliver an understanding of the impact of disturbances and parameters uncertainty on the dynamical behaviour of systems [38]. This approach has been receiving more and more attention recently

in the robotics applications [44] [45] [46] [47] [40]. For example, it was used to find an algorithm for robotic manipulators and for controlling the links of the robot, in addition, the robotics computational resources are limited, and the solution is to produce a VSC.

Sliding mode control (SMC) is a particular class of VSC, and the idea has been applied to design robust regulators, tracking systems, fault detection schemes and adaptive schemes [48]. The purpose of SMC is to drive the system states onto a specific surface in the state space, called the sliding surface. Once the sliding surface is hit, SMC keeps the states on the close neighbourhood of the sliding surface. The SMC design approach is a two-stage process. The first involves the design of a switching function to prescribe the desired system performance, and the second component consists of the selection of a control law to ensure the prescribed behaviour is attained. The design approach ensures the switching function, and thus the desired dynamics will be attractive to the system state [37]. One of the advantages of using the SMC approach can be to reduce the order of system dynamics. Furthermore, reconstructing and estimating the dynamics of an unknown input can be achieved using the principle of the equivalent control [49]. The reachability condition, which is a condition that forces sliding can be framed in terms of Lyapunov stability analysis. Then, a VSC is determined to satisfy the reachability condition [50]. The choice of switching function will determine the dynamical behaviour of the system and the choice of the control will make sure that the dynamics of the system remain on the sliding manifold. Furthermore, sliding mode systems are insensitive to a class of parameter variations and uncertainty. This has motivated the use of SMC in different applications such as biomedical applications, electric motors, furnace control and chemical models [51] [52] [53].

To generate robust predictions from a known model, understanding the modelling uncertainty and the impact of the parameters are key factors to consider. Also, the differences between the model's dynamics and the actual process must be understood. In terms of system biology, uncertainties in the model may be due to the lack of biological data for parameter estimation, the complexity of the system and the

possible range of parameters. This motivates the use of VSC in modelling because it enables assessment of parameter uncertainty on the model dynamics.

A state observer is a system that gives an approximation of the state of a system, from the knowledge of the physical systems‘ input and output measurements. Knowing the system state helps in various control problems; such as implementing controllers that are a function of the state. The observer is effectively a dynamical system model which is driven by the input and the output of the physical system. An output error is formed by comparing the output of the observer and the output of the physical system; this error is used to construct a feedback loop around the observer to drive the error between the observed output and the physical system output to zero. An observer can be considered a soft sensor as it provides estimates of unmeasured states. An observer provides robustness in the face of uncertainty between the observer model and the physical system [54]. This chapter reviews the theory of VSC, focusing on SMC and Sliding Mode Observers (SMO) which will be used later in this thesis to find the physical limitation for parameters and observe $BtuB$ from measurements of vitamin B_{12}. The chapter is organized as follows: Firstly, the underlying philosophy of VSC is presented. Next, a particular case of VSC is discussed (SMC). Finally, observation techniques are presented.

3.1.1 Philosophy of Variable Structure Control

The VSC paradigm changes the control structures of the system during operation according to a switching logic; this is frequently used to achieve desired stability and required performance. To understand the characteristics of VSC, consider the second-order oscillator system given in [37].

$$\ddot{x} - \alpha\dot{x} + u(t)\,x = 0 \tag{3.1}$$

where α is a constant value and $u(t)$ is the control. To achieve stability, the control input is selected as $u(t) = 0.5$ and $\alpha = 0.6$. The phase portrait of the dynamics is shown in Fig. 3.1. It is seen from the figure that the control input $u(t)$ generates a stable dynamics and the steady-state output goes to zero. The control input can be

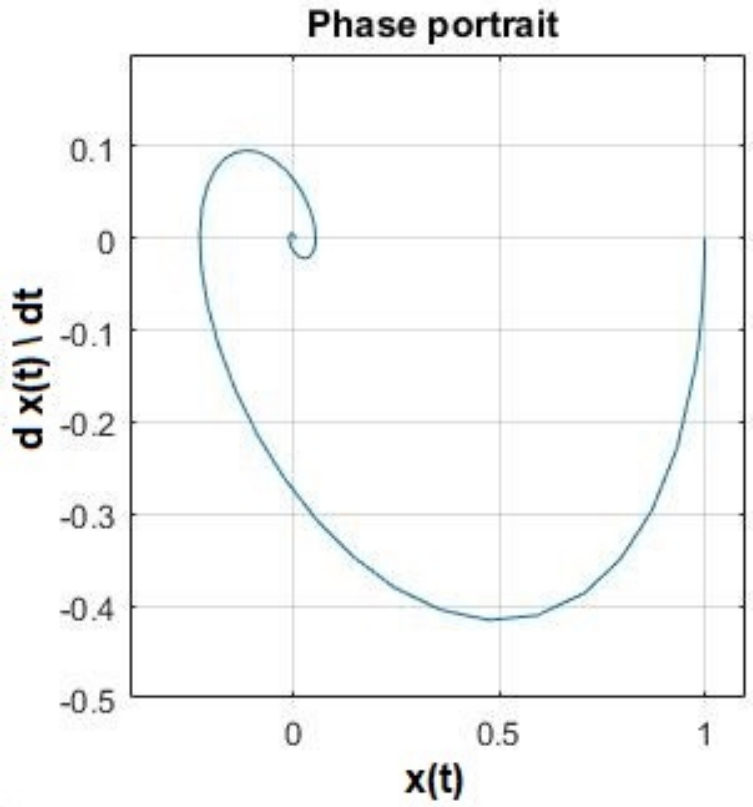

Figure 3.1: Trajectories of the oscillators system (3.1) where $X(t)$ is the variable with ($\beta = 1$ and $\alpha = 2$)

rewritten in the following law:

$$u(t) = \begin{cases} \beta \quad if \quad x(t)\ s(x(t), \frac{dx(t)}{dt}) > 0 \\ -\beta \quad if \quad x(t)\ s(x(t), \frac{dx(t)}{dt}) < 0 \end{cases} \tag{3.2}$$

where β is any positive scalar. Define a switching function by finding a linear combination of the two states of the system $(x(t) and \frac{dx(t)}{dt}))$ as shown:

$$s(x(t), \frac{dx(t)}{dt}) = Dx(t) + \frac{dx(t)}{dt} \tag{3.3}$$

where D is a positive scalar designed from system (3.1) using the stable poles. The phase portrait and the switching function of system (3.1) after applying the switching function (3.3) with $D = 0.5$ are shown in Fig. 3.2. Figure 3.2 shows

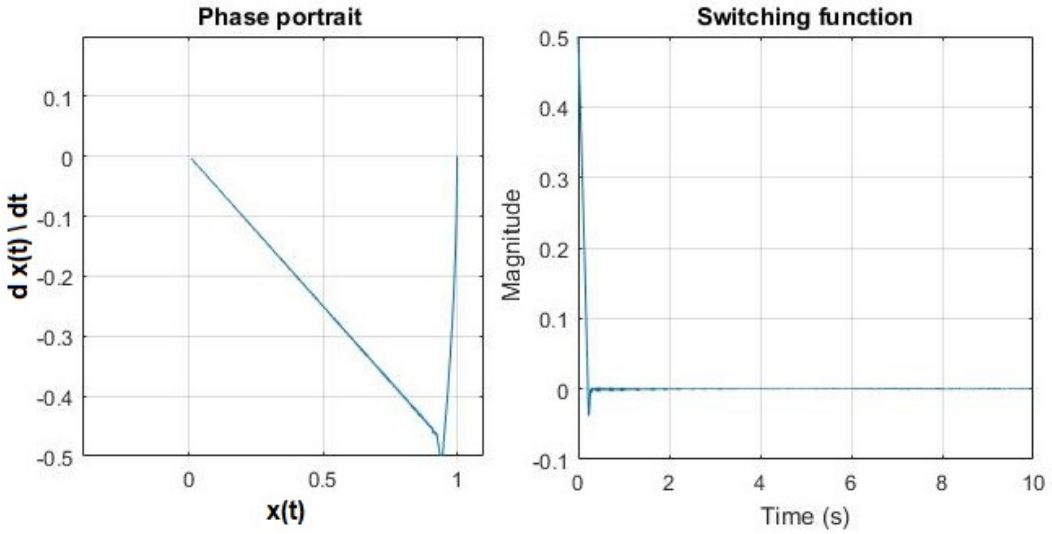

Figure 3.2: Trajectories of the oscillators system (3.1) with $D = 0.5$

that after a short transit time, the system starts to move in a straight line to the origin and the switching function goes to zero after a short time, this movement towards the origin is called the sliding mode [54] and is discussed in details in the following section. A comparison between the system with switched control and with stable feedback alone is shown in Fig. 3.3, and it shows that the system with switched control is behaving better as it reaches the stable steady-state value in a faster response.

3.2 Sliding Mode Controller

Sliding mode control (SMC) is a particular class of variable structure control [40]. [48]. It is typically composed of feedback control laws and a decision rule. The decision rule, termed the switching function, has as its input some measure of the current system performance and determines the particular feedback controller, which should be used at that time. In sliding mode control, the control is designed to drive and then constrain the system to lie within a neighbourhood of the switching function. The design thus comprises two steps; the first determines the switching function by solving the so-called existence problem and the second prescribes a control which makes the switching function attractive by solving the reachability problem. A significant advantage of the paradigm is that the dynamic behaviour

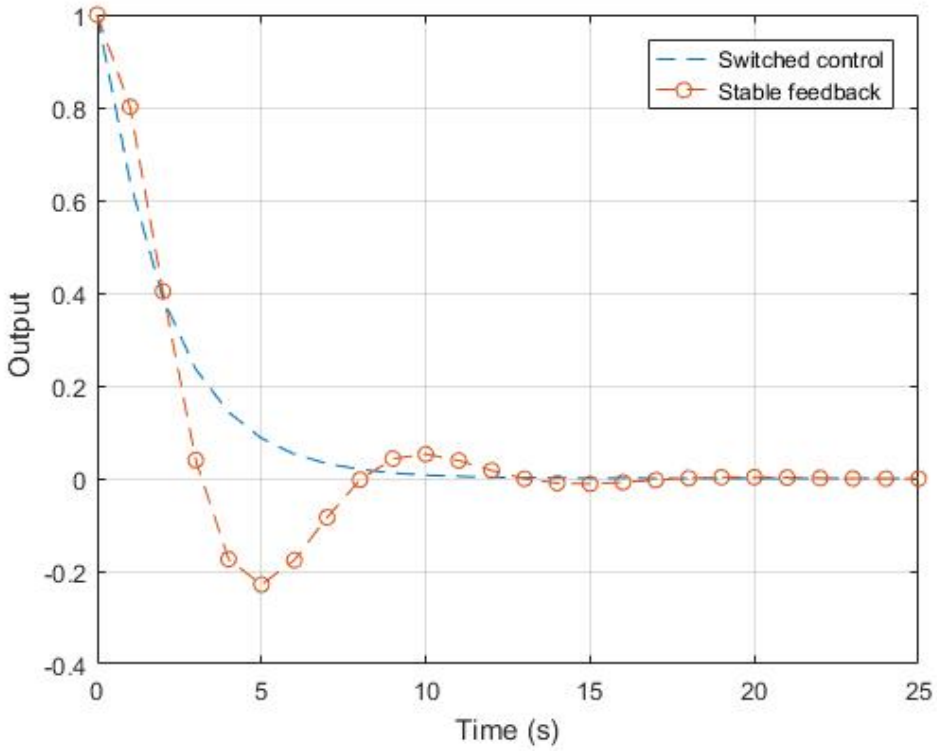

Figure 3.3: Comparison of the system output under switched control and normal stable feedback

of the system is directly tailored by choice of the switching function. Besides, the closed-loop response becomes very insensitive to a particular class of system uncertainty called matched uncertainty.

The basic design principles of sliding mode control will be shown using a pendulum system, which is simple and has been widely used to demonstrate key features in the literature [55] [48] [56]. The ordinary differential equation that represents the pendulum system is as follows:

$$\frac{d^2x(t)}{dt^2} = -\xi sin(x(t)) + u(t) \tag{3.4}$$

where ξ is a positive scaler. The variable $x(t)$ is the angular displacement variation over time and the control signal $u(t)$ is the force applied. The objective of this control is to force the trajectories to the origin. $x(t)$ and $\frac{dx(t)}{dt}$ are considered to be the state variables and the initial conditions are $x(0) = 0$ and $\frac{dx(t)}{dt} = 0$. A sliding

mode control for the system (3.4) can be designed using the switching function (3.3). When in sliding mode, the switching function $s(x(t), \frac{dx(t)}{dt}) = 0$, equation (3.3) will be:

$$\frac{dx(t_s)}{dt} = -Dx(t_s) \tag{3.5}$$

where t_s is the time when the system is on sliding mode. To simplify the writing, $s(x(t), \frac{dx(t)}{dt})$ will be replaced with s and the differential is denoted $\dot{s}(t) = \frac{ds(t)}{dt}$. The first step in the control design is to achieve sliding so that $s = 0$; the second step is to force the system state to move to and remain on the chosen sliding manifold. This step is called the reachability condition as shown in the literature [48] [56] [57]. Fundamentally, if a dynamics is needed to be attracted to the system state, then a control has to be modelled to make the direction of motion towards the origin. Because if the direction of motion is always towards the dynamics of the system, the control has to push the system back towards the origin. An advantage of having the reachability condition is that the system will stay in the sliding surface. Because every side of that dynamics will push back onto the dynamics by choice of the control [58] [59], the reachability condition can be written as:

$$s\dot{s} < 0 \tag{3.6}$$

A better version of the reachability condition is defined by Utkin, which will make the sliding mode happen in finite time is called the η-reachability [59] [58] condition and it is as shown below:

$$s\dot{s} < -\eta \mid s \mid \tag{3.7}$$

where η is a small positive number. In this case, the reaching time t_r can be found by integrating Eq. (3.7) between $t = 0$ and $t = t_r$ as: $s(t_r) - s(0) = 0 - s(0) < -\eta(t_r - 0)$, then $t_r = \frac{|s(0)|}{\eta}$. This t_r ensures the finite time converges $s = 0$.

After solving equation (3.4) when the system is in sliding mode, the value of $u(t)$ to achieve the reachability condition is as follow:

$$u(t) = -\frac{dx(t_s)}{dt} - \rho_1 sgn(s) \tag{3.8}$$

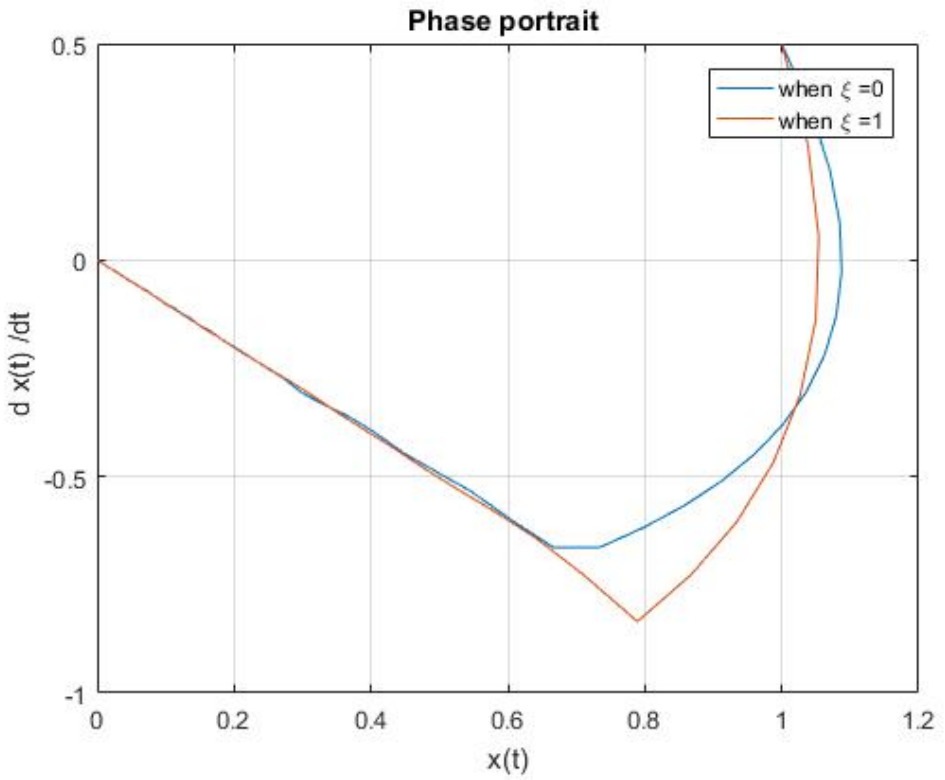

Figure 3.4: Phase portrait showing the response of the system (3.4) when $\xi = 0$ and when $\xi = 1$ with initial conditions x(0) = 1; $\dot{x} = 0.1$

where $sgn(.)$ is the sign function and value of ρ_1 should be bigger than $\xi + \eta$ to satisfy the reachability condition. Figure 3.4 shows a comparison of the phase portrait for system (3.4) when $\xi = 0$ and $\xi = 1$ and applying the control signal (3.8). Figure 3.4 show that the transit time is different between both dynamics; this difference is due to the dynamics of the sinusoid, as it is present is the case of $\xi = 1$. Once both systems reach the sliding mode, they exhibit the same dynamics of the reduced-order system with a pole at -1. The switching function is shown in Fig. 3.5. The sliding mode controller analysis is used in chapter 4 to study the robustness of models and in chapter 5 to find the physical limitations for variables using the reachability analysis.

3.3 State Observer

Three observer approaches are used; Luenberger observer, sliding mode observer and unknown input observer [60] [54] [49]. The observers block diagrams are

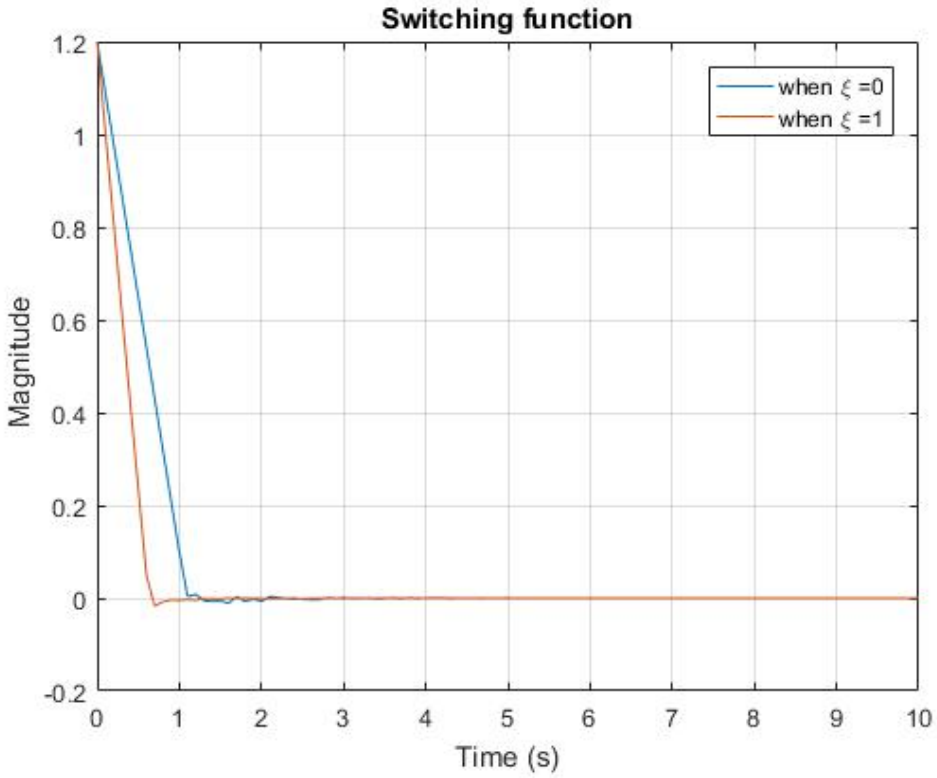

Figure 3.5: The switching function for system (3.4) when $\xi = 0$ and when $\xi = 1$

shown in the Appendix. Using three approaches gave a chance to prove that increasing the order of the system reduces the time required to estimate the wanted signal, enhances the robustness of the system and reduces the effect of external disturbance. In all cases, a model is used to define the observer, and an output error is formed by comparing the output of the observer and the output of the physical system. The analysis shows less complexity when designing the first-order observer and less accuracy compared to the second-order observer.

3.3.1 Analysis of Classical Luenberger Observer

Consider the following continuous-time system:

$$\begin{aligned} \dot{x}(t) &= Ax(t) + Bu(t) \\ y(t) &= Cx(t) \end{aligned} \tag{3.9}$$

where $x(t)$ is the system's state and $x(t) \in R^n$, $y(t)$ is the output and $y(t) \in R^p$ and $u(t)$ is the input and $u(t) \in R^m$. $A \in R^{n\times n}$, $B \in R^{n\times m}$ and $C \in R^{p\times n}$ and $p \geq m$.

Before estimating the state, it is required to investigate if the internal states can be deduced from the information of its output. This is called the observability test [61] and the system is observable if and only if the determinate of the observability matrix (3.10) does not equal to zero and it should have a full rank. In other words, the input and output measurements should be linearly independent.

$$Obsv = \begin{bmatrix} C \\ CA \\ CA^2 \\ . \\ . \\ CA^{n-1} \end{bmatrix} \tag{3.10}$$

The first step in the design of the Luenberger observer is to copy the model of the system, and then to add feedback term dependent on the error between the plant and observer.

$$\begin{aligned} \dot{\hat{x}}(t) &= A\hat{x}(t) + Bu(t) + L[y(t) - \hat{y}(t)] \\ \hat{y}(t) &= C\hat{x}(t) \end{aligned} \tag{3.11}$$

Equation (3.11) can be rewritten as:

$$\dot{\hat{x}}(t) = A\hat{x}(t) + Bu(t) + CL[x(t) - \hat{x}(t)] \tag{3.12}$$

The error between the plant and the observer is defined by:

$$e(t) = x(t) - \hat{x}(t) \tag{3.13}$$

The error dynamics between the plant and the observer will be expressed by:

$$\dot{e}(t) = \dot{x}(t) - \dot{\hat{x}}(t) = Ax(t) - A\hat{x}(t) - LCx(t) + LC\hat{x}(t) \tag{3.14}$$

and

$$\dot{e}(t) = [A - LC]\, e(t) \tag{3.15}$$

The poles of $[A - LC]$ must be negative, so an appropriate value of L will be chosen to identify the value of the eigenvalues.

3.3.2 Analysis of a Classical Sliding Mode Observer

Sliding mode observers are becoming a fundamental approach in applications [62] [63] [64] [65]. The main requirements when designing an observer is to zero the error between the plant and the observer output. One of the disadvantages of sliding mode control is that the discontinuity that is required in theory could be a problem in practice. This is not the case for a sliding mode observer that is a software entity. In the sliding mode observer, the output error is a natural sliding variable. Both outputs from the plant and the observer have to be available, and the error between them can be exactly zero in finite time using sliding mode, even in the presence of uncertainty and non-linearity. This is one of the key differences between sliding mode observer, and Luenberger observer which the error between the plant and the observer outputs goes to zero asymptotically. Consider the linear system (3.9), Assuming that (B,C) are full rank and (A,C) are observable. System (3.9) can be re-written in canonical form to make the system more straightforward by changing the coordinates $x \to Tx$ [48] where:

$$T = \begin{bmatrix} N^T \\ C \end{bmatrix} \tag{3.16}$$

where $N^T \in R^{n\times(n-p)}$ is the null space of C. The canonical form for system (3.9) is as shown:

$$\begin{aligned} \dot{x_x}(t) &= A_{11}\, x_x(t) + A_{12} y(t) + B_1\, u(t) \\ \dot{y}(t) &= A_{21}\, x_x(t) + A_{22} y(t) + B_2\, u(t) \end{aligned} \tag{3.17}$$

where

$$Tx = \begin{bmatrix} x_x \\ y \end{bmatrix} \tag{3.18}$$

In this case, y is known, which is the output, but the state x_x is not known. The observer design based on Utkin observer [66] is as shown:

$$\begin{aligned} \dot{\hat{x}_x}(t) &= A_{11}\,\hat{x_x}(t) + A_{12}y(t) + B_1\,u(t) + L\mu \\ \hat{y}(t) &= A_{21}\,\hat{x_x}(t) + A_{22}y(t) + B_2\,u(t) - \mu \end{aligned} \tag{3.19}$$

μ and L define the observer injection to be designed, so the error between the measured and the observed value is driven to zero. The error definitions are given by:

$$\begin{aligned} e_x &= \hat{x_x}(t) - x_x(t) \\ e_y &= \hat{y}(t) - y(t) \end{aligned} \tag{3.20}$$

To induce a sliding motion on the output error e_y so that the sliding condition $e_y = 0$ is enforced, it is necessary to ensure e_y and $\dot{e}_y$ have opposite signs. Consider μ defined by:

$$\mu = Msign(e_y) \tag{3.21}$$

The error dynamics are then:

$$\begin{aligned} \dot{e_x}(t) &= A_{11}\,e_x(t) + A_{12}e_y(t) + L\mu \\ \dot{e_y}(t) &= A_{21}\,e_x(t) + A_{22}e_y(t) - \mu \end{aligned} \tag{3.22}$$

It follows that for sufficiently large M, e_y and $\dot{e}_y$ have opposite signs and $e_2 = 0$ will be satisfied. When this sliding mode is attained, it follows that $e_y = 0$ and $\dot{e}_y = 0$. To complete the observer design, it is necessary to ensure the e_x subsystem exhibits stable dynamics in the sliding mode. Which, by choice of L, represents a stable system and so $e_x \to 0$ and consequently, $\hat{x_x}(t) \to x_x(t)$ infinite time. The choice of parameter L and a practical example on how the principle of the equivalent injection is shown in Chapter 6 to estimate the concentration of *BtuB* using the measured value of vitamin B_{12} concentration. The unknown input observer analysis

is described in details in chapter 6.

3.4 Conclusions

This chapter describes the primary background of the control theory that is used throughout this thesis. First, it discusses the philosophy of variable structure control, and it sheds light on the early stages of this technique, then it shows a sample example of a second-order differential equation with the creation of the switching function. It is shown in this chapter that using VSC, the system behaves better and reaches the steady-state value in transit time. The chapter then describes a particular class of variable structure control (SMC) and discuss in details using a pendulum system. The reachability condition is later addressed by finding the multiplication between the switching function and its derivative and making sure it is less than zero. Finally, the observation method is showed in details by studying two different observation approaches, one by analysing a classical Luenberger observer and then, by studying a sliding mode observer. This chapter gives the control engineering background required to investigate the control mechanisms in bacterial growth, for example, VSC is used in chapter four to study the mathematical model of a vitamin B_{12}, the reachability condition is used in chapter five to show the physical limitation of bacterial and algal growth and the observation methods are used in details to find the concentration of $BtuB$ using measurements of vitamin B_{12} concentration.

Chapter 4

Understanding the Control of a Vitamin B_{12} Riboswitch

The previous two chapters have presented the biological and control background required to study the control mechanisms of bacterial growth. This chapter will build a mathematical model of bacterial growth using the concept of the vitamin B_{12} riboswitch. The model has been developed by studying the dynamics of the vitamin B_{12} riboswitch. The simulation results have been validated using the results of *in vivo* experiments by checking the bacterial growth when using *E. coli* and *S. enterica* where the action of the vitamin B_{12} riboswitch is known to be a determinant of system behaviour and the dynamics of the growth, which when the riboswitch is ON, the bacterial growth increases and when it is OFF, the bacterial growth stops. This chapter first describes a simple model for the B_{12}-riboswitch regulatory network in *E. coli* and applies the same analysis when changing the strain to *S. enterica*. Validation of the simulation results has been undertaken by linking the dynamics of the riboswitch to bacterial growth. The literature on studying the vitamin B_{12} riboswitch focused on how it is a control element in Gram-positive and Gram-negative prokaryotes [67]. The study shows that the genes under the control of a B_{12} riboswitch are associated with the coenzyme biosynthetic pathway or involved in the transport of cobalamin compounds or metals. Many scientists studied the effect of the vitamin B_{12} riboswitch in different bacteria such as *Sinorhizobium meliloti* [68] and *Mycobacterium tuberculosis* [69]. In studying the regulation of

the vitamin B_{12} metabolism, Alexey et al. [70] showed that the regulation has a similar mechanism to those seen in riboflavin [71]. Both have the riboswitch as a regulation control element.

The mathematical model, which is used in this chapter, is based on the riboswitch regulatory pathway [6]. This riboswitch is capable, in general, of regulating *BtuB*, which is an outer membrane porin that mediates high-affinity binding and TonB- dependent active transport of vitamin B_{12} across the outer membrane. Regulation at the transcriptional level occurs when a B_{12} molecule binds the riboswitch aptamer domain and causes the formation of a terminator structure in the riboswitch expression platform. After estimating the parameters of the model, the system has been validated by creating an equation for the bacterial growth, and it is proved experimentally that the model reproduces the system behaviour and captures the system dynamics within proper bounds. For validation purposes, the growth levels in vitamin B_{12}-dependent bacteria were determined when grown in environments containing different concentrations of vitamin B_{12}. *E. coli* and *S. enterica* strains were used in the experiments, and the growth levels were measured using optical density data recorded on triplicates at 600 nm $OD600$. The verification process was performed by comparing simulation and experimental results. In addition, the assessment of the saturation effect when the concentration is high or low has been studied. The organisation of the chapter is as follows: first, a preliminary analysis for the model of vitamin B_{12} is conducted. Second, model validation is undertaken, and finally, a comparison between the analytical analysis and the experimental results is made.

4.1 Analysis of a Simple Model of the Vitamin B_{12} Riboswitch

Gene expression can be regulated at several levels in a cell and at any time before or after the processes of translation and transcription. *E. coli* is incapable of synthesizing vitamin B_{12}. Instead, these bacteria actively transport the vitamin from the environment. *BtuB*, which is encoded by gene *btuB*, is an important component of

the vitamin B_{12} transporter. Gene *btuB* is negatively regulated by vitamin B_{12} via a riboswitch. A mathematical model for the B_{12}-riboswitch regulatory network in *E. coli* was developed by Santillan et al. [6] by identifying three normalised model variables m, e and p which respectively represent the concentration of *btuB* mRNA , the concentration of *BtuB* and the concentration of vitamin B_{12}. The biological meanings of the parameters in (4.1) - (4.3) are shown in Table 5.1. The functions $\phi(p)$ and $\theta(p)$ denote the B_{12}-governed regulation at the transcriptional and translational levels respectively. These functions are shown to be given by the following Michaelis-Menten equations:

$$\phi(p) = \frac{K_\phi}{K_\phi + p}$$

$$\theta(p) = \frac{K_\theta}{K_\theta + p}$$

Table 4.1: Pre-determined parameters in the mathematical model (4.1) - (4.3)

Symbol	Biological meaning	Original [6] / New Experimental Value
γ	The mRNA degradation rate	7.1×10^{-2}
ξ	The *btuB* degradation rate	0.8×10^{-2}
δ	The B_{12} degradation rate	0.8×10^{-2}
$\varepsilon(P_{ext})$	Represent the type of the strain	25
K_ϕ	The dissociation constant at the transcriptional level	1/4 / 2.25×10^{-6}
K_θ	The dissociation constant at the translation level	1/4 / 2.25×10^{-6}

The model is described by:

$$\dot{m} = \gamma[\phi(p) - m] \tag{4.1}$$

$$\dot{e} = \xi\,[m\,\theta(p) - e] \tag{4.2}$$

$$\dot{p} = \delta\left[\varepsilon(P_{ext})\, e - p\right] \tag{4.3}$$

The development of this mathematical model started with identifying the control mechanisms for genes in the vitamin B_{12} riboswitch. Two main mechanisms are present. The first one is at the transcription level and involves the ligand formation of an essential terminator stem. The second control mechanism happens at the translation level, with vitamin B_{12} binding to control access to the ribosome binding site by causing structural changes in mRNAs. The combination of the two mechanisms creates the dynamics of the mathematical model.

Santillan et al. [6] present simulation results that have been undertaken for only 600 minutes, and the steady-state value for the concentration of the vitamin B_{12} is 1. When the simulation is run for a longer time (1500 minutes), the concentration of vitamin B_{12} increases again after 900 minutes, as shown in Fig. 4.1. This increase is an unexpected response and does not match the expected experimental results because the system should switch off when the concentration goes to zero.

The controls $\Phi(P)$ and $\Theta(P)$ in the Michaelis-Menten equations depend on the value of the concentration of vitamin B_{12}, which is the third variable in the mathematical model (4.1) - (4.3) and thus the control system response is as shown in Fig. 4.1b. As this does not match the expected experimental results, the parameters of the mathematical model (4.1) - (4.3) need to be modified. In the original model [6], the dissociation constants at the transcription (K_ϕ) and translation (K_θ) levels are considered to be 1/4. Using this value, the steady-state value for the concentration will increase after 900 minutes. Based on the literature [72], [73] the dissociation constant for the reaction has a smaller magnitude. By changing the dissociation constant to 2.25×10^{-6}, the concentration output is correct and matches the results expected from experiments. The new parameter values are shown in Table 5.1. The simulations using the modified parameters were carried out by solving (4.1) - (4.3) with MATLAB as shown in Fig. 4.2. Initial conditions of the normalised concentration of *btuB* mRNA, the concentration of *BtuB* and the concentration of vitamin B_{12} were chosen as $m(0) = 1$, $e(0) = 1$ and $p(0) = 0$. All the simulations shown in this study used the same initial conditions.

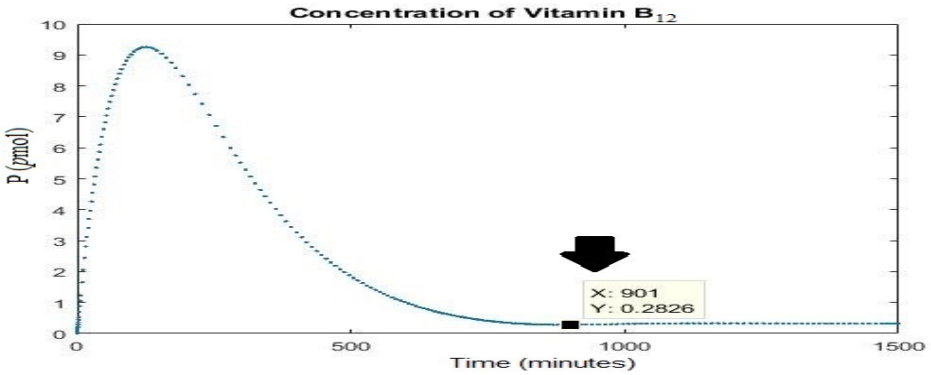

(a) Concentration of vitamin B_{12}

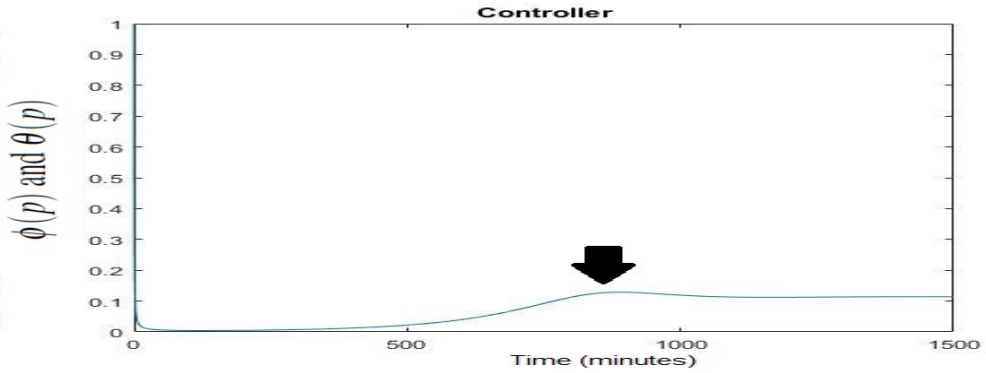

(b) $\phi(p)$ and $\theta(p)$

Figure 4.1: The simulation results for the concentration of vitamin B_{12} and the controller in the original model [6]

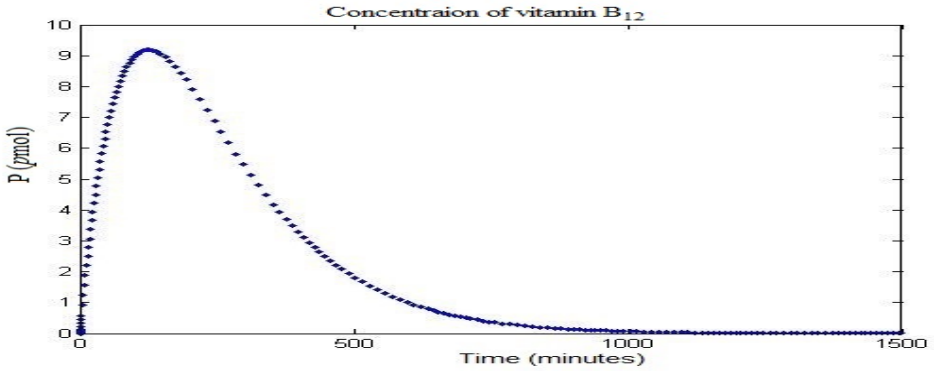

Figure 4.2: Concentration of Vitamin B_{12} following simulation for 1500 minutes

It is seen from the simulation results of model (4.1) - (4.3) that the concentration of *btuB* mRNA has a rapid transient, and thus it is assumed that this has reached steady-state in the subsequent analysis. The reason for this is because γ is one order of magnitude larger than ξ and δ.

This will make the dynamics of *btuB* mRNA faster than the concentration of *BtuB* and the concentration of vitamin B_{12}. Applying a quasi-steady-state assumption whereby $\dot{m} = 0$, this yields to $m = \phi(p)$, and substituting the corresponding steady-state value of m in the concentration of the *BtuB* equation (4.2), the system's order is reduced to yield:

$$\dot{e} = \xi \left[\phi(p)\,\theta(p) - e\right] \tag{4.4}$$

$$\dot{p} = \delta \left[\varepsilon(P_{ext})\,e - p\right] \tag{4.5}$$

Several parameters affect the reduced order mathematical model of the regulation equations for the B_{12} riboswitch as shown in (4.4) - (4.5). These parameters are the *BtuB* degradation rate, the B_{12} degradation rate and the value that is used to show which strain has been used (ε). The effect of varying these parameters on the concentration of vitamin B_{12} and the bacterial growth rate will now be considered.

4.2 Model Validation

To validate the model, it is necessary to model the growth curve from (4.4) - (4.5) and compare it with the growth curve obtained from experiments. The comparison will include different levels of the concentration vitamin B_{12} ($50p$M - $1n$M). The effect of the parameters will be described in detail. For example, the relation between the concentration of vitamin B_{12} and the growth will be considered. A model incorporating the effect of varying concentration of vitamin B_{12} with the OD600 bacterial growth output (which denotes the absorbance, or optical density, of a sample measured at a wavelength of 600 nm) is shown below:

$$OD_{600} = \begin{cases} OD_{Lag\,phase}, \text{ if } t \le t_l \\ [(\dfrac{0.057 \times P_{max}}{t_s - t_l}) \times (t - t_l)] + OD_{Lag\,phase} \text{ if } t_l \le t \le t_s \\ OD_{t_s}, \text{ if } t \ge t_s \end{cases} \tag{4.6}$$

The parameters used in this equation with their biological meanings and experimental values are listed in Table 4.2.

The initial number of bacteria, bacterial types and experimental environments de-

Table 4.2: Pre-determined parameters in the growth equation (OD_{600})

Symbol	Biological meaning	Experimental Value
$OD_{Lag\ phase}$	The absorbance at OD_{600} when the growth is at the lag phase	0.1
t_l	Time to reach the log phase	400
t_s	Time to reach the saturation phase	Varies depending on vitamin B_{12} concentration
OD_{t_s}	The absorbance at OD_{600} when the growth is at the saturation phase	Varies depending on vitamin B_{12} concentration

pend on the particular experimental conditions. Table 4.2 presents a set of parameters consistent with the experiments performed by Naziyat Khan in the bioscience laboratory at University of Kent under the supervision of Professor Martin Warren. This choice may be justified by considering Fig. 4.3. It is shown from Fig. 4.3 that the bacterial growth remained the same for a period of time, this value was counted to be 0.1 in the $OD600$ scale. Then, the binary fission started and the equation of it was calculated based on the value of P_{max} and a constant value of 0.057 to fit the simulation results with the experimental results. P_{max} is defined to be the maximum value of the concentration of vitamin B_{12} and t_s is defined to be the time at which the maximum is reached. These values have been computed directly from the model (4.4) - (4.5) and can also be identified from the experimental results. After that, the growth reached the saturation level and the growth remained as the maximum value of the previous phase. This value is named as OD_{t_s}. It is clear that P_{max} and t_s vary with the change of $Btub$ degradation rate ξ. Figure 4.4 shows P_{max} corresponding to different values of ξ. Changing the bacterial strain will also change P_{max}, and this is demonstrated both from simulation and experimental results, as shown in Fig. 4.5.

Simulations were carried out by solving (4.4) - (4.5) and applying the simulation results in the growth equation. It is seen that by increasing the concentration of vitamin B_{12}, the absorbance at OD600 will increase and the time required to reach the steady-state value will decrease. The time needed to reach the stationary phase

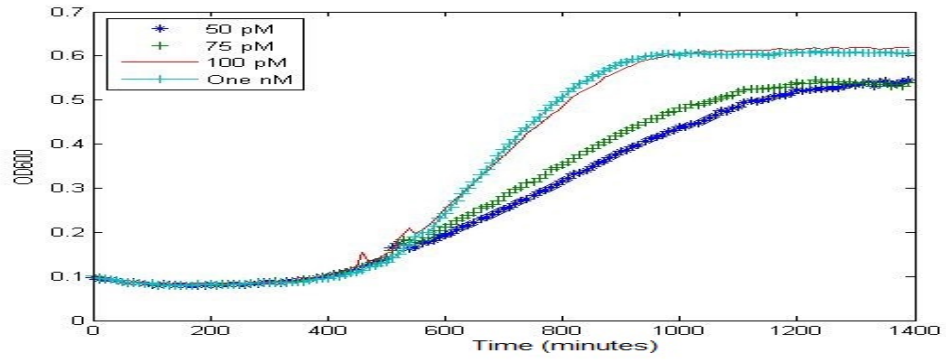

Figure 4.3: Experimentally measured *E. coli* growth curves with varying vitamin B_{12} concentration (50pM to 1nM)

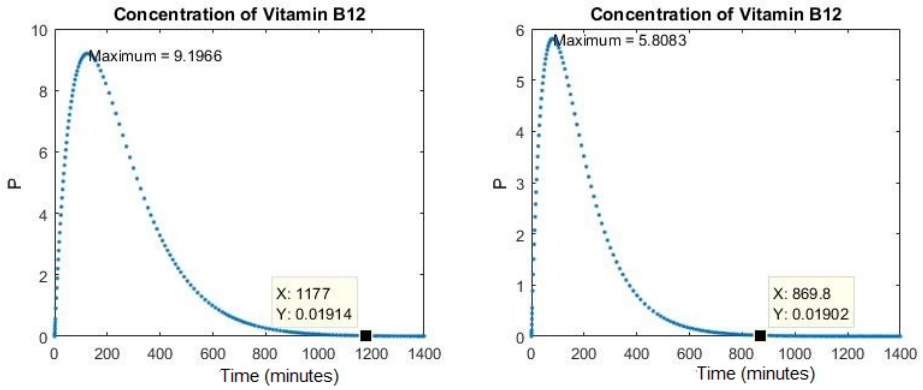

(a) 0.8×10^{-2} **(b)** 1.8×10^{-2}

Figure 4.4: The concentration of Vitamin B_{12} when changing the *Btub* degradation rate ξ from 0.8×10^{-2} to 1.8×10^{-2}

and the absorbance at OD600 for both simulation and experimental results for all concentrations is shown in Table 4.3 and Table 4.4. Fig. 4.3 shows the experimentally measured growth curve of *E. coli* with varying B_{12} concentration between 50pM and 1nM across three growth phases. In the lag phase, there is no change between the curves, even when the concentration is changed. That is because the system requires time to detect the environment and synthesise components necessary for rapid growth while in the exponential phase. By changing the concentration of vitamin B_{12}, the growth curve changes. From Fig. 4.3, it is seen that the OD600 during the lag phase is 0.1 and t_s is 400 minutes. These two values vary from one plate reader to another as they are dependent on the number of bacteria present when the experiment is initialised and the atmospheric conditions in the laboratory,

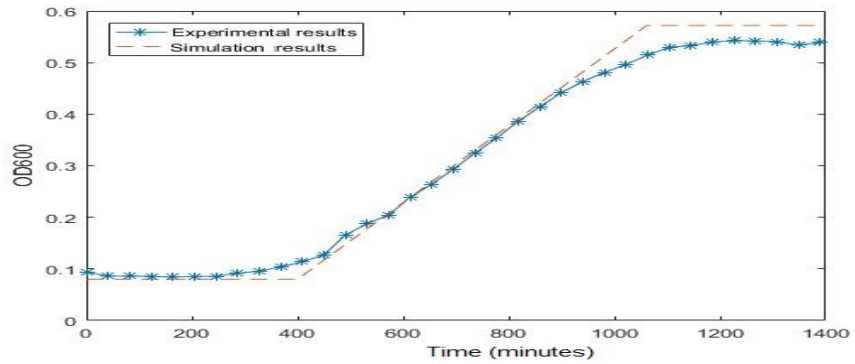

(a) Growth curve for 75pM when *E. coli* strain is used $\varepsilon = 25$

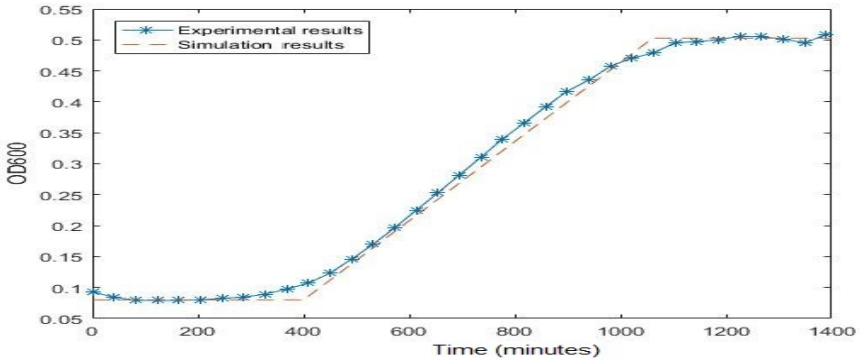

(b) Growth curve for 75pM when *Salmonella enterica* strain is used $\varepsilon = 21.5$

Figure 4.5: Comparison between the experimental and the simulation results when changing the value of bacterial strain ε

which may change. The exponential phase starts from 400 minutes to reach t_s. The value of t_s has a negative relation with the concentration of vitamin B_{12}, so when the concentration of vitamin B_{12} increases, the value of t_s decreases. In the stationary phase, bacterial growth stops, and there is no net increase or decrease in the number of cells. Varying the concentration of vitamin B_{12} will change the steady-state value of absorbance. For example, when the concentration of vitamin B_{12} is $50pM$, the value of absorbance at OD600 is 0.53, and when the concentration of vitamin B_{12} is 100pM, the value of absorbance at OD600 is 0.61 as shown in Fig. 4.6.

4.3 Discussion

To validate the model, a comparison has been made between the experimental results and the simulation results as shown in Fig. 4.5. Table 4.3 shows a comparison between the time required to reach the stationary phase in simulation and

Table 4.3: Comparison between the time required to reach the stationary phase experimentally and the time required for the concentration to reach zero mathematically.

Concentration of Vitamin B_{12}	Time required to reach the stationary phase in *E. coli* Fig. 4.5 (mins) Simulation Results	Time required to reach the stationary phase in *E. coli* Fig. 4.5 (mins) Experimental Results
50 pM	1330	1497
75 pM	1170	1170
85 pM	1140	1135
100 pM	1090	1061

experimentally while varying the concentration of vitamin B_{12}. It is clear that by increasing the concentration, growth is faster, and it reaches the stationary phase more rapidly. In addition, by increasing the concentration, the maximum value of the simulated concentration will increase and thus the absorbance at 600 nm will increase, as shown in Table 4.4. Growth reaches the stationary phase when the concentration of vitamin B_{12} goes to zero. By increasing the concentration, the time to reach the stationary phase decreases. Fig. 4.6 shows a comparison between the experimental results and the simulation results for the growth curve when the concentration of vitamin B_{12} is $50pM$, and when it is 100pM. The simulation results have a similar trend to the experimental observations in terms of bacterial growth, peak values and steady-state values. The value of ε is related to the strain for each bacteria that has been used. Here, *E. coli* and *S. enterica* are used and have different growth curves, as shown in Fig. 4.5. The experiments correspond to the wild-type *E. coli* and 375 mutant strain *S. enterica* [74]. The values of ε employed in these simulations are as follows: $\varepsilon = 25$ (wild-type strain), $\varepsilon = 21.5$ (375 mutant strain). The value of absorbance at OD600 increases when the value of ε increases. From

Table 4.4: Comparison between the absorbance at OD600 in the experiment and in the simulation.

Concentration of vitamin B_{12}	Simulation	Experiment
50 pM	0.503	0.532
75 pM	0.57	0.53
85 pM	0.61	0.57
100 pM	0.66	0.61

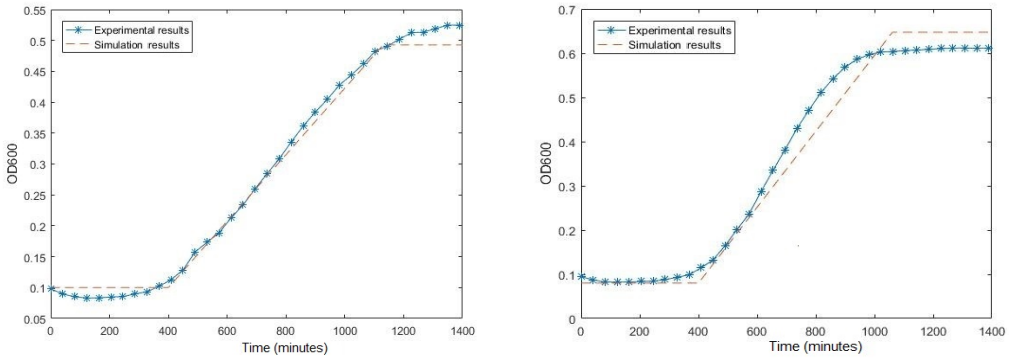

(a) 50pM **(b)** 100pM

Figure 4.6: Comparison between the experimental and the mathematical growth curve with different concentration of Vitamin B_{12} when growing *E. coli*

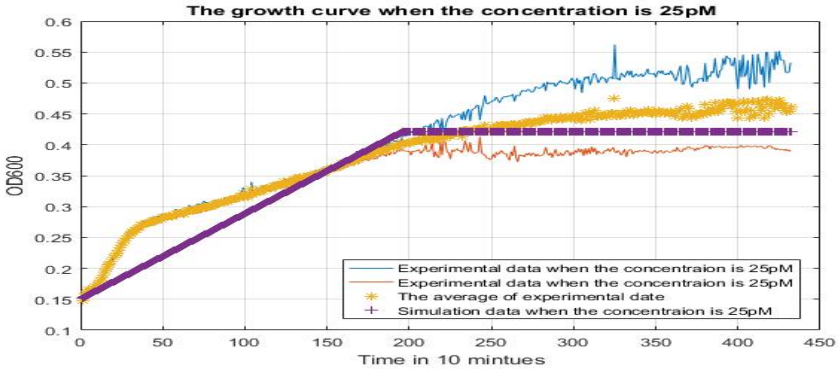

Figure 4.7: Comparison between the simulation and experimental growth curve for *E. coli* with concentration of 25pM

Fig. 4.5, the absorbance at OD600 is 0.63 when ε = 25 and it decreases to 0.52 when $\varepsilon = 21.5$.

After the model has been validated, an expected growth curve when the concentration of vitamin B_{12} is $25pM$ has been generated based only on the mathematical model. Experimental results were then obtained to verify the predictions. Fig. 4.7 shows the comparison between the simulated and experimental growth curve for *E. coli* with a concentration of 25pM. The model parameter t_l in (4.6) is zero and OD600 at the lag phase is 0.15. This setting is based on the plate that has been used for the experiments where it should be noted that results vary between plates.

It can be concluded that there is a positive relationship between the concentration of vitamin B_{12} and bacterial growth, as when the concentration of vitamin B_{12}

increases, the growth curve increases. Moreover, when the concentration of vitamin B_{12} increases to a certain level, it should be noted that bacterial growth will saturate. Comparing simulation and experimental results, it can be seen that the value of the concentration when the growth saturates is 1 nM; increasing the concentration of vitamin B_{12} by more than 1 nM, produces no change in the growth curve. Using the experimental results shown in Fig. 4.8a which are the experimental growth curve results for *E. coli* when the concentration of vitamin B_{12} is between 1nM and 100 μM, the experimental results agreed with the observed simulation results. In addition, this shows that for all the concentrations (1nM - 100 μM), the bacterial growth curve is approximately the same.

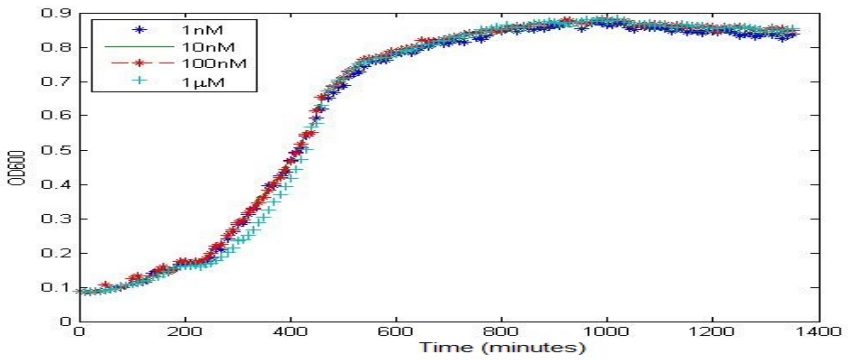

(a) Time evaluation of OD600 when applying high vitamin B_{12} concentration

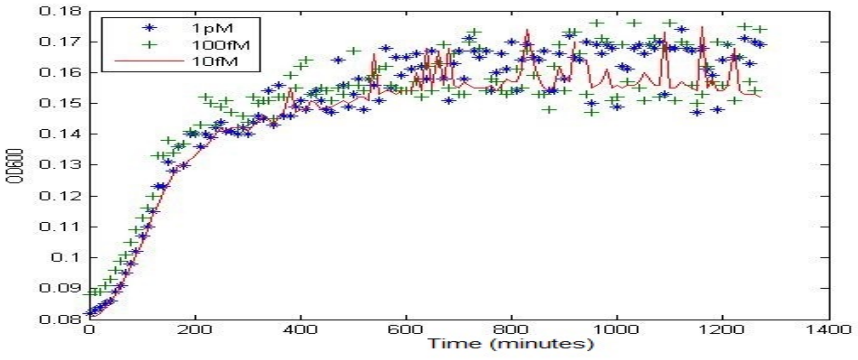

(b) Time evaluation of OD600 when applying low vitamin B_{12} concentration

Figure 4.8: Bacterial growth curve when the concentration of vitamin B_{12} are high and low

Fig. 4.8b shows the growth curve for *E. coli* when varying the concentration of vitamin B_{12} between $1pM$ and $10fM$. It also shows that when the growth is in the exponential phase, the growth is increasing slowly, and the absorbance at OD600 is

low. This also accords with the simulation results, as when the concentration is low, the amplitude of the output is low. The growth curve remains in the exponential phase. When the concentration is decreased further, the absorbance at OD600 will also decrease to reach the same value as in the lag phase, as shown in table 5.2.

Table 4.5: Simulation results for absorbance at OD600 with low vitamin B_{12} concentration.

Concentration of vitamin B_{12}	Simulation results
10 pM	0.2
5 pM	0.16
1 pM	0.11

4.4 Conclusions

In this chapter, the effect of the vitamin B_{12} riboswitch has been tested at the cellular level. The concentration of *btub* mRNA, the concentration of the *BtuB* and the concentration of vitamin B_{12} have been studied to determine how they affect the cells during transcription and translation. The dynamics of the vitamin B_{12} riboswitch have been incorporated in a model with *E. coli* bacterial growth. The effect of varying the concentration of vitamin B_{12} has been tested on the bacterial growth curves of *E. coli*. The same analysis has been performed with different bacterial strains, the simulation results fit with the experimental results and the mathematical model worked well. The effect of changing the concentration of vitamin B_{12} in bacterium *S. enterica* has been tested. The results have been linked, and the simulation results obtained replicated the experimental results. The next chapter will discuss the effect of vitamin B_{12} riboswitch in the population level and how it affects the co-culture of bacteria and algae.

Chapter 5

Growth Dynamics of Algal-bacterial Cocultures: A Control Engineering Perspective

5.1 Introduction

Despite internal complexity, algae and bacteria have coexisted since the early stages of evolution. This co-evolution follows relatively simple laws that can be expressed using mathematical models. This chapter performs quantitative analysis, motivated from the perspective of control theory, of a classical model from the literature. The model has been developed using data from an in *vivo* experimental two-species system where the bacterium $M.\ loti$ supplies the vitamin B_{12} required for growth to the freshwater green alga $L.\ rostrata$ and where the action of the B_{12} riboswitch

is known to be a determinant of system behaviour. This model was created by Matthew et. al [19] and analysis of the model both before and after the add-back of nutrients is carried out, which is the case where the nutrients are added externally to the system. A focus is on exploring the robustness of the system when varying the parameters and check the steady state values. The chapter first describes a simple model of algal-bacterial growth and analysis is undertaken. The effect of system parameters and control mechanisms is quantified. Motivated by the inherent switching action within the biology, a sliding mode interpretation of the control mechanism is hypothesized based on knowledge of the maximum carrying capacities for growth. The results of a range of experiments reported in the literature are used to validate the assertions.

The co-evolution between algae and bacteria has revolutionized life on earth. Amin et al. [75] studied the interaction and signalling between a cosmopolitan phytoplankton and associated bacteria and they proved the linkage in growth between the two populations.

A study performed by Croft et al. [76] investigated how algae acquire vitamin B_{12} through a symbiotic relationship with bacteria. It is important to understand these interactions from an evolutionary and ecological standpoint. Many studies have shown that algal and bacterial growth are coupled. Rhee et al. [77] showed that the growth of Scenedesmus algae increases exponentially, hitting a saturation level of 40×10^6 when growing alone without Pseudomonas bacteria. When Pseudomonas bacteria is added, the steady-state population of algae reduces to 15×10^6.

This is because the population of the bacteria is determined by the number of bacteria required to reach half the maximum carrying capacity. Haines et. al [78] experimentally measured the algal growth with and without bacteria. The algal growth without bacteria was 5×10^4, and the algal growth increased to 10^6 with bacteria added.

The most critical parameters regulating algal and bacterial growth are nutrient quantity and quality, light, pH, turbulence, salinity and temperature [79] and the interaction is complex [80]. For growth, bacteria require nutrient supply and organic matter which are produced by plants and algae.

In comparison, the stoichiometry of plants and algae is more flexible [81]. Algae take up nutrients such as phosphorus and nitrogen from the water, thus growing in open water, and capture their energy from sunlight. Dissolved organic carbon (DOC) is essential for bacteria and provided by algae to maintain energy and carbon. In exchange, over 50% of microalgae are dependent on an exogenous source of cobalamin synthesized by bacteria only for growth [19].

Systems models are required to associate the input effects on such a complex biological system, as well as capture the factors that affect the quality of the final product. A recent survey paper [82] has emphasized the importance of developing such models which can contribute to understanding ecosystems as varied as oceans to lichens as well as processes in biotechnology. The interaction between algae and bacteria is often considered as contamination during commercialization. However, some recent studies have shown that bacteria not only enhance algal growth but also

help in flocculation, both essential processes underpinning algal biotechnology.

Models underpinning algal growth [83] [84], bacterial growth [85] [86] [87] and growth of an algal-bacterial co-culture in the literature [88] include that of Matthew et al. [19]. This model describes the behaviour of the co-culture *L. rostrata* and *M. loti* including the B_{12} riboswitch. As the vitamin B_{12} riboswitch changes between ON and OFF behaviours, the output will be stabilised, thus influencing the vitamin B_{12} concentration. Therefore, in this case, depending on the switching mechanisms, the supply of bacteria for algal growth will be determined. This reliance on switching mechanisms motivates this work, which considers the control process for the perspective of discontinuous control theory.

The organisation of the chapter is as follows: first, a preliminary analysis for the model of algal and bacterial growth before the add-back of nutrients is conducted, the steady-state analysis, the robustness and the analytical analysis for a sliding mode control perspective, in this case, will be considered. Next, the same analysis is considered when the carbon and vitamin B_{12} are added as nutrients.

5.2 Analysis of a Simple Model Before the Add-back of Nutrients

This section will consider the algal and the bacterial growth equations before the add-back of nutrients such as vitamin B_{12} and carbon, which is the first step towards the analysis of the feedback control mechanisms inherent in the biology. The model of Matthew et. al [19] is considered, which describes the behaviour of the *L.*

rostrata / *M. loti* co-cultures. A model containing a minimal set of terms, which will elucidate the main processes is described as:

$$\dot{a} = \alpha a\Big[1 - a\Big(\frac{K_a\, b}{b_c + b}\Big)^{-1}\Big], \tag{5.1}$$

$$\dot{b} = \beta b\Big[1 - b\Big(\frac{K_b a}{a_c + a}\Big)^{-1}\Big]. \tag{5.2}$$

where α and β are the growth rate of *L. rostrata* and *M.loti* respectively, a and b are the algal and the bacterial growth respectively, K_a is the maximum number of algae that the bacteria can support, K_b is the maximum number of bacteria that the algae can support, b_c is the number of bacteria required to reach half the maximum carrying capacity and a_c is the number of algae required to reach half the maximum carrying capacity. Comparing equations (5.1), (5.2) with the logistic equation (2.2), it is clear that α and β are the growth rate, a and b are the algal and the bacterial growth respectively and $\left(\frac{K_a\, b}{b_c+b}\right)$ and $\left(\frac{K_b a}{a_c+a}\right)$ are the carrying capacity for the algae and the bacteria respectively. This means that the rate of change in the algal population with respect to time will have a limitation defined by the carrying capacity $\left(\frac{K_a\, b}{b_c+b}\right)$. From this carrying capacity, as the maximum value for $\frac{b}{b_c+b} = 1$ when $b>>b_c$, the maximum carrying capacity in the algal growth equation will be K_a, which is named as the maximum number of algae that the bacteria can support as shown in Table 5.1. The same thing applies in the case of bacterial growth. The carrying capacity is $\left(\frac{K_b a}{a_c+a}\right)$ and, as the maximum value of $\frac{a}{a_c+a} = 1$ when $a>>a_c$, the maximum carrying capacity in the bacterial growth equation will be K_b. This

is also shown in Table 5.1 as the maximum number of bacteria that the algae can support.

The biological meaning of the parameters in (5.1) - (5.2) is shown in Table 5.1. The values in Table 5.1 were taken from the literature where possible [19], with the

Table 5.1: Parameters in the mathematical model (5.1) - (5.2)

Symbol	Biological Meaning	Value [19]
α	Growth rate of L. rostrata	1.5 log2 days^{-1}
K_a	Maximum number of algae that the bacteria can support	4×10^6 ml^{-1}
b_c	Number of bacteria required to reach half K_a	10^4 ml^{-1}
δ_a	Fractional decrease in carbon production by algae when vitamin B_{12} is provided externally	0.4
K_v	Maximum number of algae when vitamin B_{12} is provided externally	4×10^6 ml^{-1}
β	Growth rate of *M. loti*	4 log2 days^{-1}
K_b	Maximum number of bacteria that the algae can support	10^7 ml^{-1}
a_c	Number of algae required to reach half K_b	5×10^3 ml^{-1}
δ_b	Fractional decrease in vitamin B_{12} production by bacteria when carbon is provided externally	0.9
K_c	Maximum number of bacteria if carbon is provided externally	2×10^8 ml^{-1}

remainder being established to achieve a satisfactory qualitative fit to experimental data [89]. From (5.1) and (5.2), it is seen that the algal growth is affected by K_a and

$\frac{b}{b_c+b}$. The bacterial growth is affected by K_b and $\frac{a}{a_c+a}$. The switches present in the system are $\frac{b}{b_c+b}$ and $\frac{a}{a_c+a}$. In biological terminology, the switch represents positive or negative feedback depending on the system conditions. If the switch corresponds to increasing the value of the output, it is denoted as positive feedback with:

$$\frac{X(t)}{\delta + X(t)} \tag{5.3}$$

where δ is a constant value. This switch will increase the value of the output, and it will enforce a steady-state value depending on the value of δ and $X(t)$. The corresponding negative feedback is given by :

$$\frac{\delta}{X(t) + \delta} \tag{5.4}$$

where δ is a constant value. By increasing the value of $X(t)$, the output of the switch will go to zero, and this switch decreases the value of the desired output. In the algal and bacterial growth equations, $X(t)$ is the value of b and a respectively and the corresponding value of δ is b_c and a_c respectively. Robustness is the ability of the closed-loop system to be insensitive to component variations and disturbances. It is one of the most useful properties of feedback, and it is useful to understand the robustness properties of systems. From (5.1) and (5.2), the system is affected by two different types of parameters. These may be characterised by those parameters that are included in the effective control signal (5.2) or (5.2) and those that are not. The parameters that determine this control are K_b, K_a, a_c and b_c and the parameters

that impact on the remaining dynamics are α and β. The algal growth rate has been determined experimentally in many studies and different algae. Original experimental conditions frequently differ in work reported across the literature. To enable comparison, work that has applied conditions corresponding to a temperature of 25 $^{\circ}$C and light intensity of 2500 Lux is considered here. Harris et al. experimentally found the *L. rostrata* growth rate to be 1.03 divisions per day [90], and under the same conditions, Fogg et al. found the growth rate of *XanthophyceaeMonodus* subterranean and *BacillariophyceaeAsterionellajaponica* to be 0.3 and 0.52 respectively [91]. As the variation in the algal growth rate appears in the same channel as the switched control, the effect of such changes on the dynamics can be expected to be small by appealing to well-known robustness properties of switched control systems in engineering [92]. Section 5.2.3 will show the exact components that affect the growth and will show that varying some parameters will not affect the control system.

5.2.1 Steady-state analysis

The first step towards the analysis of a closed-loop control system is the preparation of a mathematical model suitable for analysis. For ease of analysis, frequently a model is selected that is linear over a satisfactory range of operating conditions. Linear model is design to use the system in different applications such as, finding the exact time required to reach the steady state value. In this thesis , the non-linear system was enough as the sliding mode control theory is used.

To investigate the dynamic behaviour, an appropriate steady-state operating

condition is first identified. Setting the derivatives equal to zero in equations (5.5) and (5.6) whereby $\dot{a} = \dot{b} = 0$, and denoting $U_1 = \left(\frac{K_a\, b}{b_c + b}\right)$ and $U_2 = \left(\frac{K_b\, a}{a_c + a}\right)$ so that they are considered to be control signals within the closed-loop system (5.1)-(5.2). The mathematical model (5.1), (5.2) can now be rewritten as:

$$\dot{a} = \alpha\, a\left[1 - \frac{a}{U_1}\right], \tag{5.5}$$

$$\dot{b} = \beta\, b\left[1 - \frac{b}{U_2}\right]. \tag{5.6}$$

The following equilibrium conditions are obtained:

$$U_1 = \bar{x_1} \tag{5.7}$$

$$U_2 = \bar{x_2} \tag{5.8}$$

where $\bar{x}$ denotes the steady-state value, $\bar{x_1} = a_{ss}$ and $\bar{x_2} = b_{ss}$. The corresponding state matrices are found to be:

$$A = \begin{bmatrix} \frac{\partial \dot{a}}{\partial a} & \frac{\partial \dot{a}}{\partial b} \\ \\ \frac{\partial \dot{b}}{\partial a} & \frac{\partial \dot{b}}{\partial b} \end{bmatrix} = \begin{bmatrix} \alpha - \frac{2\,\alpha\, a_{ss}}{U_1} & 0 \\ \\ 0 & \beta - \frac{2\,\beta\, b_{ss}}{U_2} \end{bmatrix} \tag{5.9}$$

$$B = \begin{bmatrix} \frac{\partial \dot{a}}{\partial U_1} & \frac{\partial \dot{a}}{\partial U_2} \\ \\ \frac{\partial \dot{b}}{\partial U_1} & \frac{\partial \dot{b}}{\partial U_2} \end{bmatrix} = \begin{bmatrix} \frac{2\alpha a_{ss}^2}{(U_1)^2} & 0 \\ \\ 0 & \frac{2\beta b_{ss}^2}{(U_2)^2} \end{bmatrix} \tag{5.10}$$

After substituting the values of a and b with their steady-state values a_{ss} and b_{ss} in matrices A and B, the corresponding matrices become:

$$A = \begin{bmatrix} -\alpha & 0 \\ \\ 0 & -\beta \end{bmatrix} \tag{5.11}$$

$$B = \begin{bmatrix} 2\alpha & 0 \\ \\ 0 & 2\beta \end{bmatrix} \tag{5.12}$$

The stability of the system can be determined by calculating the poles of the linear system (5.11). The system is stable as it has negative open-loop poles located at $[-\alpha, -\beta]$. It is clear from the structure of the equations (5.11) and (5.12) that the parameters are all matched to the input signals and thus any parameter variations belong to the class of matched uncertainty to which a well-designed feedback control can expect to provide robustness, as in matrix A, the first line has a value related to the first variable $(-\alpha)$ and the second value is 0, and the second line has a value related to the second variable $(-\beta)$and the first value is 0. The same analysis applies to equation (5.12). From the mathematical model (5.1), (5.2), it is clear that

there is a feedback from variable a to b and from variable b to a. Moreover, this is a multivariable problem, because U_1 is a function of b and it is controlling a and U_2 is a function of a, and it is controlling b. This means the system is coupled. The parameters used in these normalised mathematical equations with their biological meanings and experimental values are as previously listed in Table 5.1.

Let $(\bar{x_1}, \bar{x_2}) = (4 \times 10^6, 10 \times 10^6)$. The corresponding equilibrium inputs are from (5.7) - (5.8):

$\bar{u_1} = 4 \times 10^6$ and $\bar{u_2} = 10 \times 10^6$. To define the linear model, state variables are defined as deviations from the equilibrium point:

$\delta_x(t) = x(t) - \bar{x}$

$\delta_u(t) = u(t) - \bar{u}$

The following linearised model can be expected to be valid for small deviations $\delta_x(t)$ and $\delta_y(t)$:

$\dot{\delta_x}(t) = A\,\delta_x(t) + B\,\delta_u(t)$

Simulation experiments are carried out to validate the performance of the linear model when compared with the non-linear model. The non-linear differential equations (5.25), (5.26) are simulated subject to the following conditions:

$$x(0) = \begin{bmatrix} 4 \times 10^6 \\ \\ 10^7 \end{bmatrix} \text{ and } u(t) = \begin{bmatrix} 4 \times 10^6 \\ \\ 10^7 \end{bmatrix}$$

For the linear model, the corresponding initial conditions are $\delta_x(0) = \begin{bmatrix} 3.9 \times 10^6 \\ 9.9 \times 10^6 \end{bmatrix}$

$$\delta_u(t) = \begin{bmatrix} 3.9 \times 10^6 \\ 9.9 \times 10^6 \end{bmatrix}$$

The response of the linear and non-linear models are compared in Figure 5.1.

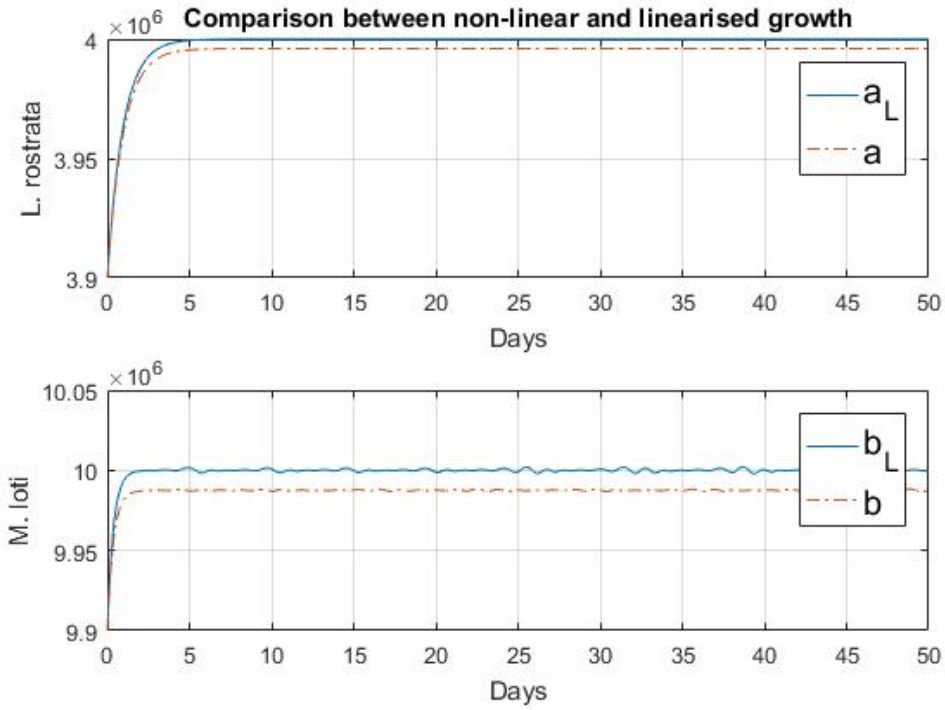

Figure 5.1: Comparison between non-linear and linearised growth of *L. rostrata* and *M.loti*

The relative error between the linear and the non-linear model responses is shown in Figure 5.2, which is calculated by finding the differences between the linear and the non-linear value, divided by the non-linear value.

In the previous simulation, the initial conditions for the system were taken close to

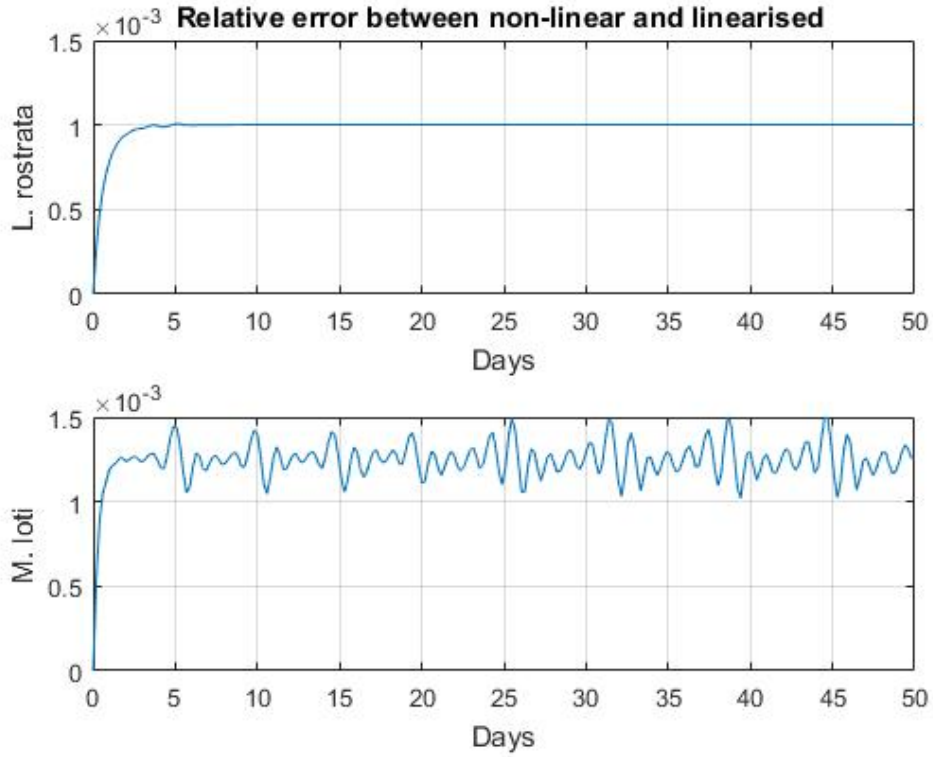

Figure 5.2: The relative error between non-linear and linearised growth of *L. rostrata* and *M.loti*

the equilibrium points. The initial conditions of the non-linear model are changed to $x_1(0) = 3 \times 10^6, 9 \times 10^6$. Figure 5.3 shows the comparison between the non-linear and linearised models. The relative error between the linear and the non-linear models is shown in Figure 5.4.

As the initial conditions move away from the equilibrium point, the accuracy

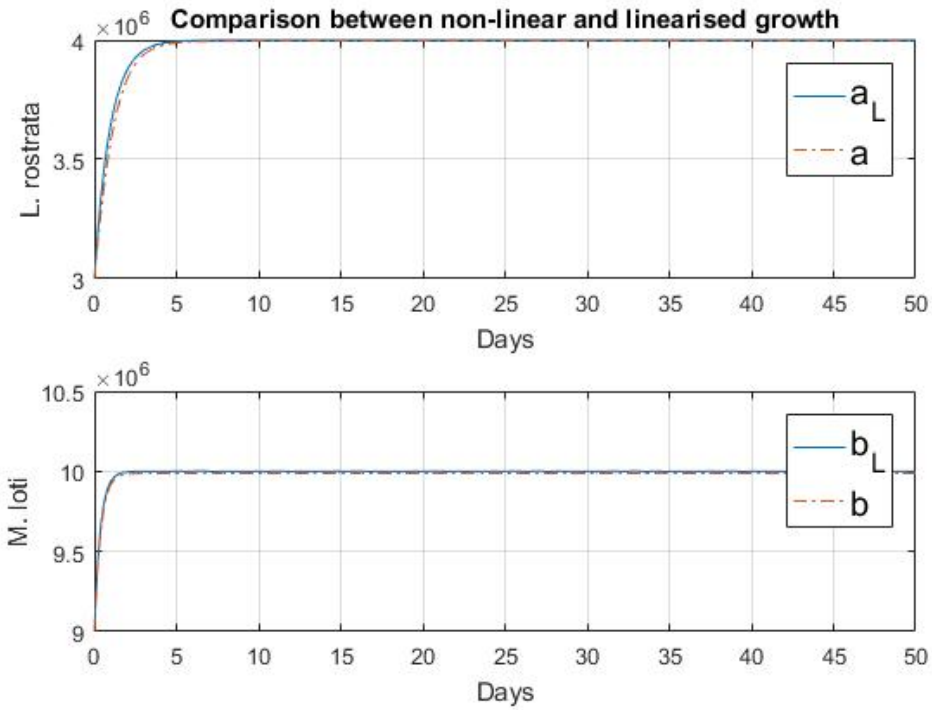

Figure 5.3: Comparison between non-linear and linearised growth of *L. rostrata* and *M.loti* when $x_1(0) = 3 \times 10^6, 9 \times 10^6$

of the linearisation will degrade. For example, if $x_1(0) = 1 \times 10^6, 5 \times 10^6$, the relative error is shown in Fig. 5.5. The impact of the parameters on the behaviour of the system is now explored. From equations (5.1) - (5.2), it is seen that the algal growth is affected by K_a and $\frac{b}{b_c+b}$. The bacterial growth is affected by K_b and $\frac{a}{a_c+a}$. To understand the limitation of the switches $\frac{b}{b_c+b}$ and $\frac{a}{a_c+a}$,it is crucial to study how the parameters affect the output.

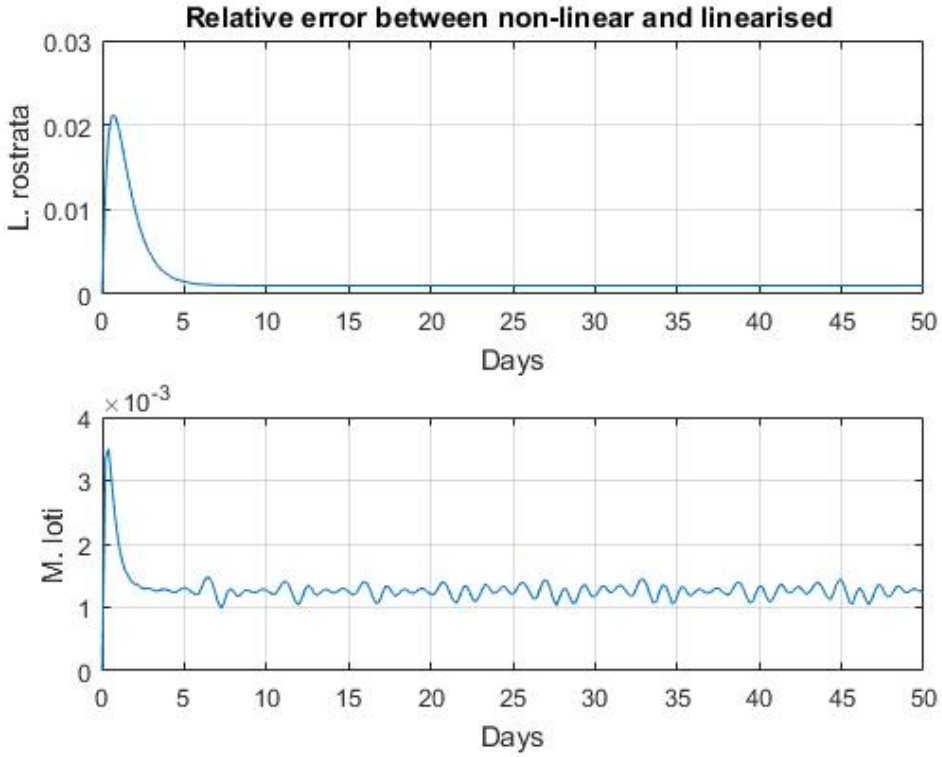

Figure 5.4: The relative error between non-linear and linearised growth of *L. rostrata* and *M.loti* when $x_1(0) = 3 \times 10^6, 9 \times 10^6$.

5.2.2 Robustness analysis and the effect of varying the parameters

In engineering, robustness is what makes it possible to design feedback systems based on simplified models. In biology, control systems can be inherently robust. When robustness breaks down, this can be an indicator of, for example, ill-health [92]. It is thus of interest to use tools from control engineering to study why

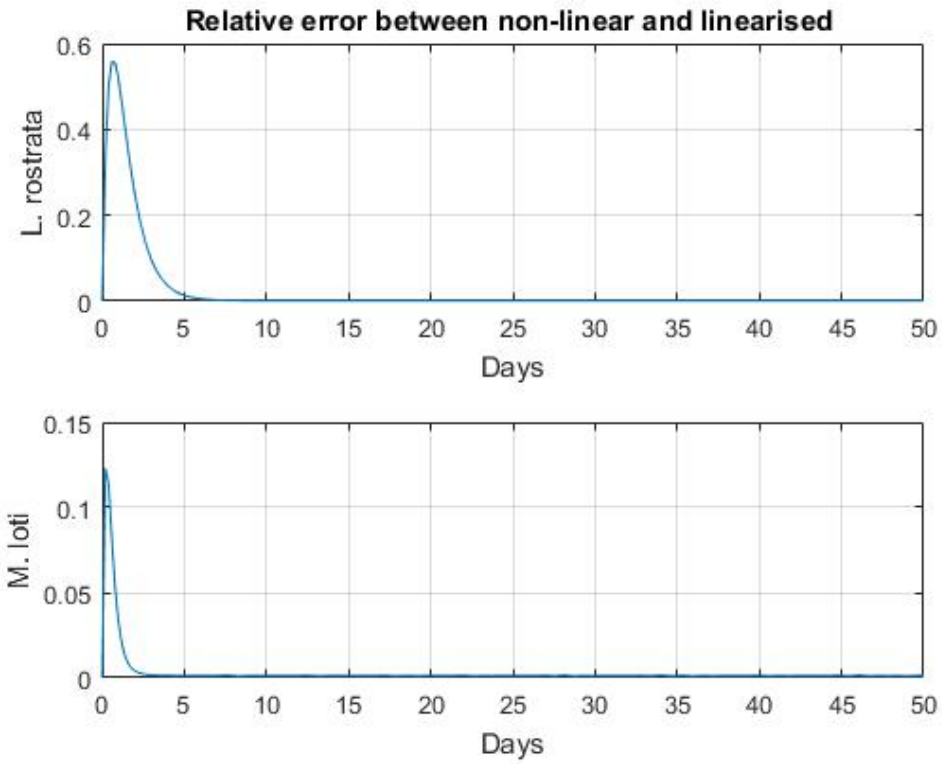

Figure 5.5: The relative error between non-linear and linearised growth of *L. rostrata* and *M.loti* when $x_1(0) = 1 \times 10^6, 5 \times 10^6$

biological control systems can be so robust as well as to understand how robustness breaks down. As discussed in the previous subsection, equations (5.1) - (5.2) are affected by two different types of parameter. These may be characterised by those parameters that are included in channels implicit in the control impact and those that are not.

The effect of varying K_b, K_a,a_c and b_c on algal growth The algal growth rate has been determined experimentally in many studies and different algae [82] [83] [94]. As the value of the algal growth rate is small compared with the value of the other parameters in the equation, its effect on the dynamics may be expected to be small. This is verified in Figure 5.6a. When the algae and the bacteria are

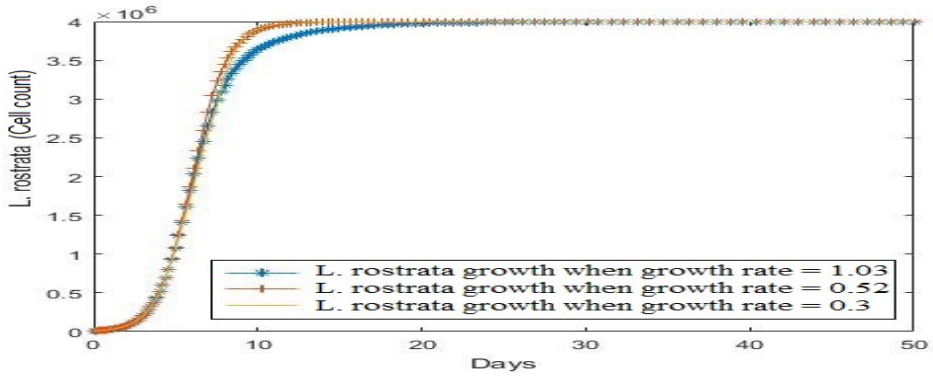

(a) The growth curve of *L. rostrata* when varying the growth rate of *L. rostrata* α

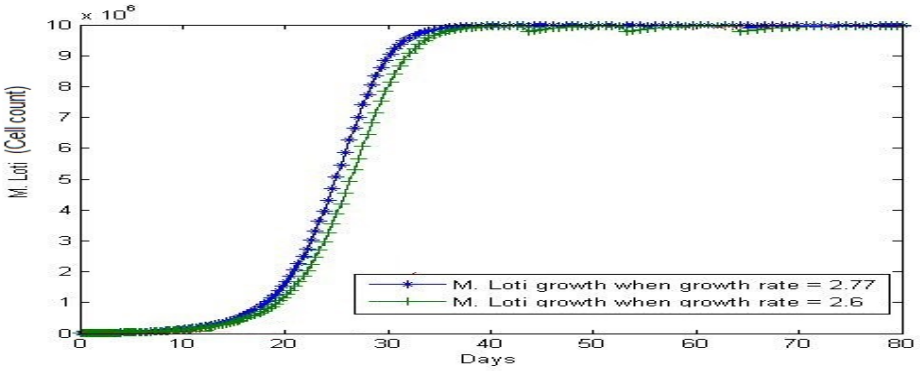

(b) The growth curve of *M. loti* when varying the growth rate of *M. loti* β

Figure 5.6: The growth curve of *L. rostrata* when varying the growth rate of *L. rostrata* α and *M. loti* when varying the growth rate of *M. loti* β

growing in the same medium, the factors that affect the *L. rostrata* algal growth are K_a and the switch $\frac{b}{b_c+b}$ where b is the *M. loti* bacterial growth. From the *L. rostrata* algal growth equation (5.1), increasing K_a will increase the algal growth. The algal growth is also affected by the switch $\frac{b}{b_c+b}$. It is clear that by increasing the value of b_c, the overall *L. rostrata* algal growth will decrease. Using the parameters provided in the original model [19], b_c was 10^4, and the algal growth was 4×10^6. By increasing the value of b_c to 10^7, the overall growth decreases to 2×10^6 as shown in Figure 5.7. The relation between b and b_c will also affect the algal population where the maximum value of b is K_b. If $K_b >> b_c$, the algal growth will be at the maximum value given by K_a as shown in Figure 5.8. To determine the value of K_b that will saturate the algal growth, fix the value of b_c as given in Table 5.1, $b_c = 10^4$. Varying K_b, the value of K_b that saturates algal growth is $K_b = 10^6$. To validate the result, take $K_b = 10^8$. The growth curve is the same as when $K_b = 10^6$, as shown in figure 5.9. As $K_b = 10^6$, is set to be the saturation limit for K_b, by decreasing the value of K_b to 10^4, algal growth will decrease, as shown in Figure 5.10.

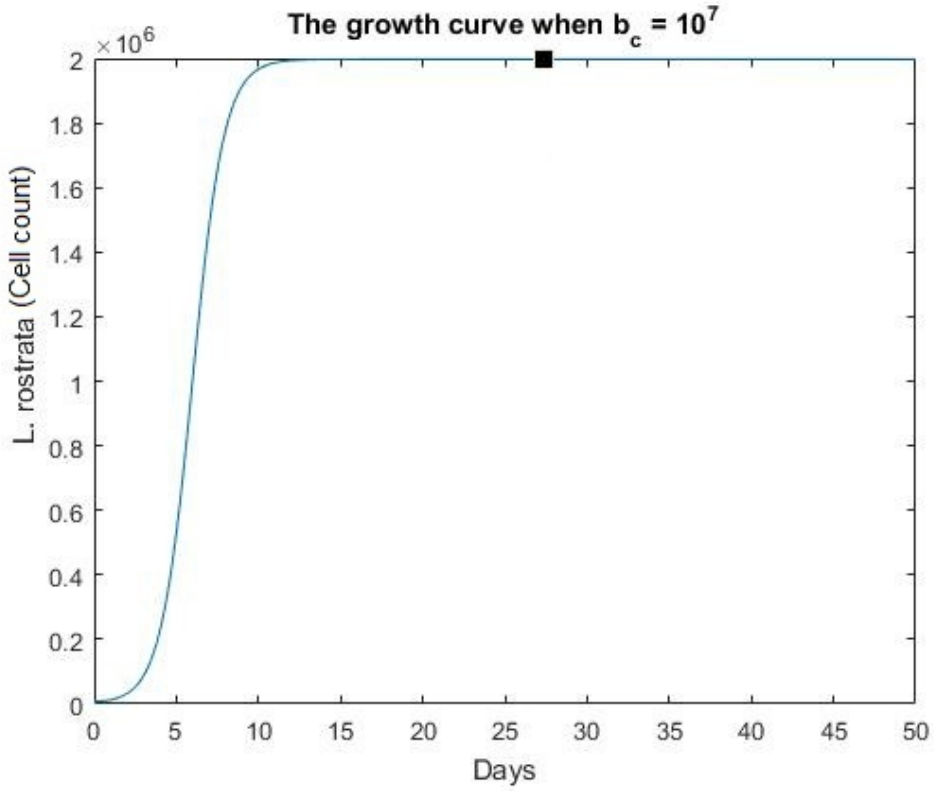

Figure 5.7: *L. rostrata* growth curve when the number of bacteria required to reach half of the number that the algae can support to $b_c = 10^7$

The effect of varying K_b, K_a, a_c and b_c on bacterial growth The bacterial growth rate has been determined experimentally in many studies and different bacteria. M. Mason [93] made a comparison of the maximal growth rates of various bacteria under optimal conditions showing that the bacterial growth rate of Streptococcus Liquefaciens is equal to 1.54 and the bacterial growth rate of Escherichia communior is equal to 2.6. Harris et. al [90] experimentally found the *M. loti* growth rate

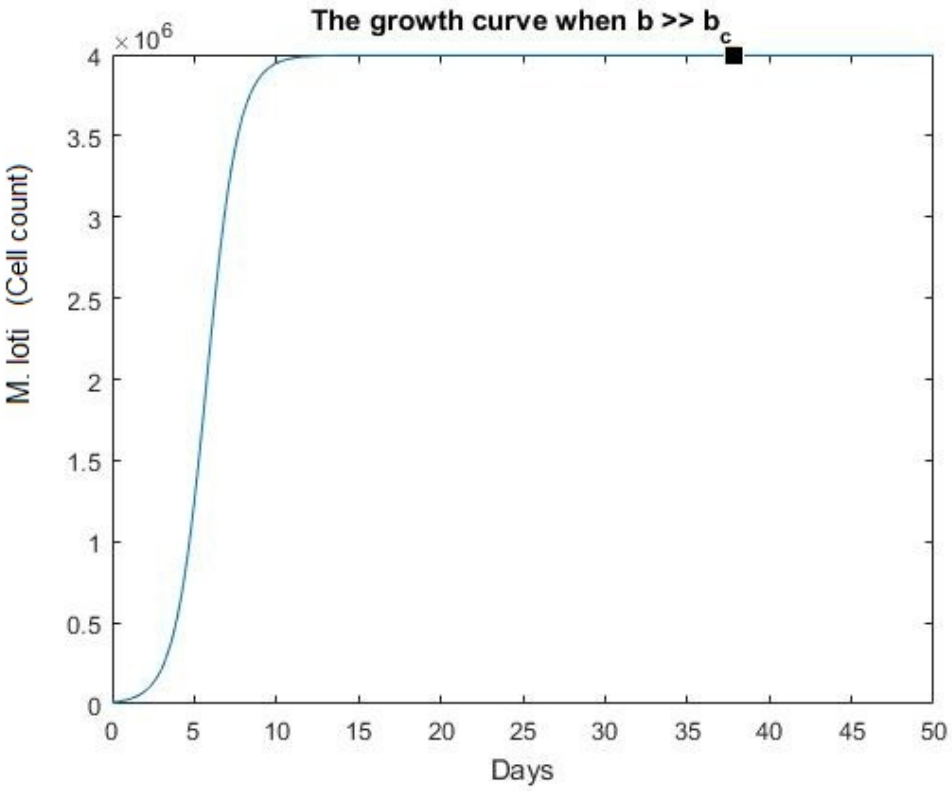

Figure 5.8: *M.loti* growth curve when the number of bacteria that the algae can support is larger than the number of bacteria required ro reach half of algae that the bacteria can support $K_b >> b_c$

to be 2.7726 divisions per day. The effect of the bacterial growth rate is shown to be small in Figure 5.11. The factors that affect bacterial growth are K_b and the switch $\frac{a}{a_c+a}$. Equation (5.2) shows that as the variable a varies which is the *L. rostrata* growth, the bacterial growth will vary. Increasing K_b increases bacterial growth. The other factor that affects the bacterial growth is the switch $\frac{a}{a_c+a}$. It is clear that

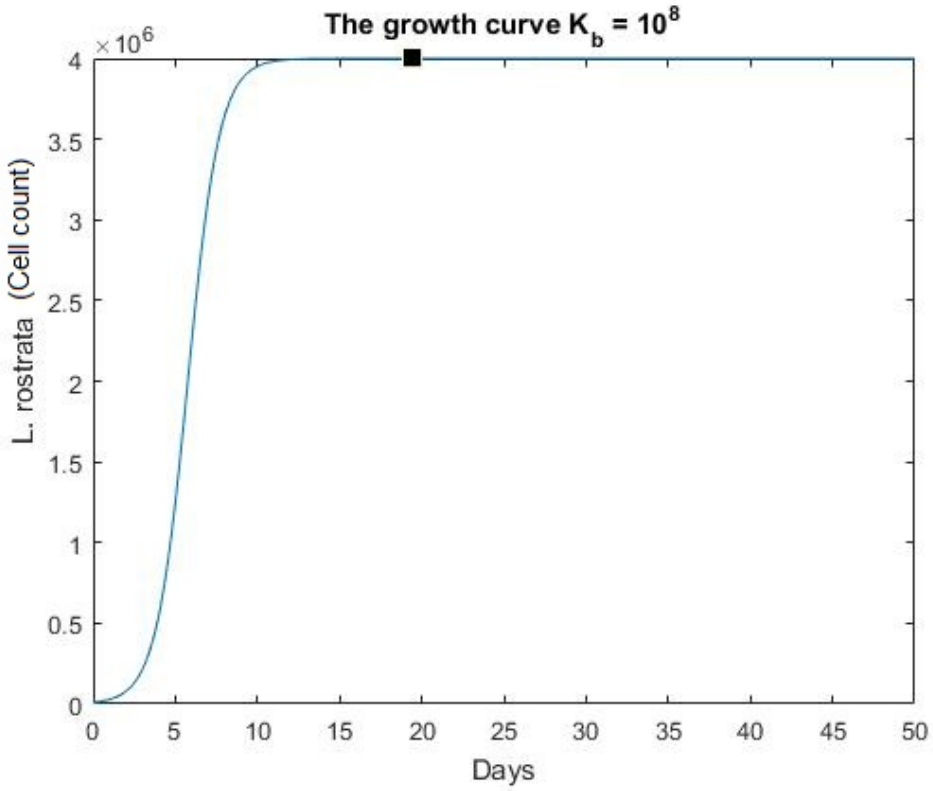

Figure 5.9: *L. rostrata* growth curve when the number of bacteria that the algae can support $K_b = 10^8$

by increasing the value of a_c, bacterial growth will decrease. Using the original parameters provided in Matthew et. al [19], the value of a_c is 5×10^3 and the bacterial growth is 10^7. By increasing the value of a_c to be 4×10^6, the overall growth decreases to 5×10^6 as shown in Figure 5.12. In addition, the relationship between a and a_c will affect the bacterial population. It is shown from the simulation that K_a is the main factor that affects algal growth and the maximum value of a is K_a. The

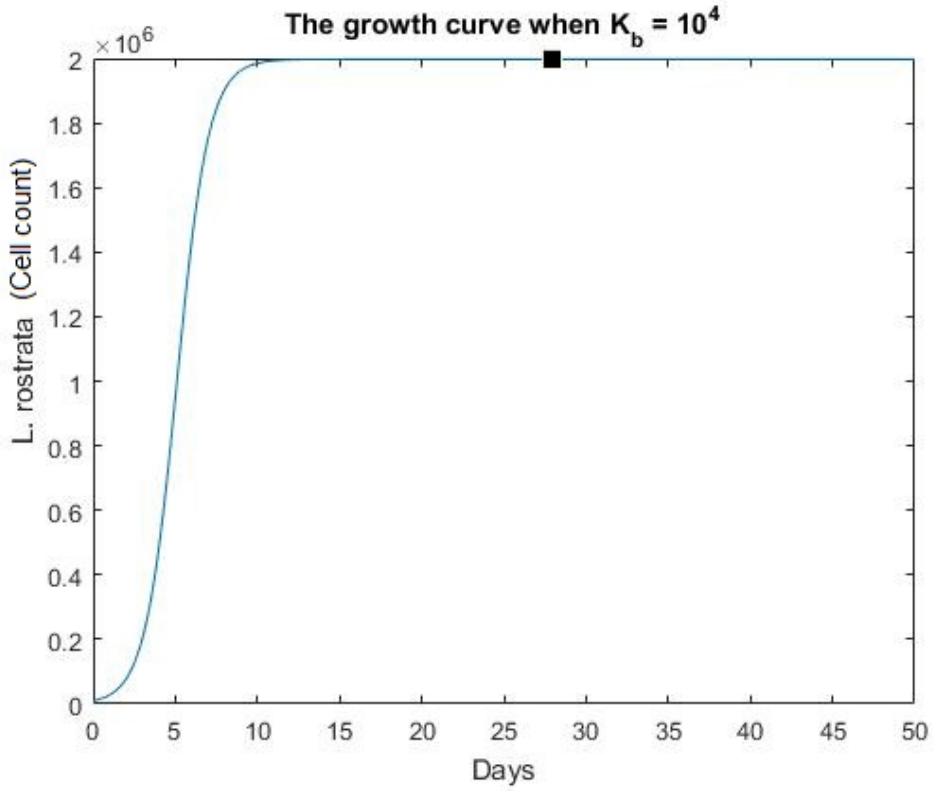

Figure 5.10: *L. rostrata* growth curve when the number of bacteria that the algae can support $K_b = 10^4$

main parameters that affect bacterial growth are the value of K_b and the relationship between K_a and a_c. K_a is the maximum number of algae that the bacteria can support. It affects algal growth by determining the switching behaviour. The value of K_a that saturates the growth of the algae is $K_a = 5 \times 10^7$. The simulation output for algal growth when $K_a = 10^8$ is shown in Figure 5.13, and it is seen that the growth curve is similar to the growth curve when $K_a = 5 \times 10^7$ shown in figure 5.14.

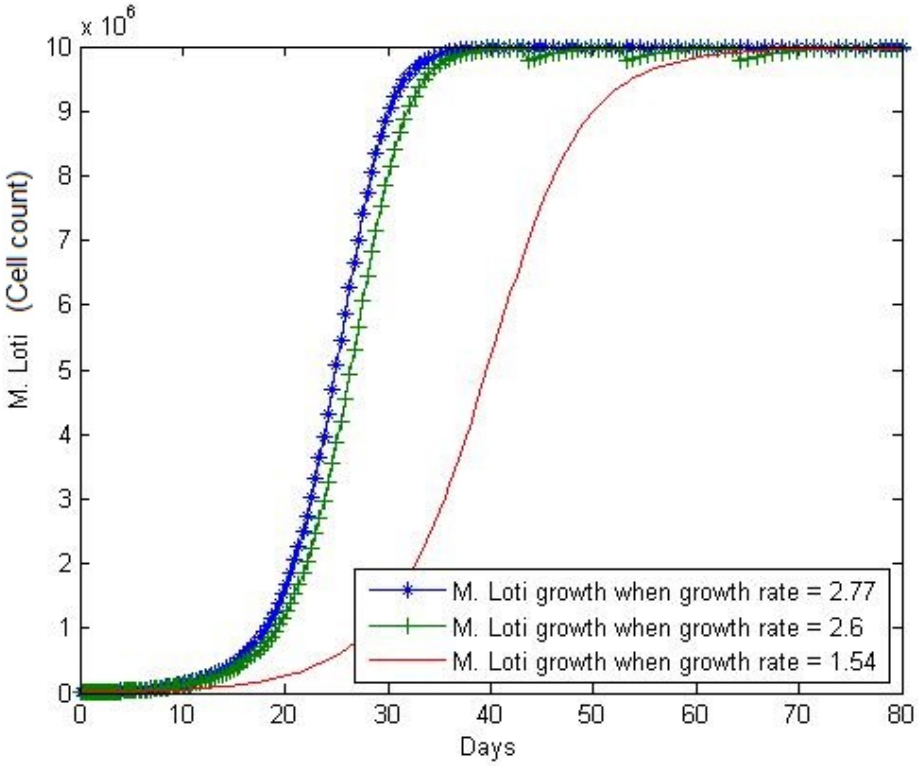

Figure 5.11: The growth curve of $M.\ loti$ when varying $M.\ loti$ growth rate β

The effect of the parameters on the dynamics when growing algae may be summarised as follows:

- α: α should be positive and does not affect the steady-state value. It has a transient effect. For example, when $\alpha = 1.5 \times log(2)$, the time required to reach the steady-state value is 10 days and when $\alpha = 3.5 \times log(2)$, the time required is 5 days

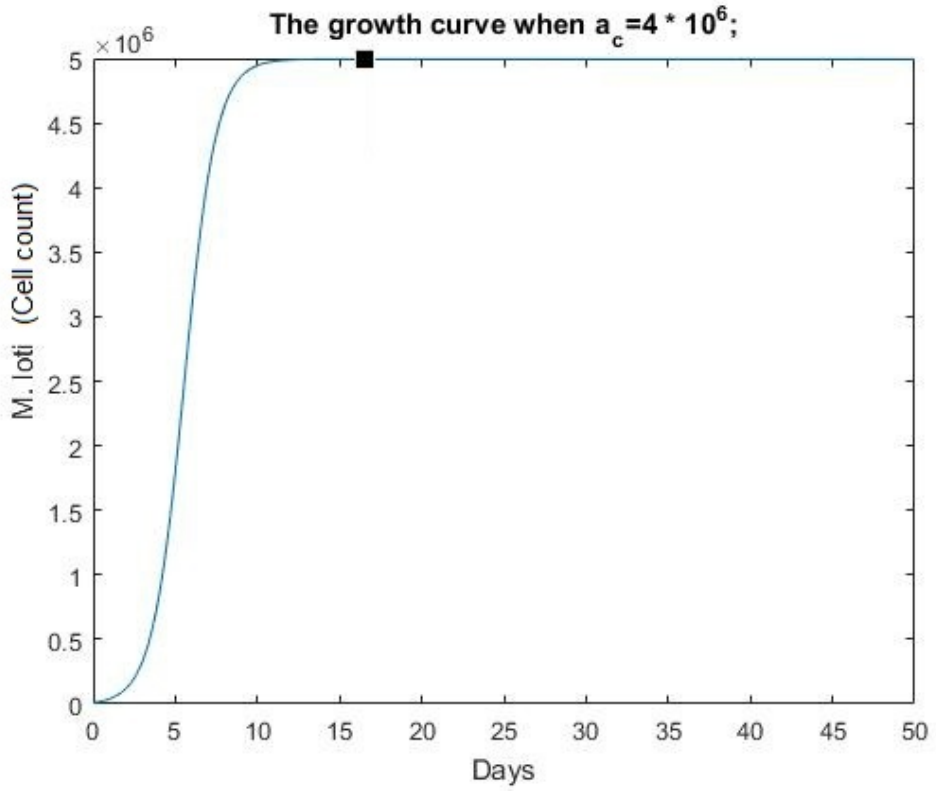

Figure 5.12: *M. loti* growth curve when the number of algae required to rach half of the number of bacteria that the algae can support $a_c = 4 \times 10^6$

- β : β is the growth rate of bacteria. It reduces the time required to reach the steady-state. It has no impact on algal growth.

- K_a: K_a will increase algal growth

- K_b: Algae will grow when $K_b > b_c$. It will continue growing until the value of the switch reaches one when it will saturate to the value of K_a.

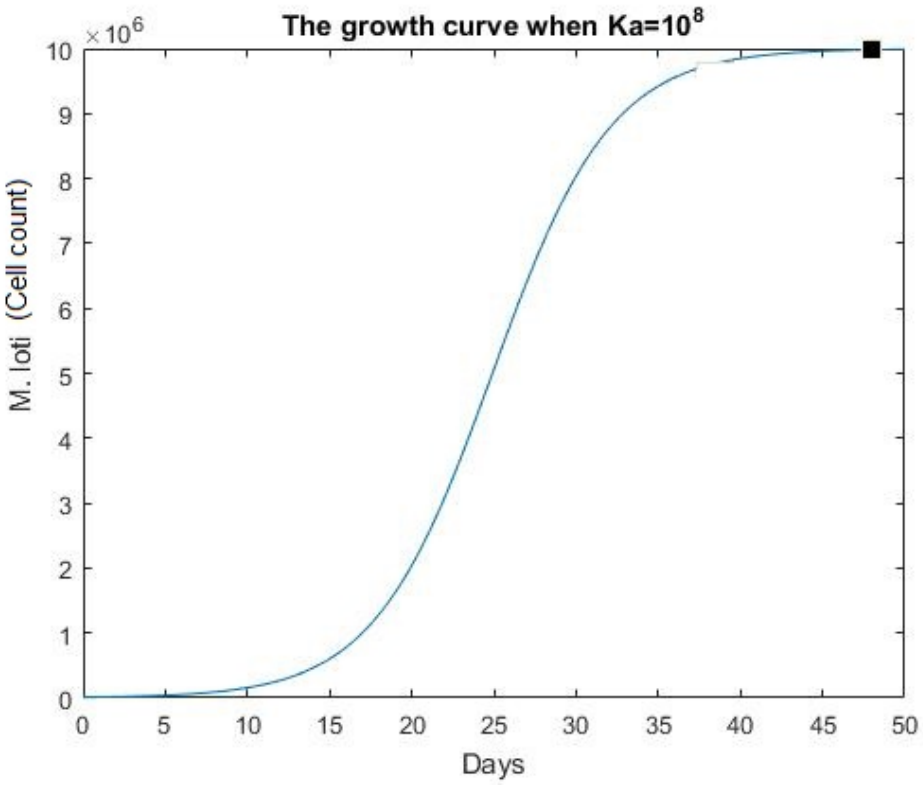

Figure 5.13: *M. loti* growth curve when the number of algae that the bacteria can support $K_a = 10^8$

- a_c : There is no direct relation between a_c and a. As long as $a >> a_c$, the growth will not be affected by increasing a_c and the steady-state output will be the same. To have a noticeable change in a while changing a_c , the value of a_c should be similar to a and the value of b_c should be similar to b.

- b_c : If the value of b_c is smaller than K_b, the growth of algae will decrease, and if the value of b_c is greater than K_b, the growth of algae will increase until

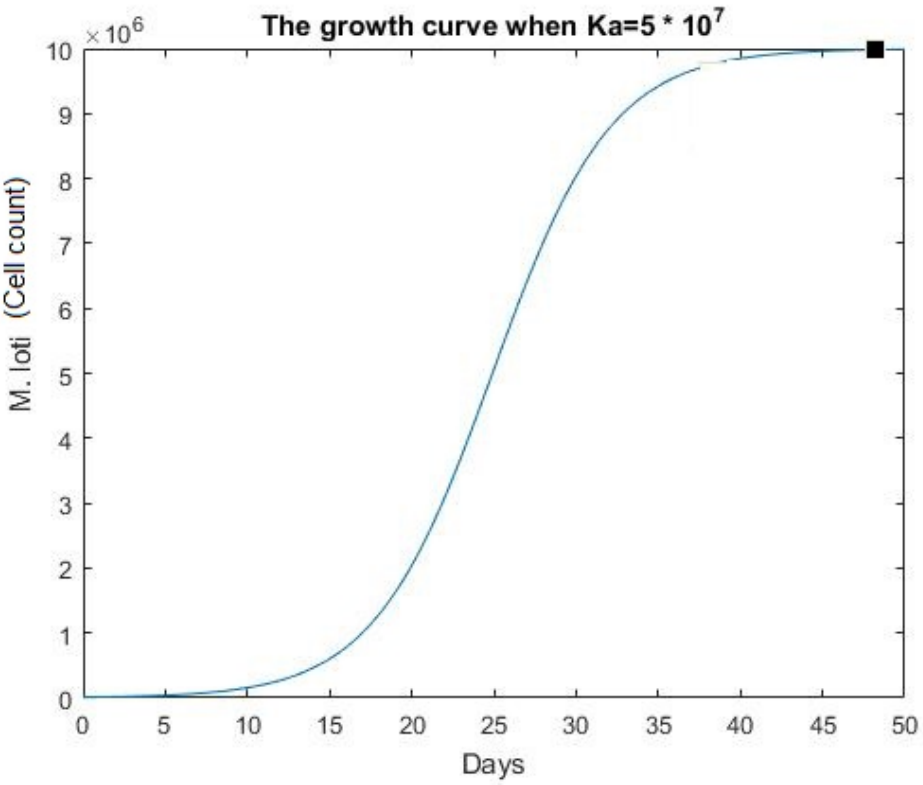

Figure 5.14: *M. loti* growth curve when the number of algae that the bacteria can support $K_a = 5 \times 10^7$

it reaches the value K_a.

Table 5.2 summarizes the effect of the parameter ranges on algal growth. The effect of the range of parameters on bacterial growth will now be summarised.

- α does not affect bacterial growth.
- β: β should be positive. It does not affect the steady-state value. It has a

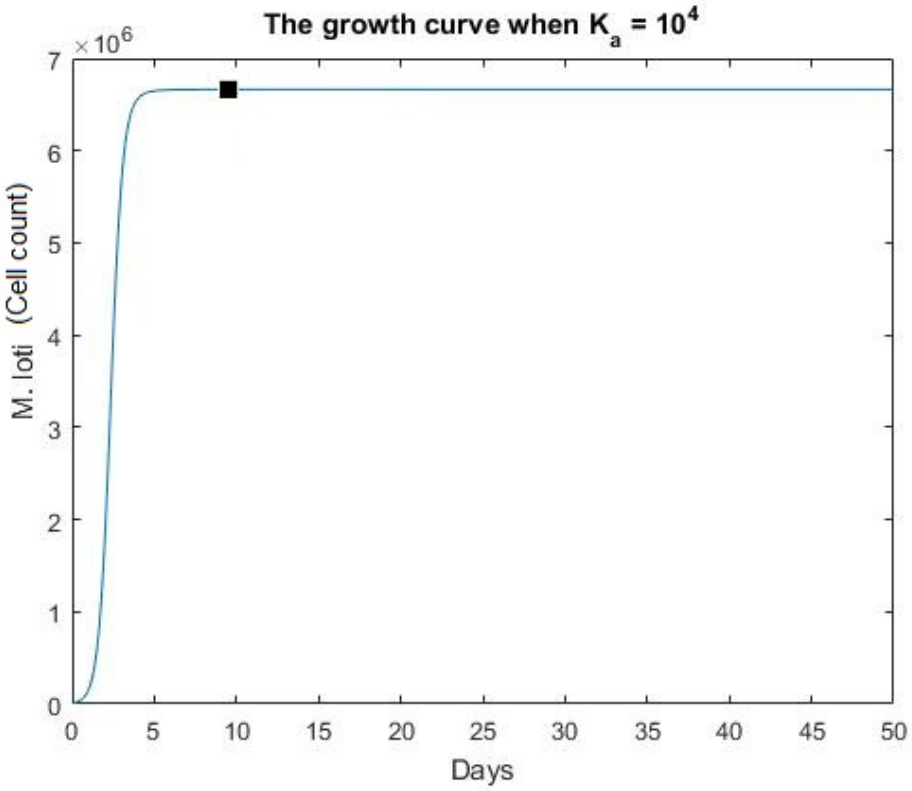

Figure 5.15: *M. loti* growth curve when the number of algae that the bacteria can support $K_a = 10^4$

transient effect.

- K_a: Bacteria will start to grow when $K_a > a_c$. Growth will continue until the value of the switch reaches one. The number of bacteria will then saturate to the value of K_b.

- K_b: K_b will increase bacterial growth.

Symbol	Range
1) α	Any positive value
2) β	Does not affect the growth
3) K_a	$K_a > 0$, $K_a \uparrow a \uparrow$
4) K_b	$b_c < K_b < K_{b_{max}}$ $a \uparrow$, $K_b < b_c$ $a \downarrow$
5) a_c	Does not affect the growth as long as $a_c > b$
6) b_c	$b_c > K_b$ $a \downarrow$, $b_c < K_b$ $a \uparrow$ until it reaches K_a

Table 5.2: Range for parameters when growing *L. rostrata*

- a_c : If the value of a_c is smaller than K_a, the bacterial growth will decrease, and if the value of a_c is greater than K_a, the bacterial growth will increase to the value of K_b.

- b_c : As there is no direct relation between b_c and b, as long as $b_c > b$, the growth will not be affected by increasing b_c and the steady-state output will be the same.

Table 5.3 summarizes the effect of the parameter ranges on bacterial growth. When

Symbol	Range
1) α	Does not affect the growth
2) β	Any positive value
3) K_a	$a_c < K_a < K_{a_{max}}$ $b \uparrow$, $K_a < a_c$ $b \downarrow$
4) K_b	$K_b > 0$, $K_b \uparrow b \uparrow$
5) a_c	$a_c > K_a$ $b \downarrow$, $a_c < K_a$ $b \uparrow$ until it reaches K_b
6) b_c	Does not affect the growth as long as $b_c > a$

Table 5.3: Range for parameters when growing *M. loti*

α and β are negative values, the population is in the death phase. For example, when

the bacterial growth rate is $-4 \times log(2)$, both the algal and bacterial populations will decrease to zero depending on the speed of the negative growth as shown in Figure 5.16, and that is when it will be in the death phase. So far, the steady state

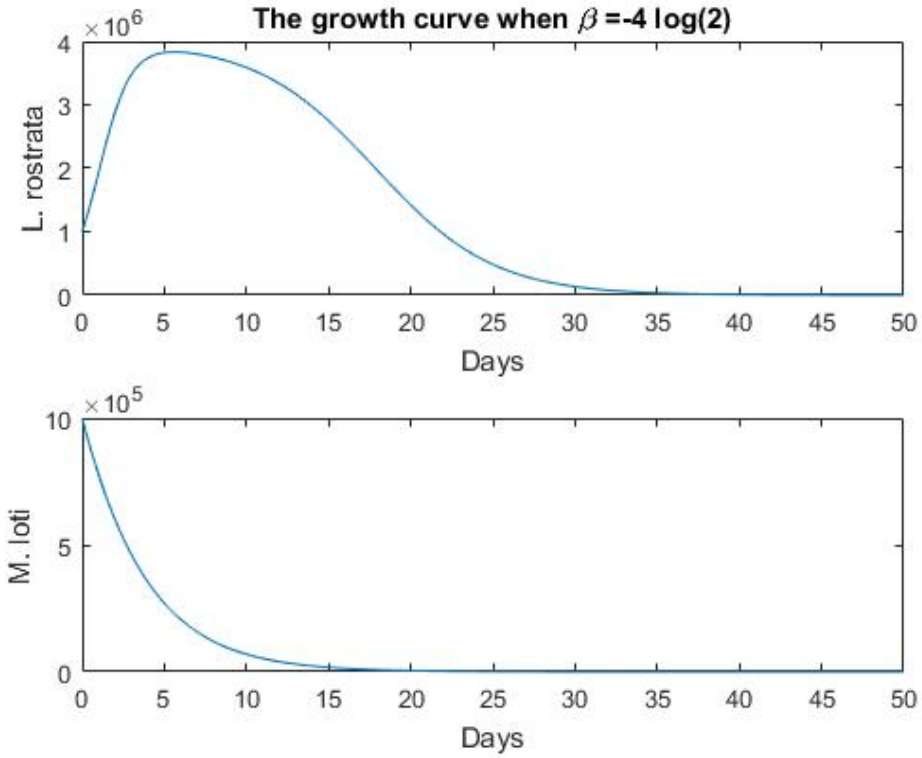

Figure 5.16: *L.rostrata* and *M.loti* growth curves when the growth rate is negative (death phase)

analysis of the system and robustness of varying the parameters when the model is behaving before the add-back of nutrients, those results are important to understand the system and apply a control system to it, which will be shown in the coming

section 5.2.3

5.2.3 A Sliding Mode Control Perspective

The simulation results in Fig. 5.6a-5.11 indicate that the system may exhibit a natural sliding mode. Consider the corresponding candidate switching functions for the algal and bacterial growth before the add-back of nutrients:

$$S_1 = a - K_a \tag{5.13}$$

$$S_2 = b - K_b \tag{5.14}$$

where S_1 is the sliding surface for the algal growth and S_2 is the sliding surface for the bacterial growth. Surfaces S_1 and S_2 will become zero when the values of a and b are equal to the values of K_a and K_b, respectively, and thus reach the carrying capacity.

When in the sliding mode, it follows that $S_1 = 0$ and $S_2 = 0$ and, if the sliding mode is to be maintained, the following must also hold: $\dot{S_1} = 0$ and $\dot{S_2} = 0$. The system dynamics in the sliding mode satisfy the following:

$$\dot{S_1} = \dot{a} = \alpha a\left[1 - \frac{a}{U_1^{eq}}\right] = 0, \tag{5.15}$$

$$\dot{S_2} = \dot{b} = \beta b\left[1 - \frac{b}{U_2^{eq}}\right] = 0. \tag{5.16}$$

where U_1^{eq} and U_2^{eq} represent the corresponding equivalent control signals required

to maintain sliding as mentioned earlier in Chapter 3. Solving for U_1^{eq} and U_2^{eq} from (5.15) and (5.16) yields:

$$\begin{aligned} U_1^{eq} &= a \\ U_2^{eq} &= b \end{aligned} \tag{5.17}$$

To ensure a sliding mode is attained, the so-called reaching condition (3.6) must be satisfied. Application of the reachability condition (3.6) shows that the sliding surfaces are reached if:

$$R_1 = S_1(\alpha a\Big[1-\frac{a}{U_1}\Big]) < 0 \tag{5.18}$$

$$R_2 = S_2(\beta b\Big[1-\frac{b}{U_2}\Big]) < 0. \tag{5.19}$$

where R_1 is the reachability condition corresponding to the algal sliding surface, R_2 is the reachability condition for the bacterial sliding surface, $U_1 = \left(\frac{K_a\, b}{b_c+b}\right)$ and $U_2 = \left(\frac{K_b\, a}{a_c+a}\right)$ are the applied control signals.

Consider first S_1 in (5.13). As a is a population, it will be positive and, given the set-point, is the carrying capacity of the population. It follows that $a \leq K_a$ and thus S_1 is negative. As α is a positive parameter, the reachability condition (5.18) is satisfied if the following holds:

$$1-\frac{a}{U_1} > 0 \tag{5.20}$$

So that $U_1 > a$ if the system is to satisfy the reachability condition and attain a sliding mode. As previously defined, the applied control signal is given by $U_1 = \left(\frac{K_a\, b}{b_c+b}\right)$ and for the sliding condition to be attained, it follows that:

$$\frac{K_a b}{b_c + b} > a \tag{5.21}$$

Performing the same computation for the reachability condition in (5.19) yields:

$$\frac{K_b a}{a_c + a} > b \tag{5.22}$$

If the reachability conditions (5.21) and (5.22) are satisfied, and a sliding mode is exhibited, then the system will be insensitive to parameter variations. In this case, knowing the parameters physical limitation, the amount of the carying capacity will be known, and this will save time instead of doing the experiment, the simulation results will give an approximation of the maximum growth that can be achieved. Simulations have been performed with different values of the algal and bacterial growth rate α, and β to test this hypothesis and the results are shown in Fig. 5.17. Fig. 5.17A shows the algal sliding surface S_1 from equation (5.13) when varying the algal growth rate α between $\log 2$ and $10 \log 2$. It is seen that a sliding mode is exhibited and as previously asserted the dynamics of the sliding mode is insensitive to variations in the the algal growth rate. The same test is carried out for the bacterial sliding surface S_2 in (5.14) and the results are shown in Fig. 5.17B. Here the bacterial growth rate β is varied between $\log 2$ and $15 \log 2$. Fig. 5.17C and Fig.

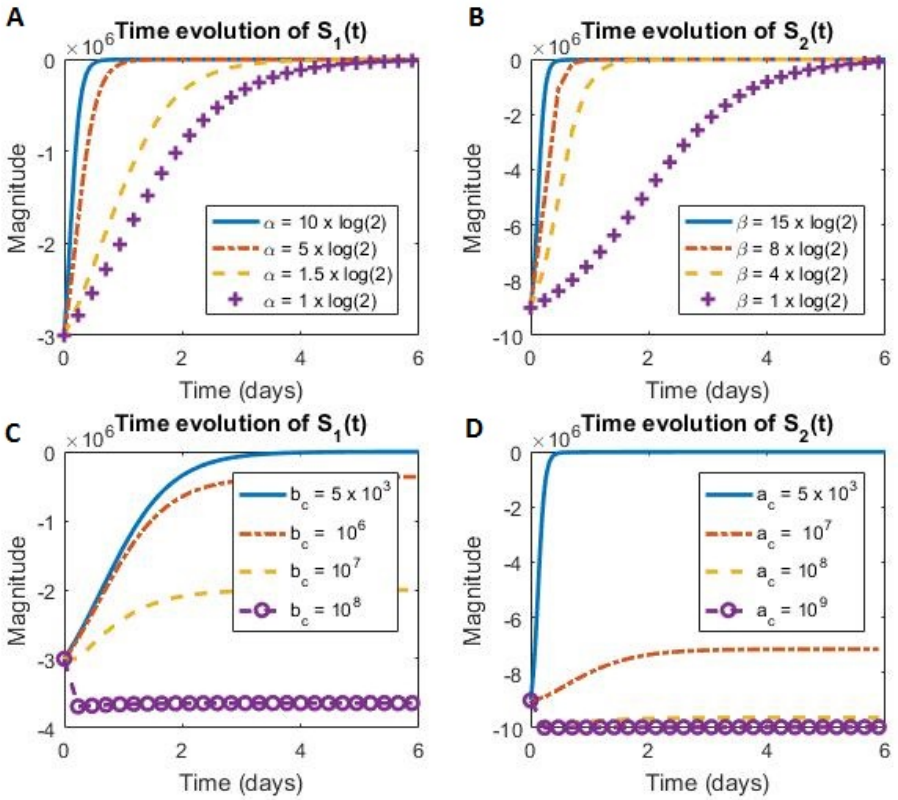

Figure 5.17: Time evolution of the sliding surface S_1 (5.13) and S_2 (5.14) when varying the the growth rates α, β, and the number of bacteria to reach half of algae b_c and number of algae required to reach half of bacteria a_c

5.17D show the sliding surfaces (5.13), (5.14) when varying b_c between 5×10^3 and 10^8 and a_c between 5×10^3 and 10^9 respectively. Both figures show that varying a_c and b_c affect the ability of the system to attain a sliding mode. Equation (5.21) shows that the reachability condition R_1 in (5.18) depends on the value of b_c and

the value of b_c that breaks the reachability condition is as follows:

$$b_c > b\left(\frac{K_a}{a} - 1\right) \tag{5.23}$$

Once the sliding condition ceases to hold, the system becomes sensitive to all parameter variations. Performing the same computation for the bacterial reachability condition R_2 in (5.19) shows that the reachability condition is broken when:

$$a_c > a\left(\frac{K_b}{b} - 1\right) \tag{5.24}$$

Simulations have been performed with different values of b_c to find the exact value of b_c that breaks the reachability condition (5.18). The results in Fig. 5.18 show that the value that breaks the reachability condition is $b_c = 3 \times 10^6$. Fig. 5.18 shows the time evolution of the reachability condition (5.21) when varying b_c between 10^5 and 10^8. It is clear from Fig. 5.18C that when $b_c = 3 \times 10^6$, the value of $a(t)$ will start to be bigger than $\frac{K_a b(t)}{b_c + b(t)}$ which breaks the reachability condition. Fig. 5.18D shows the simulation when $b_c = 10^8$ which demonstrates that the simulation for $\frac{K_a b(t)}{b_c + b(t)}$ is bigger than $a(t)$. The simulation results in Fig. 5.18 tie in with the analytical results presented in equation (5.23) using the parameters values provided in Table 5.1. Corresponding results for the reachability condition in (5.22) with the sliding surface (5.14) are obtained by varying a_c between 10^5 and 10^8. In Fig. 5.19 it is seen that $a_c = 9 \times 10^6$ will break the reachability condition (5.22). This is also supported by the analytical results presented in (5.24) using the parameter values

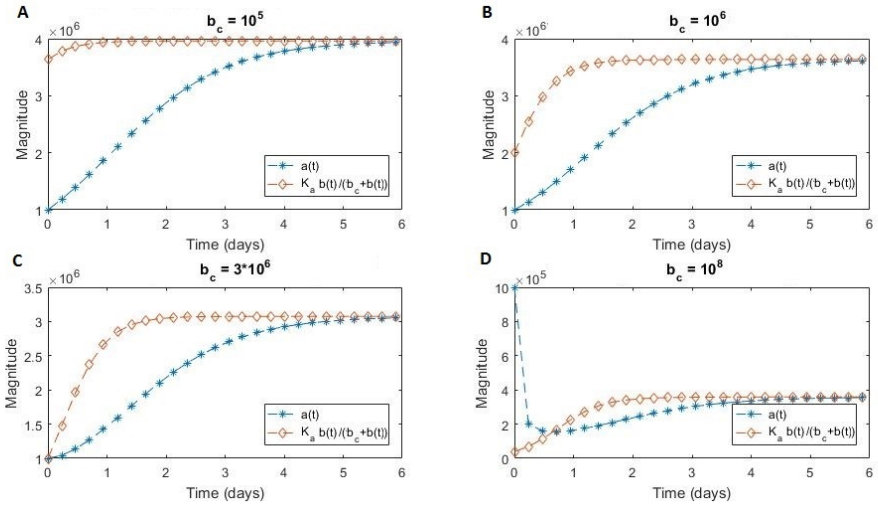

Figure 5.18: Time evolution of the reachability condition (5.21) when varying the number of bacteria required to reach half of algae b_c between 10^5 and 10^8.

provided in Table 5.1.

5.3 Model Behaviour After the Add-back of Nutrients

This section will consider the algal and bacterial growth equations when add-back of nutrients is considered. The nutrients that have been used in this system are vitamin B_{12} and carbon. The mathematical model that describes the algal and bacterial growth after the add-back of nutrients is assumed to have the following form [19]:

$$\dot{a} = \alpha a\left[1 - a\left(\frac{K_a b(1-\hat{H}(K_c)\delta_b)}{b_c + b} + K_v\right)^{-1}\right], \tag{5.25}$$

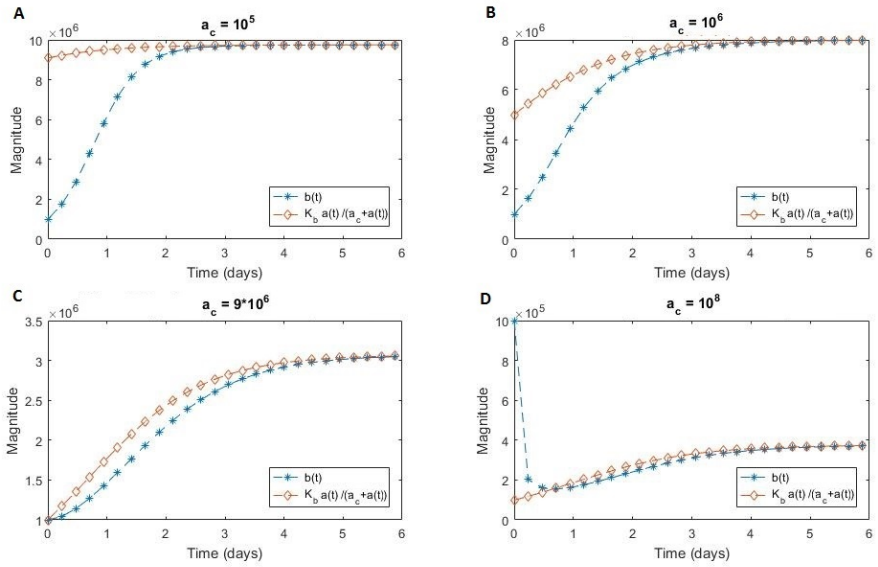

Figure 5.19: Time evolution of the reachability condition (5.22) when varying the number of algae required to reach half of bacteria a_c between 10^5 and 10^8.

$$\dot{b} = \beta\, b\Big[1 - b\Big(\frac{K_b\, a(1-\hat{H}(K_v)\delta_a)}{a_c + a} + K_c\Big)^{-1}\Big]. \tag{5.26}$$

where a and b are the *L. rostrata* algal population and *M. loti* bacterial population respectively, after the add back of nutrients.

The values and the biological meanings of K_v, K_c, δ_a and δ_b are shown in Table 5.1 and $\hat{H}$ is the Heaviside step function:

$$\hat{H}(x) = \begin{cases} 0 & x \leq 0 \qquad (5.27) \\ 1 & x > 0 \qquad (5.28) \end{cases}$$

Previous work in the literature [89] has considered these values to be constant. Mod-

els are available [19] relating the concentration of vitamin B_{12} with bacterial growth, so changing the concentration of vitamin B_{12} will change the value of K_v. Fig. 5.20

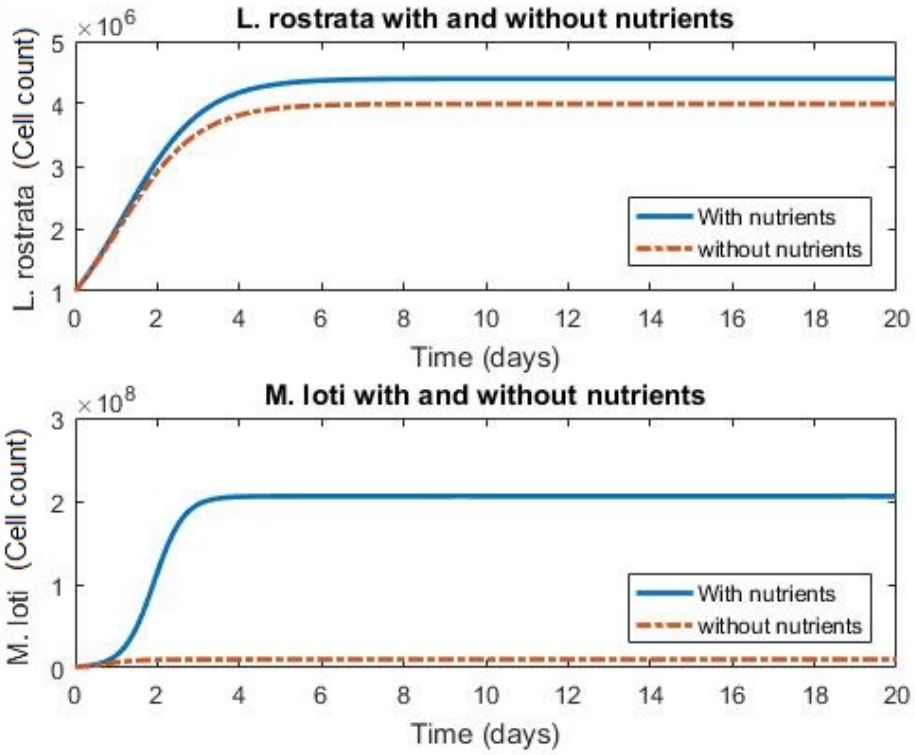

Figure 5.20: Algal and bacterial growth before and after the add-back of nutrinets

shows a comparison of both algal and bacterial growth before and after the add-back of nutrients, using the parameter values in Table 5.1 and the system model (5.25) and (5.26), and it shows that the amount of $M.loti$ increased massively after adding the nutrients.

5.3.1 Steady-state analysis

Consider the algal and bacterial growth equations after the add-back of nutrients. Let the inputs be the two flow rates $K_v(t)$ and $K_c(t)$. The equations for growth are shown in equations (5.25), (5.26). Let the state vector x and input vector u be defined as:

$$x(t) = \begin{bmatrix} a(t) \\ \\ b(t) \end{bmatrix}, \; u(t) = \begin{bmatrix} K_v(t) \\ \\ K_c(t) \end{bmatrix} \tag{5.29}$$

$$f_1(x,u) = \alpha x_1 \Big[1 - x_1 \Big(\frac{K_a x_2 (1 - \hat{H}(K_c)\delta_b)}{b_c + x_2} + u_1 \Big)^{-1} \Big], \tag{5.30}$$

$$f_2(x,u) = \beta x_2 \Big[1 - x_2 \Big(\frac{K_b x_1 (1 - \hat{H}(K_v)\delta_a)}{a_c + x_1} + u_2 \Big)^{-1} \Big]. \tag{5.31}$$

Intuitively, any algal population $\bar{a} > 0$ and any bacterial population $\bar{b} > 0$ should be a possible equilibrium point (after specifying the correct values of the equilibrium inputs). In fact, with $\bar{a}$ and $\bar{b}$ chosen, the equation $f(\bar{x}, \bar{u}) = 0$ can be written as:

$$\bar{u_1} = \bar{x_1} - K_a \Big(\frac{\bar{x_2}(1 - \hat{H}(\bar{u_2})\delta_b)}{b_c + \bar{x_2}} \Big), \; \bar{u_2} = \bar{x_2} - K_b \Big(\frac{\bar{x_1}(1 - \hat{H}(\bar{u_1})\delta_a)}{a_c + \bar{x_1}} \Big). \tag{5.32}$$

Since u_i represent flow rates of nutrients, physical considerations restrict them to be non-negative real numbers. This implies that when $\delta_b, \delta_a < 1$ $\bar{x_1} > K_a \Big(\frac{\bar{x_2}(1-\hat{H}(\bar{u_2})\delta_b)}{b_c+\bar{x_2}} \Big), \; \bar{x_2} > K_b \Big(\frac{\bar{x_1}(1-\hat{H}(\bar{u_1})\delta_a)}{a_c+\bar{x_1}} \Big)$.

Looking at the differential equations for a and b , it is seen that their rates of change are coupled. Hence, the model is valid when:

$u_1(t) < \bar{x_1} - K_a\left(\frac{\bar{x_2}(1-\hat{H}(\bar{u_2})\delta_b)}{b_c+\bar{x_2}}\right)$, $u_2(t) < \bar{x_2} - K_b\left(\frac{\bar{x_1}(1-\hat{H}(\bar{u_1})\delta_a)}{a_c+\bar{x_1}}\right)$. Under these restrictions, the state $\bar{x}$ is indeed an equilibrium point, and there is a unique equilibrium input given by the equations above. To linearise the system, it is necessary to consider:

$$A = \begin{bmatrix} \frac{\partial f_1}{\partial x_1} & \frac{\partial f_1}{\partial x_2} \\ \\ \frac{\partial f_2}{\partial x_1} & \frac{\partial f_2}{\partial x_2} \end{bmatrix}, B = \begin{bmatrix} \frac{\partial f_1}{\partial u_1} & \frac{\partial f_1}{\partial u_2} \\ \\ \frac{\partial f_2}{\partial u_1} & \frac{\partial f_2}{\partial u_2} \end{bmatrix} \tag{5.33}$$

where:

$$\frac{\partial f_1}{\partial x_1} = \alpha - 2\,\alpha\, x_1\left(\frac{K_a x_2(1-\hat{H}(u_2)\delta_b)}{b_c+x_2} + u_1\right)^{-1}.$$
$$\frac{\partial f_1}{\partial x_2} = \alpha\, x_1^2\left(\frac{K_a x_2(1-\hat{H}(u_2)\delta_b)}{b_c+x_2} + u_1\right)^{-2}\left(\frac{K_a(1-\hat{H}(u_2)\delta_b)(b_c+x_2) - K_a x_2(1-\hat{H}(u_2)\delta_b)}{(b_c+x_2)^2}\right).$$
$$\frac{\partial f_2}{\partial x_1} = \beta\, x_2^2\left(\frac{K_b x_1(1-\hat{H}(u_1)\delta_a)}{a_c+x_1} + u_2\right)^{-2}\left(\frac{K_b(1-\hat{H}(u_1)\delta_a)(a_c+x_1) - K_b x_1(1-\hat{H}(u_1)\delta_a)}{(a_c+x_1)^2}\right).$$
$$\frac{\partial f_2}{\partial x_2} = \beta - 2\,\beta\, x_2\left(\frac{K_b x_1(1-\hat{H}(u_1)\delta_a)}{a_c+x_1} + u_2\right)^{-1}.$$
$$\frac{\partial f_1}{\partial u_1} = \alpha\, x_1^2\left(\frac{K_a x_2(1-\hat{H}(u_2)\delta_b)}{b_c+x_2} + u_1\right)^{-2}$$
$$\frac{\partial f_1}{\partial u_2} = 0$$
$$\frac{\partial f_2}{\partial u_1} = 0$$
$$\frac{\partial f_2}{\partial u_2} = \beta\, x_2^2\left(\frac{K_b x_1(1-\hat{H}(u_1)\delta_a)}{a_c+x_1} + u_2\right)^{-2}$$

The linearisation requires that the matrices of partial derivatives are evaluated at the equilibrium points. After selecting realistic parameters and using the values in Table 5.1 , $\bar{x_1} = \bar{a} = K_a$ or $K_a + K_v$ and $\bar{x_2} = \bar{b} = K_b$ or $= K_b + K_c$, four combinations are obtained:

- $(\bar{x_1}, \bar{x_2}) = (K_a, K_b)$. The equilibrium inputs are:
  $\bar{u_1} = \bar{k_v} = 3.6 \times 10^6$ and $\bar{u_2} = \bar{k_c} = 9 \times 10^6$.
  The linearised matrices are:

$$A = \begin{bmatrix} -1.0397 & 0 \\ 0 & -0.9257 \end{bmatrix}, B = \begin{bmatrix} 1.0397 & 0 \\ 0 & 1.2333 \end{bmatrix} \tag{5.34}$$

- $(\bar{x_1}, \bar{x_2}) = (K_a + K_v, K_b + K_c)$. The equilibrium inputs are:
  $\bar{u_1} = \bar{k_v} = 7.6 \times 10^6$ and $\bar{u_2} = \bar{k_c} = 2.04 \times 10^8$.
  The linearised matrices are:

$$A = \begin{bmatrix} -1.0397 & 0 \\ 0 & -2.7726 \end{bmatrix}, B = \begin{bmatrix} 1.0397 & 0 \\ 0 & 2.7726 \end{bmatrix} \tag{5.35}$$

- $(\bar{x_1}, \bar{x_2}) = (K_a + K_v, K_b)$. The equilibrium inputs are:
  $\bar{u_1} = \bar{k_v} = 7.6 \times 10^6$ and $\bar{u_2} = \bar{k_c} = 1.94 \times 10^8$.
  The linearised matrices are:

$$A = \begin{bmatrix} -1.0397 & 0 \\ 0 & -2.7726 \end{bmatrix}, B = \begin{bmatrix} 1.0397 & 0 \\ 0 & 2.7726 \end{bmatrix} \tag{5.36}$$

- $(\bar{x_1}, \bar{x_2}) = (K_a, K_b + K_c)$. The equilibrium inputs are:
  $\bar{u_1} = \bar{k_v} = 3.6 \times 10^6$ and $\bar{u_2} = \bar{k_c} = 2.0401 \times 10^8$.
  The linearised matrices are:

$$A = \begin{bmatrix} -1.0397 & 0 \\ 0 & -2.7726 \end{bmatrix}, B = \begin{bmatrix} 1.0397 & 0 \\ 0 & 2.7726 \end{bmatrix} \tag{5.37}$$

Because of the large difference between the values of k_a, k_b and the values of k_v, k_c, matrices A and B in equations (5.35), (5.36) and (5.37) have similar values and only the matrices A and B in equation (5.34) differ. The non-linear differential equations (5.25), (5.26) will be simulated subject to the following conditions:

$$x(0) = \begin{bmatrix} 4 \times 10^6 \\ \\ 2 \times 10^8 \end{bmatrix} \text{ and } u(t) = \begin{bmatrix} 4 \times 10^6 \\ \\ 2 \times 10^8 \end{bmatrix}$$

This is close to the fourth equilibrium condition shown in equation (5.37) and the following conditions will be used:

$$\delta_x(0) = \begin{bmatrix} 0 \\ \\ 0.1 \times 10^8 \end{bmatrix}.$$

$$\delta_u(t) == \begin{bmatrix} 0.4 \times 10^6 \\ \\ -4.01 \times 10^6 \end{bmatrix}$$

The corresponding simulation results of the linear and non-linear models are shown

in figure 5.21. To check the range of validity of the linear model, the initial condi-

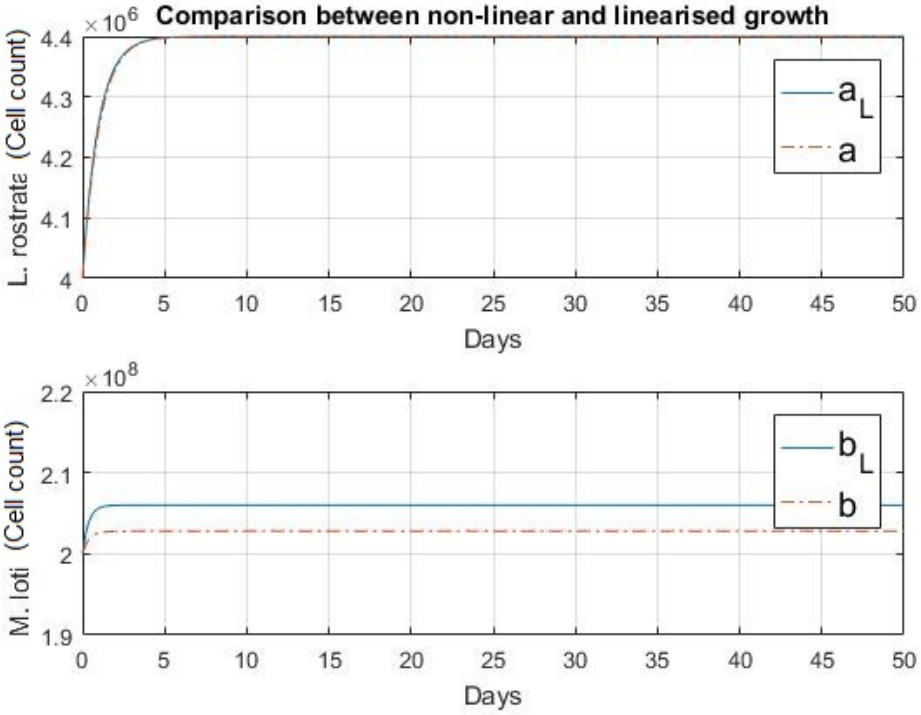

Figure 5.21: Comparison between non-linear and linearised of *L.rostrata* and *M.loti* growths after the add-back of nutrients

tions are moved further away from the equilibrium point used to define the linearisation. Select $x(0) = \begin{bmatrix} 3 \times 10^6 \\ \\ 1.5 \times 10^8 \end{bmatrix}$, Figure 5.22 shows the corresponding response of the linear and non-linear models. The corresponding error between the linear and the non-linear model is shown in Figure 5.23.

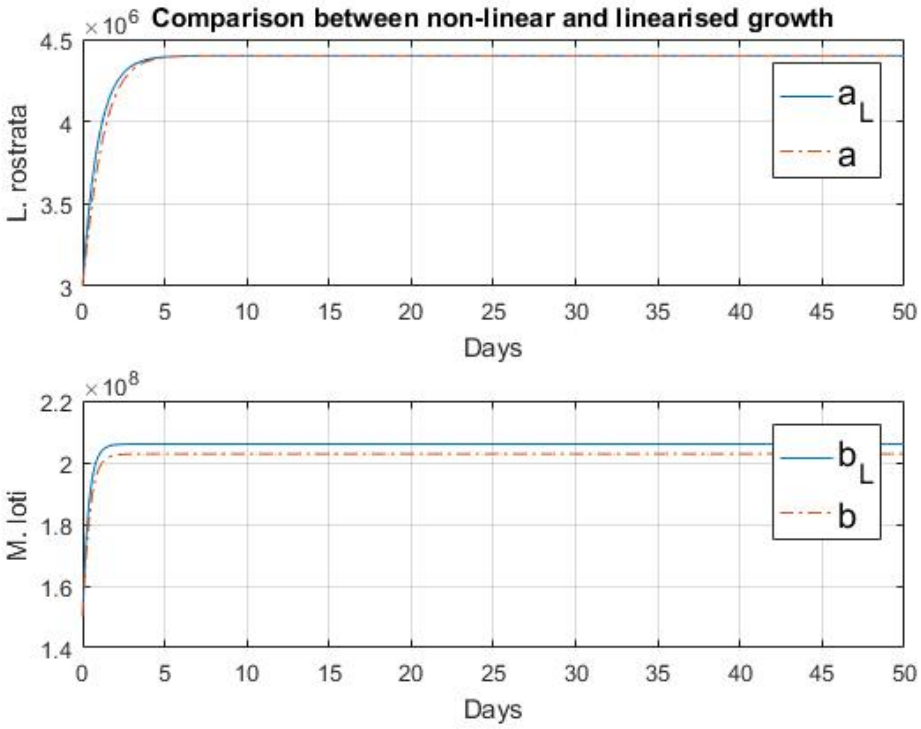

Figure 5.22: Comparison between non-linear and linearised of *L.rostrata* and *M.loti* growths after the add-back of nutrients when $x(0) = 3 \times 10^6, 1.5 \times 10^8$ where a_L and b_L represent the linarised model

Moving the initial conditions away from the equilibrium point will cause the response of the linear model to degrade still further. For example, if $x(0) = \begin{bmatrix} 1 \times 10^6 \\ \\ 1 \times 10^8 \end{bmatrix}$ the corresponding error is shown in Figure 5.24.

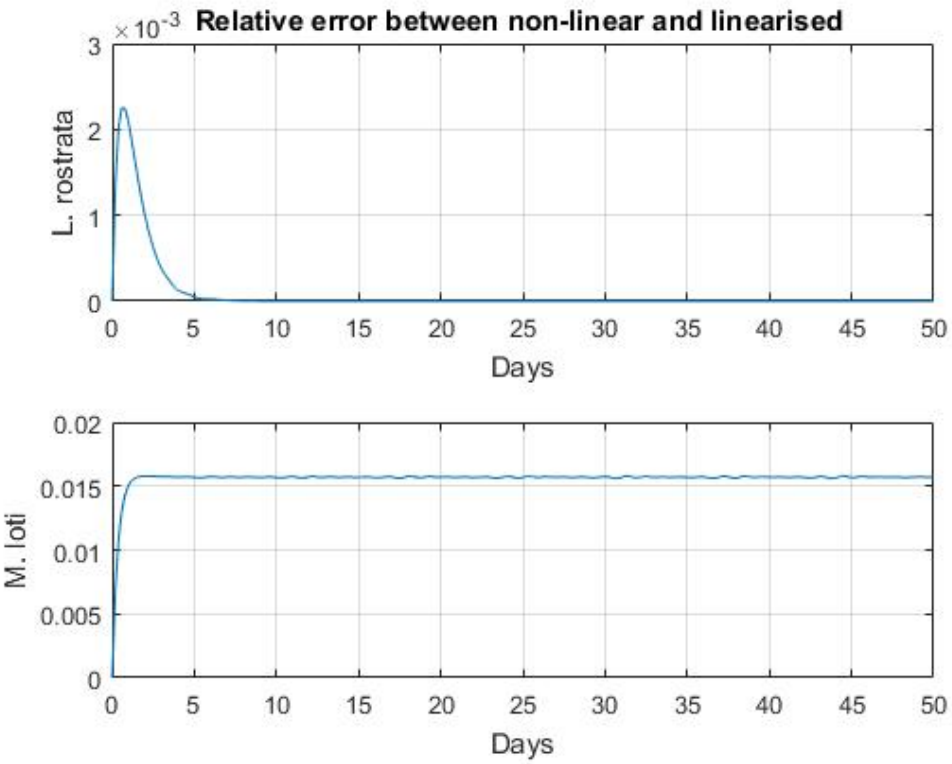

Figure 5.23: The relative error between non-linear and linearised of *L.rostrata* and *M.loti* growths

5.3.2 Robustness analysis and the effect of varying the parameters

Kazamia et al. [89] experimentally showed that the interactions between vitamin B_{12}-dependent algae and heterotrophic bacteria exhibit regulation. The experiments prove that by increasing the amount of vitamin B_{12}, the overall growth will increase. Moreover, Cole [94] experimentally validated the impact of adding vitamin B_{12}

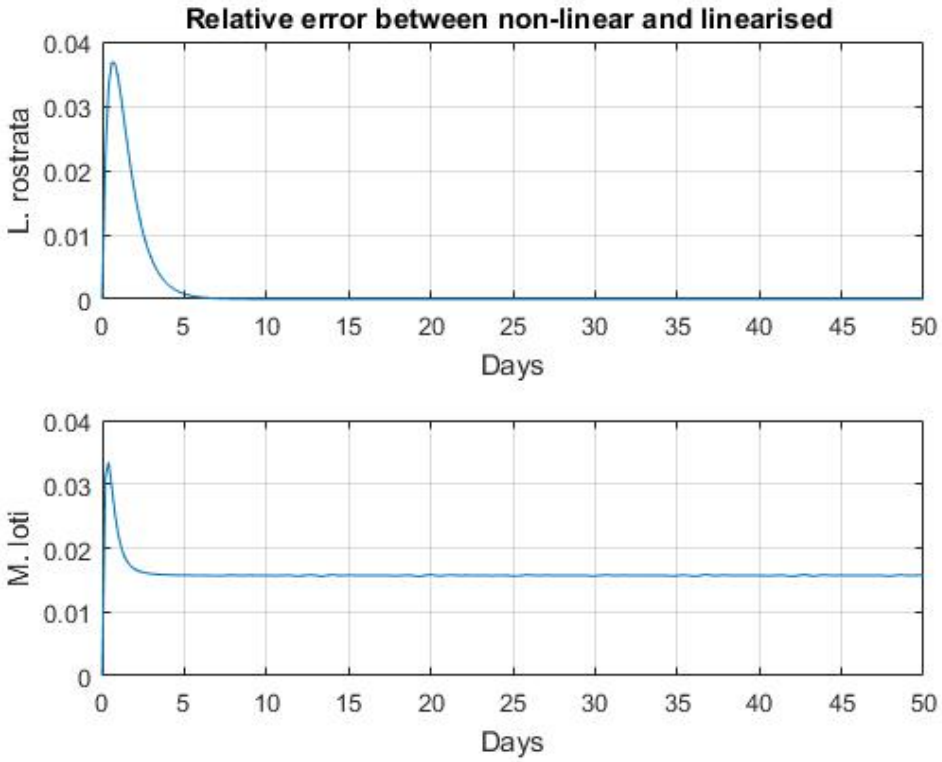

Figure 5.24: The relative error between non-linear and linearised of *L.rostrata* and *M.loti* growths when $x_1(0) = 1 \times 10^6, 1 \times 10^8$

to Thallasiosira pseudonanna algal growth. The Thallasiosira pseudonanna algal growth before adding vitamin B_{12} was 9×10^3, and after adding vitamin B_{12} became 2×10^6. In the previous section, the system was studied before the add-back of nutrients. Considering equations (5.25) and (5.26), there are more parameters that affect the switching dynamics. As an example, the first switch depends now on the value of b, b_c and δ_b and the second switch depends on the value of a, a_c and

δ_a. Before adding nutrients, there was not algal growth unless there was bacterial growth, but now if vitamin B_{12} or carbon is added externally, equations (5.25) and (5.26) show that growth is possible. Matthew et al. [89], measured the value of K_v to be 4×10^6 and the value of K_c to be 2×10^8. The simulation result for algal growth shows that the algal growth will be the summation of [($K_a \times$ (1-δ_b)) and K_v] as shown in Figure 5.25. For bacterial growth, the amount of the bacteria will be the summation of [($K_b \times$ (1-δ_a)) and K_c] as shown in Figure 5.26. If the value of K_a decreases, the number of algae will decrease, and the value of the switch ($\frac{a}{a_c+a}$) will decrease. In this case, the algal growth will reduce below the saturation level. From the constants in [19], the values of K_v and K_c are much bigger than K_a and K_b, so the overall growth will not be significantly affected by the switch, in this case, if the switch increased the value of the growth by 10%, this increment will not increase the overall growth by much. The effect of the additional parameters on algal growth is first described.

- δ_a: To determine the effect of δ_a on a, select K_c close to K_b and K_v close to K_a. Let the number of bacteria be close to b_c. In this case, changing δ_a will affect a

- δ_b: As δ_b has a value between 0 and 1, the algal growth will not be affected unless the values of K_v and K_a are close to each other. For example, if $K_v = 10^8$ and $K_a = 10^7$, then the value of δ_b will not affect the output as the value of a will be $K_a(1-\delta_b)+K_v$, but if the value of K_v is close to K_a, then increasing δ_b will decrease the value of a.

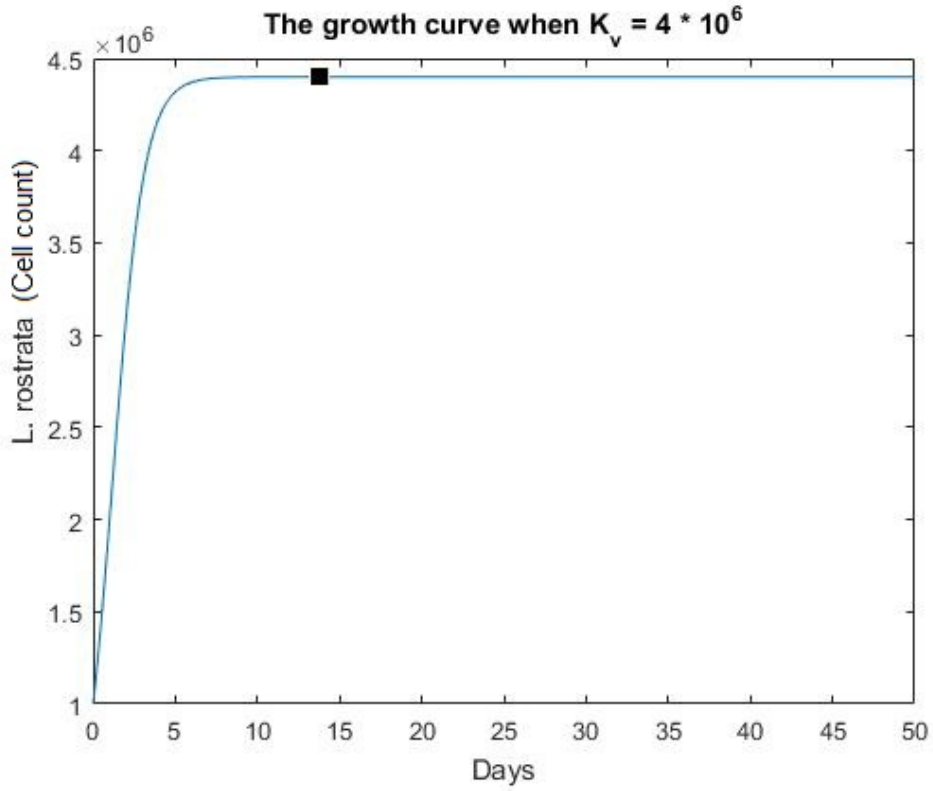

Figure 5.25: *L.rostrata* growth curve when the number of algae when vitamin B_{12} is provided externally $K_v = 4 \times 10^6$

- K_v: Changing K_v will affect the algal growth as by increasing K_v, the total number of algae increases.
- K_c: Changing K_c will not affect the algal growth unless the value of K_c is close to the value of b_c. If the value of K_c is equal to b_c, the total amount of algae will reduce to half of its original population.

The effect of the parameters corresponding to the add-back of nutrients on bacterial

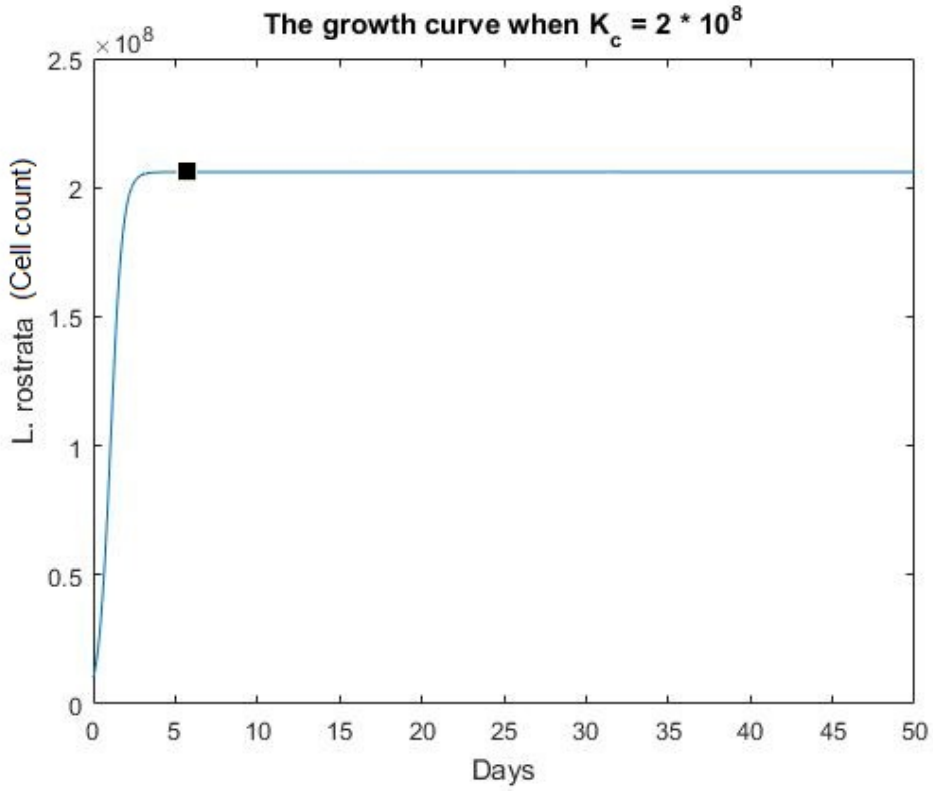

Figure 5.26: *L.rostrata* growth curve when the number of algae when carbon is provided externally $K_c = 2 \times 10^8$

growth is now outlined.

- δ_a: As δ_a is a fraction and its value between 0 and 1, the system will be stable whatever was the value of it. The bacterial growth will not be affected unless the value of K_c and K_b are close to each other. For example, if $K_c = 10^8$ and $K_b = 10^7$, then the value of δ_a will not affect the output as the value of b will be $K_b(1-\delta_a)+K_c$, but if the value of K_c is close to K_b, then increasing δ_b

will decrease the value of b.

- δ_b: To determine the effect of δ_b on b, the value of K_v is selected close to K_a and K_c should be close to K_b. The number of algae should be close to a_c. In this case changing δ_b will affect b.

- K_v: Changing K_v will not affect the growth of bacteria unless the value of K_v is close to the value of a_c. If the value of K_v is equal to a_c, the total amount of bacteria will reduce to half of its original population.

- K_c: Changing K_c will affect the growth of bacteria as by increasing K_c, the total number of algae will increase.

Table 6.1, 5.5 summarize the effects of the additional parameters corresponding to the add-back of nutrients; δ_a, δ_b, K_v and K_c.

Symbol	Range
1) δ_a	When K_b is close to K_c and b is close to b_c, $\delta_a \uparrow a \downarrow$
2) δ_b	When K_a is close to K_v , $\delta_b \uparrow a \downarrow$
3) K_v	When $K_v > 0$, $K_v \uparrow a \uparrow$
4) K_c	When K_a is close to K_v and b is close to b_c, $K_c \uparrow a \uparrow$

Table 5.4: Range for parameters when growing *L. rostrata* after the add-back of nutrients

Symbol	Range
1) δ_a	When K_b is close to K_c , $\delta_a \uparrow b \downarrow$
2) δ_b	When K_a is close to K_v and a is close to a_c, $\delta_b \uparrow b \downarrow$
3) K_v	When K_b is close to K_c and a is close to a_c, $K_v \uparrow b \uparrow$
4) K_c	$K_c > 0$, $K_c \uparrow b \uparrow$

Table 5.5: Range for parameters when growing $M.\ loti$ after the add-back of nutrients

5.3.3 A Sliding Mode Control Perspective

Consider the following switching functions for the algal and bacterial growth after the add-back of nutrients:

$$S_3 = a - (K_a(1 - \hat{H}(K_c)\delta_b) + K_v) \tag{5.38}$$

$$S_4 = b - (K_b(1 - \hat{H}(K_c)\delta_a) + K_c) \tag{5.39}$$

where S_3 and S_4 are the sliding surface for the algal and bacterial growth after the add-back of nutrients respectively. Note that add-back of nutrients effectively modifies the carrying capacity. The surfaces S_3 (5.38) and S_4 (5.39) will become zero when the values of a and b are equal to the new carrying capacities. When in the sliding mode, it follows that $S_3 = 0$ and $S_4 = 0$ and, if the sliding mode is to be maintained, $\dot{S}_3 = 0$ and $\dot{S}_4 = 0$. From (5.38) and (5.39), a and b are the only variables that vary with time if K_v and K_c are assumed constant. This yields $\dot{S}_3 = \dot{a}$ and $\dot{S}_4 = \dot{b}$. Going back to (5.25) and (5.26), and denoting $U_3 = \frac{K_a b(1-\hat{H}(K_c)\delta_b)}{b_c+b}$, $U_4 = \frac{K_b a(1-\hat{H}(K_v)\delta_a)}{a_c+a}$ so that they are considered to be control signals within the

closed-loop system (5.25) - (5.26), the system dynamics in the sliding mode satisfies the following:

$$\dot{S_3} = \dot{a} = \alpha a\Big[1 - \frac{a}{U_3^{eq}}\Big] \tag{5.40}$$

$$\dot{S_4} = \dot{b} = \beta b\Big[1 - \frac{b}{U_4^{eq}}\Big]. \tag{5.41}$$

Where U_3^{eq} and U_4^{eq} represents the corresponding equivalent control signals required to maintain sliding. Solving for U_3^{eq} and U_4^{eq} from equations (5.40) and (5.41) yields

$$\begin{aligned} U_3^{eq} &= a \\ U_4^{eq} &= b \end{aligned} \tag{5.42}$$

Note that the value of $\dot{S_3}$ and $\dot{S_4}$ will be different if the amount of vitamin B_{12} and carbon varies with time as the derivative of S_3 and S_4 will involve the derivative of K_v and K_c. Application of the reachability condition (3.6) shows that the sliding surfaces after the add-back of nutrients are reached if:

$$R_3 = S_3(\alpha a\Big[1 - \frac{a}{U_3}\Big]) < 0 \tag{5.43}$$

$$R_4 = S_4(\beta b\Big[1 - \frac{b}{U_4}\Big]) < 0. \tag{5.44}$$

where R_3 and R_4 are the reachability conditions for the algal and bacterial growth after the add back of nutrients, respectively.

Consider first (5.43). As a is a population, it will be positive and, given the set-point

is the maximum value of cells following the add back of nutrients, it follows that $a < (K_a(1-\hat{H}(K_c)\delta_b)+K_v)$ and thus S_3 in (5.43) is negative. As α is a positive parameter, the reachability condition (5.43) is satisfied if the following holds:

$$1-\frac{a}{U_3}>0 \tag{5.45}$$

so that $U_3 > a$ if the system is to satisfy the reachability condition and attain a sliding mode. As previously defined, the applied control signal is given by $U_3 = \left(\frac{K_a b(1-\hat{H}(K_c)\delta_b)}{b_c+b}+K_v\right)$ and it follows that

$$\frac{K_a b(1-\hat{H}(K_c)\delta_b)}{b_c+b}+K_v > a \tag{5.46}$$

for the sliding condition to be attained. Performing the same computation for the reachability condition in (5.44) yields:

$$\frac{K_b a(1-\hat{H}(K_v)\delta_a)}{a_c+a}+K_c > b \tag{5.47}$$

If a sliding mode is reached, the dynamic behaviour will be independent of variations in the algal and bacterial growth rate α and β. Equations (5.46) and (5.47) show that the reachability conditions after the add back of nutrients are affected by more parameters than in the case before the add back (5.21),(5.22). Note that when $K_v = K_c = \delta_a = \delta_b = 0$, the reachability conditions before and after the add back of nutrients will be the same, as expected.

First consider (5.46). The parameters that affect the reachability conditions are δ_b and K_v. Note that the value of δ_b is between 0 and 1 [19]. The values of b_c that breaks the reachability condition R_3 satisfy:

$$b_c > b\,(\frac{K_a\,(1-\delta_b)}{a-k_v}-1) \tag{5.48}$$

The system then becomes sensitive to all parameters variations. Performing the same computation for the bacterial reachability condition R_4 (5.44) yields that the values of a_c that breaks the reachability condition satisfy:

$$a_c > a\,(\frac{K_b\,(1-\delta_a)}{b-k_c}-1) \tag{5.49}$$

The value of K_v that breaks R_3 is as follows

$$k_v < a-\,(\frac{K_a\,b\,(1-\delta_b)}{b_c+b}) \tag{5.50}$$

Performing the same computation for the bacterial reachability condition (5.47) yields that the values of a_c that break the reachability condition satisfy:

$$k_c < b-\,(\frac{K_b\,a\,(1-\delta_a)}{a_c+a}) \tag{5.51}$$

Performing the same analysis on the reachability condition corresponding to the algal sliding surface after the add-back of nutrients (5.46) yields that $K_v = 0.604\times 10^6$ is the value that breaks the reachability condition and the results of the simulations

are shown in Fig. 5.27. These results match with the analytical results presented in (5.50) using the same parameters values provided in Table 5.1.

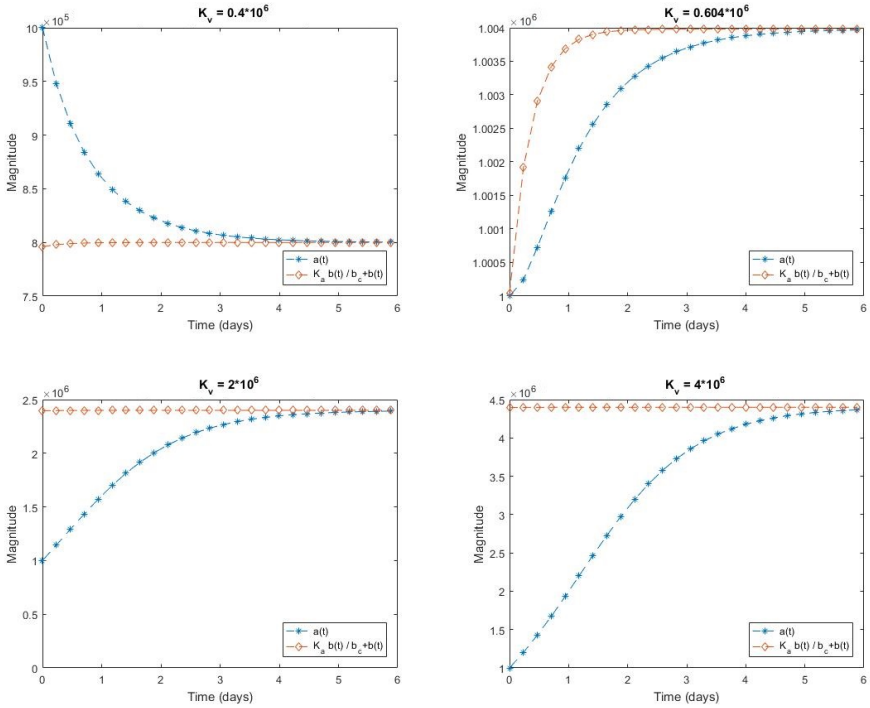

Figure 5.27: Time evolution of the reachability condition (5.46) when varying the number of algae when vitamin B_{12} is provided externally K_v between 0.4×10^6 and 4×10^6

5.4 Conclusions

In this chapter, mathematical models for the growth of *L. rostrata* algae and *M. loti* bacteria have been studied both before and after the add-back of nutrients. The spe-

cific nutrients studied are vitamin B_{12} and carbon. The physical limitations on the parameters have been identified, and simulations show how the growth saturates. Linearised models have been identified and the degree to which they are useful to represent the dynamics explored. Sliding mode analysis has been carried out to quantify the action of the control mechanisms and the system robustness explicitly. Robustness is the distinctive feature of the sliding mode control as the control can merely be switching between the two states. In this model, switches of the algal and bacterial growth between exponential or saturation phases demonstrated a natural sliding mode. This case was studied in the chapter by checking the reachability condition and finding the physical limitations on growth both before and after the add-back of nutrients. The next chapter will study the mathematical model of vitamin B_{12} presented in chapter 4 and will use a sliding mode observer to estimate the concentration of $BtuB$. The results of this chapter demonstrate the use control engineering methods in the analysis of biological systems. The reachability condition and be used to determine the carrying capacity without the need to perform experiments. This chapter demonstrates how sliding mode control paradigms can be applied to systems that exhibit inherent switching mechanisms. The analysis directly determines the physical limitations of the systems.

Chapter 6

Using sliding mode observers to estimate *BtuB* concentration from measured vitamin B_{12} concentration

6.1 Introduction

Successful metabolism in gram-negative bacteria requires many cofactors that cannot be synthesised within the cell. These bacteria must obtain these metabolites and nutrients from their surrounding environment to survive. *BtuB* exist as part of the phospholipid bilayer that composes the outer shell of bacteria. The primary function of *BtuB* is that of a transporter; it binds with several molecules to carry them into the cell. This is an essential part of the bacterial cell, and experimentally, scientist found it hard to measure the dynamics of it. Hence, techniques from the control

engineering field will be used to find a way of measuring the dynamics.

In control theory, a state observer is a dynamic system that provides an estimate of the internal state of a given physical system, from measurements of the input and output (the available measurements) of the real system as described in details in Chapter 3.

Many studies show the impact of using observation methods in linear and non-linear systems in industry [95], [65]. There may be difficulty in measuring quantities in biological systems. It may be expensive to perform measurements or the act of taking a measurement may unduly affect the process. Observers or soft sensors can be used as seen for example in the work of Gonzalez et al. [96]. Equations (4.2) - (4.3) present a direct relationship between the concentration of vitamin B_{12} and the concentration of *BtuB*. This motivates the use of observation methods to estimate *BtuB* concentration based on measurement of the vitamin B_{12} concentration.

6.2 Analysis of a Simple Model of a *BtuB* Observer

In this section, two observer candidates will be presented. Before developing the observers, in the Luenburger observer, it is necessary to verify that the model is observable. A system with an initial state, $x(t_0)$ is observable if and only if the value of the initial state can be obtained from measurements of the system output that have been obtained over a finite time $t_0 < t < t_f$. If the initial state cannot be obtained, then the system is unobservable. A straightforward observability check is to produce the input-output form of the system. The input-output form is a mathematical model of a physical system as a function of the input and output and the derivatives

of the input and output. In equations (4.4), (4.5), the product $\phi(p)\,\theta(p)$ is set to be the input signal and p is set to be the output. The corresponding input-output form is given by:

$$\ddot{p(t)} = \delta\,\xi\,[\varepsilon(P_{ext})\,[U - e(t)] - \dot{p(t)}] \tag{6.1}$$

where $U = \phi(p)\,\theta(p) = \frac{K_\phi}{K_\phi + p}\,\frac{K_\theta}{K_\theta + p}$. The system state can be observed from a knowledge of the output measurement $p(t)$ and the corresponding control inputs. The objective is to formulate a soft sensor to reconstruct *BtuB* concentration based on measurements of the concentration of vitamin B_{12}. The observation methods that are presented in Chapter 3 will be discussed in details here, the first observer strategy is based on an unknown input observer formulation and uses a first-order model representation. The second observer uses a second-order model representation to estimate the concentration of *BtuB* directly.

6.2.1 An Unknown Input Approach to Estimate *BtuB* using Luenberger and Sliding Mode Observation Mechanisms

This observer will use the measured concentration of vitamin B_{12}, $p(t)$ as the known output and use the corresponding dynamical equation (4.5) to reconstruct *BtuB* concentration. An unknown input observer technique will be used [49]. Referring to Eq. (4.5), $[\delta\,\varepsilon(P_{ext})\,e]$ will be considered as the unknown input as the value of p in the equation is measured and considered as the output. The assumed observer is as

follows where μ is an observer injection to be designed:

$$\dot{\hat{p}} = -\delta\, p + \mu \tag{6.2}$$

Define the error between the plant and observer by

$$e_1 = \hat{p} - p \tag{6.3}$$

The error dynamics is then given by

$$\dot{e_1} = \dot{\hat{p}} - \dot{p} = \mu - \delta\, \varepsilon(P_{ext})\, \hat{e} \tag{6.4}$$

where $\hat{e}$ is the observed concentration of *BtuB*. The injection must be designed, so the error is driven to zero. When this holds $(\dot{e_1} = 0)$, the designed injection compensates for the unknown input and the *BtuB* concentration can then be estimated as follows:

$$\hat{e} = \frac{\mu}{\delta\, \varepsilon(P_{ext})} \tag{6.5}$$

μ can be designed using numerous techniques. Appealing to sliding mode concepts, define:

$$\mu = Q\, sgn(e_1) \tag{6.6}$$

Q should be greater than $\delta\, \varepsilon(P_{ext})$ in magnitude to enforce a sliding mode, whereby $e_1 = 0$. This selection ensures the error becomes zero infinite time. An alternative

approach is to use a Luenberger observer paradigm:

$$\mu_1 = Q_1 e_1 \tag{6.7}$$

Figure 6.1 shows a comparison between the first order sliding mode observer and the first order luenburger observer when $Q = 1$ and $Q1 = 10$. It is seen that the sliding mode observer behaves better in terms of accuracy and response to the *BtuB* results from the original system (4.2).

The performance of the first order Luenberger observer can be expected to approach that of the first order sliding mode observer when Q_1 is selected to be very large so that a high gain observer results. Figure 6.2 shows the performance of the first order Luenberger observer when $Q_1 = 1000$ and when $Q = 10$. In practice, the observer dynamics is an approximation of the system dynamics. The observer performance will now be considered in the presence of a realistic range of the parameter variations in the system dynamics (4.4), (4.5). The sliding mode observer is expected to exhibit greater robustness than the Luenberger observer; infinite gain Q_1 would be required for the Luenberger observer to achieve the same performance as the sliding mode observer in the presence of parameter variations. The first parameter variation considered is the bacterial growth rate which will be bacteria dependent. The growth rate of $E.coli$ cultured in a minimal medium can be calculated from:

$$\mu = \frac{ln(2)}{t_d} \tag{6.8}$$

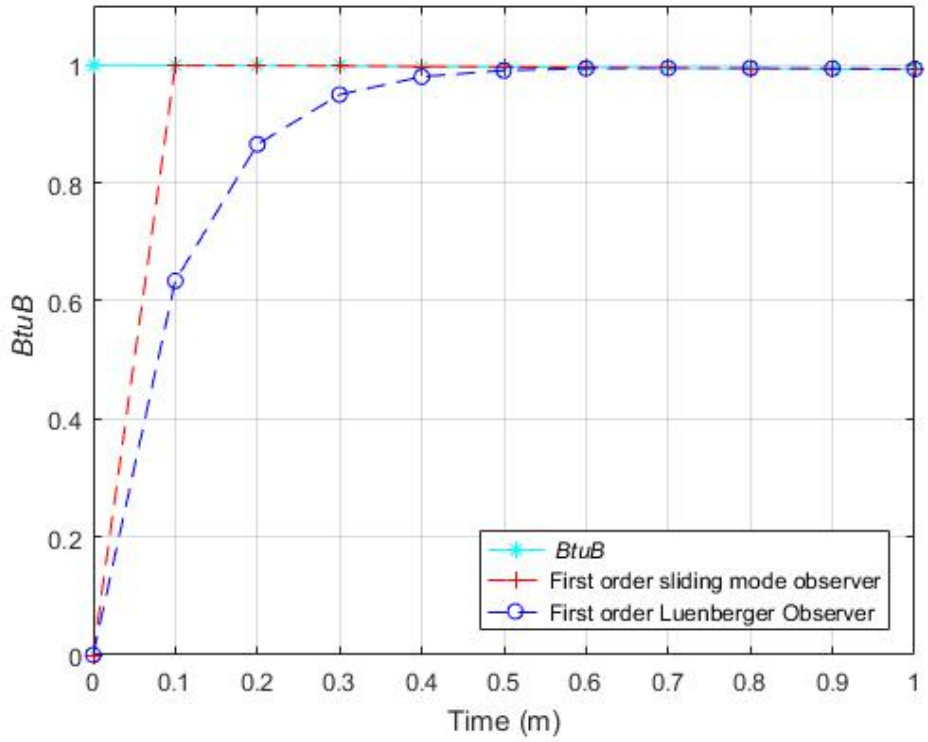

Figure 6.1: Comparison between the first order sliding mode observer and the first order Luenberger observer with the original *BtuB* from equation (4.2)

where t_d is the time required to double the number of cells. The bacterial growth rate can be calculated in practice using $OD600$ data, as shown in Fig. 4.3 when the vitamin B_{12} concentration is $100pM$ and using equations:

$$\ln OD - \ln OD_0 = \mu t \tag{6.9}$$

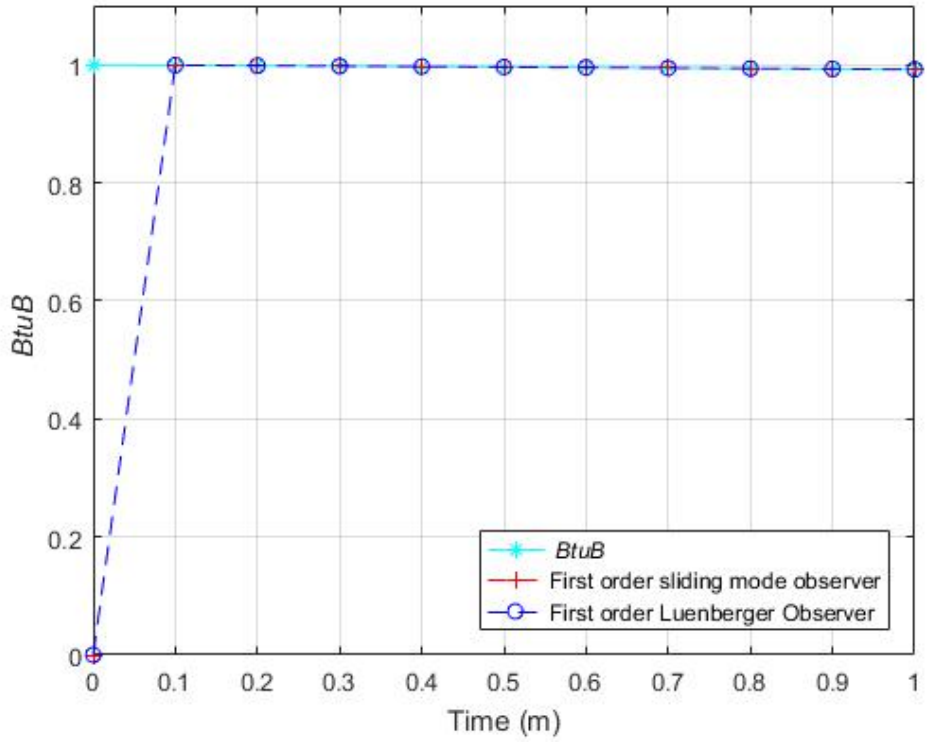

Figure 6.2: Comparison between the first order sliding mode observer and the first order Luenberger observer with the original *BtuB* from equation (4.2) when $Q1 = 1000$ and $Q = 10$

$$\ln OD_2 - \ln OD_1 = 2.303 \times (\log OD_2 - \log OD_1) = \mu(t_2 - t_1) \tag{6.10}$$

$$\mu = \frac{2.303 \times (\log OD_2 - \log OD_1)}{t_2 - t_1} = 0.008 \tag{6.11}$$

The full set of parameter ranges considered for the model are as given in Table 6.1. The growth rates of different types of bacteria are compared in [93]. The *btuB* and vitamin B_{12} degradation rates depend on the bacterial growth rate and a

realistic range for both rates is shown in Table 6.1. The assumed range for $\varepsilon(P_{ext})$ is based on the work of Santillan et al. [6] which demonstrates that the wild-type, 375 mutant, 434 mutant, 343 mutant strains are represented by $25, 21.5, 15.75$ and 5.8, respectively. The dissociation constant at the transcriptional and translation level should be small, and the selected range is based on the results reported in [97], [98] and [99]. In the tests that follow the model used to represent the physical system which generates $p(t)$ and the model used to define the observer are assumed to take different parameter values from the defined ranges. This test is replicating the fact that the parameters used to define the observer will be an approximation of any physical system.

Table 6.1: Range for parameters in the mathematical model (4.1) - (4.3)

Symbol	Biological meaning	Realistic Range
ξ	The *btuB* degradation rate	[0.693 - 0.4 $\times$ 10^{-2}]
δ	The B_{12} degradation rate	[0.693 - 0.4 $\times$ 10^{-2}]
$\varepsilon(P_{ext})$	Represent the type of the strain	[25 - 5.8]
K_ϕ	The dissociation constant at the transcriptional level	[2$\times10^{-9}$ - 2$\times10^{-4}$]
K_θ	The dissociation constant at the translation level	[2$\times10^{-9}$ - 2$\times10^{-4}$]

Figure (6.3) shows the comparison between the first-order sliding mode observer and the first order Luenberger observer when $Q1 = 1000$, $Q = 10$ and ξ changes from 0.008 to 0.2. It is seen from the figure that both observers behave well in estimating the original *BtuB*.

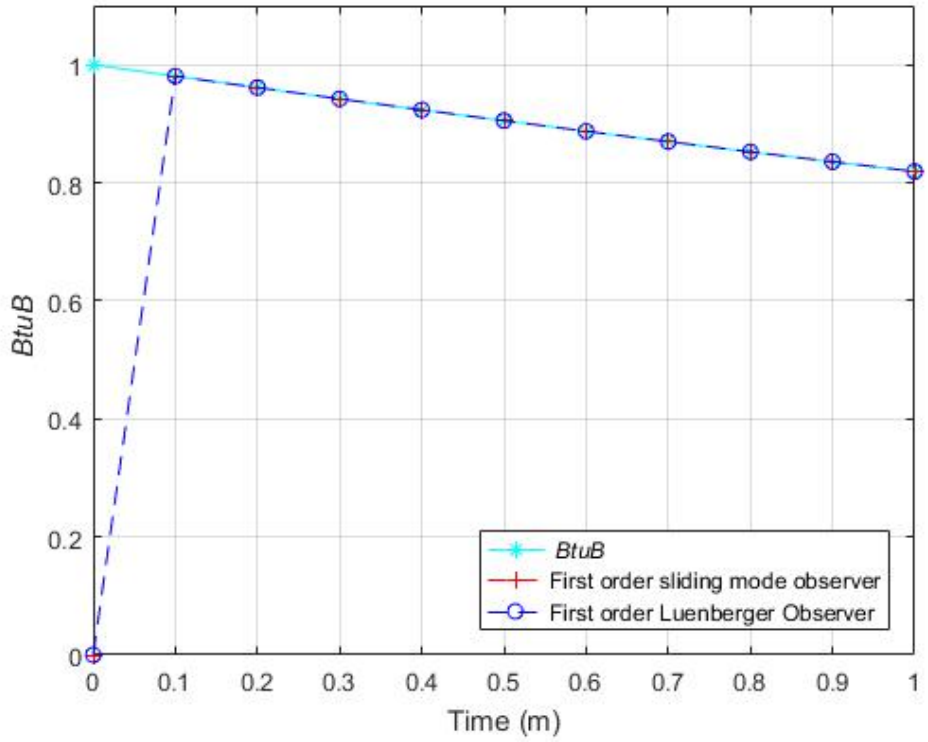

Figure 6.3: Comparison between the first order sliding mode observer and the first order Luenberger observer with the original *BtuB* from equation (4.2) when $Q1 = 1000$ and $Q = 10$ and $\xi = 0.2$

6.2.2 A Full Order *BtuB* Observer

In this section, a second-order observer will be implemented using equations (4.4) and (4.5) to determine the model. Luenberger [100] and Utkin [54] injection signals will be used to force the observation error to zero. This observer will be studied to make sure that any disturbance for each variable can be observed as this system can

observe the full order of the system instead of only observing the unknown signal. The corresponding *Luenberger observer* is given by:

$$\dot{\hat{e}} = \xi\,[\phi(p)\,\theta(p) - \hat{e}] + L_1(\hat{p} - p) \tag{6.12}$$

$$\dot{\hat{p}} = \delta\,[\varepsilon(P_{ext})\,\hat{e} - \hat{p}] + L_2(\hat{p} - p) \tag{6.13}$$

If the error between the plant and the observer is defined by:

$$\begin{aligned} e_1 &= e - \hat{e} \\ e_2 &= p - \hat{p} \end{aligned} \tag{6.14}$$

the error dynamics between the plant and the observer may be expressed by:

$$\begin{aligned} \dot{e_1} &= -\xi\, e_1 + L_1 e_2 \\ \dot{e_2} &= \delta\,\varepsilon\, e_1 - \delta\, e_2 + L_2 e_2 \end{aligned} \tag{6.15}$$

The poles of the closed-loop error dynamics (6.15) using the technique mentioned in Chapter 5 are the roots of the following characteristic equation:

$$s^2 + s(-L_2 + \delta + \xi) + \xi\,(\delta - L_2) - L_1\delta\varepsilon \tag{6.16}$$

Appropriate adjustment of the gains L_1 and L_2 enables the closed-loop poles of the observer to be placed in any desired location. With the parameter values from Table

5.1 and $\varepsilon = 25$, the selection $L_1 = -1000$ and $L_2 = -30$ yields closed-loop observer poles at -10 and -20.

The second observer will be based on an Utkin observer formulation discussed in Chapter 3. The observer is defined based on the nominal model in equations (4.4) and (4.5) as follows:

$$\dot{\hat{e}} = \xi\,[\phi(p)\,\theta(p) - \hat{e}] + L\mu \tag{6.17}$$

$$\dot{\hat{p}} = \delta\,[\varepsilon(P_{ext})\,\hat{e}] - \mu \tag{6.18}$$

where μ and L define the observer injection to be designed, so the error between the measured and the observed concentration of vitamin B_{12} is driven to zero. Using the error definitions in (6.14), the error dynamics are given by:

$$\begin{aligned} \dot{e_1} &= -\xi\, e_1 - L\mu \\ \dot{e_2} &= -\delta\,\varepsilon\, e_1 - \delta\, e_2 + \mu \end{aligned} \tag{6.19}$$

To induce a sliding motion on the output error e_2 so that the sliding condition $e_2 = 0$ is enforced, it is necessary to ensure e_2 and $\dot{e}_2$ have opposite signs. Consider μ defined by:

$$\mu = -M sign(e_2) \tag{6.20}$$

It follows that for sufficiently large M, e_2 and $\dot{e}_2$ have opposite signs and $e_2 = 0$ will be satisfied. When this sliding mode is attained, it follows that $e_2 = 0$ and $\dot{e}_2 = 0$.

Using the principle of the equivalent injection it follows from (6.19) that on average, the effect of the applied injection signal (6.20), denoted μ_{eq}, is given by:

$$\mu_{eq} = -\delta\,\varepsilon\,e_1 \tag{6.21}$$

To complete the observer design, it is necessary to ensure the e_1 subsystem in (6.19) exhibits stable dynamics in the sliding mode. Substituting (6.21) in (6.19)

$$\dot{e_1} = -(\xi - L\delta\,\varepsilon)e_1 \tag{6.22}$$

It follows that for stability of (6.22)

$$L < \frac{\xi}{\delta\,\varepsilon} \tag{6.23}$$

The Utkin observer (6.17)-(6.18) with the injections defined by (6.20) and (6.23) will ensure stable evolution of the error trajectories as shown in Figure (6.4). The parameters are selected as $M = 1$ and $L = -100$.

To test the robustness of the observers in the presence of parameter uncertainty, two tests have been performed. The first considers variation in the parameter ξ. ξ is the *btuB* degradation rate, and from [6], it is determined by the summation of the bacterial growth rate and the *BtuB* degradation rate. The value of the *BtuB* degradation rate is assumed negligible in [6] and because of that, the value of ξ is set equal to the bacterial growth rate, which is 0.008 for *E.coli*. In this robustness

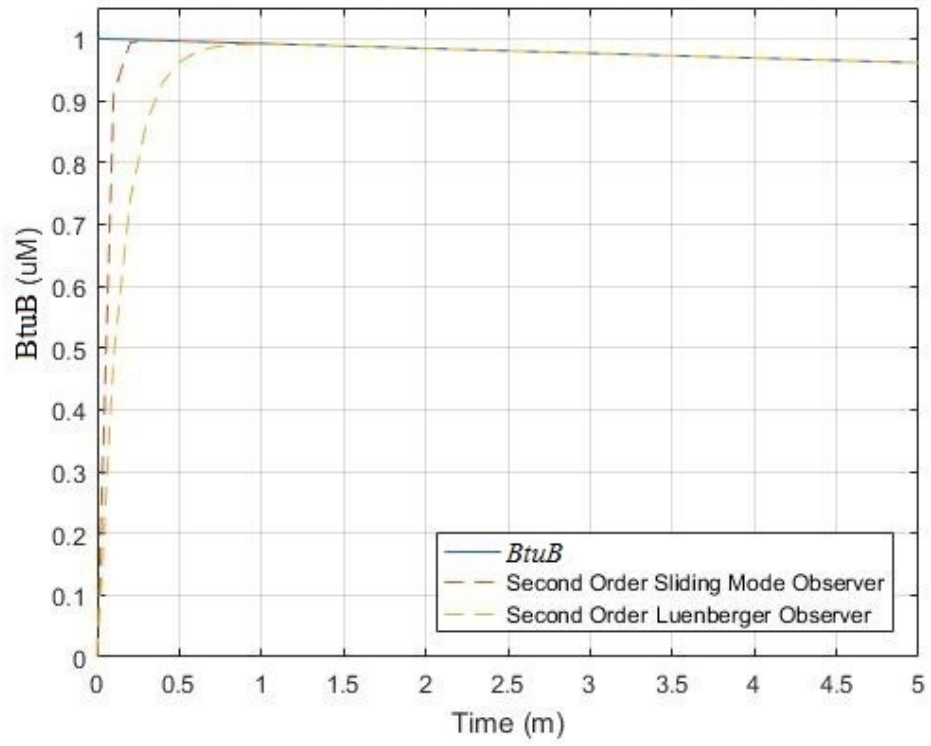

Figure 6.4: Time evaluation for measured and observed *BtuB* dynamics when applying Utkin and Luenburger observation methods with no disturbance

test, the *BtuB* degradation rate is not neglected, and an additional value will be added to the bacterial growth rate to define ξ. Fig 6.5 compares the dynamics of *BtuB* obtained from the model with $\xi = 0.016$ as well as the estimates obtained from the Utkin and Luenberger observers, wherein the observers $\xi = 0.008$.

It is seen from Fig. 6.5 that varying the parameter ξ does not affect the estimate of the *BtuB* concentration. Despite the uncertainty, both observers converge to

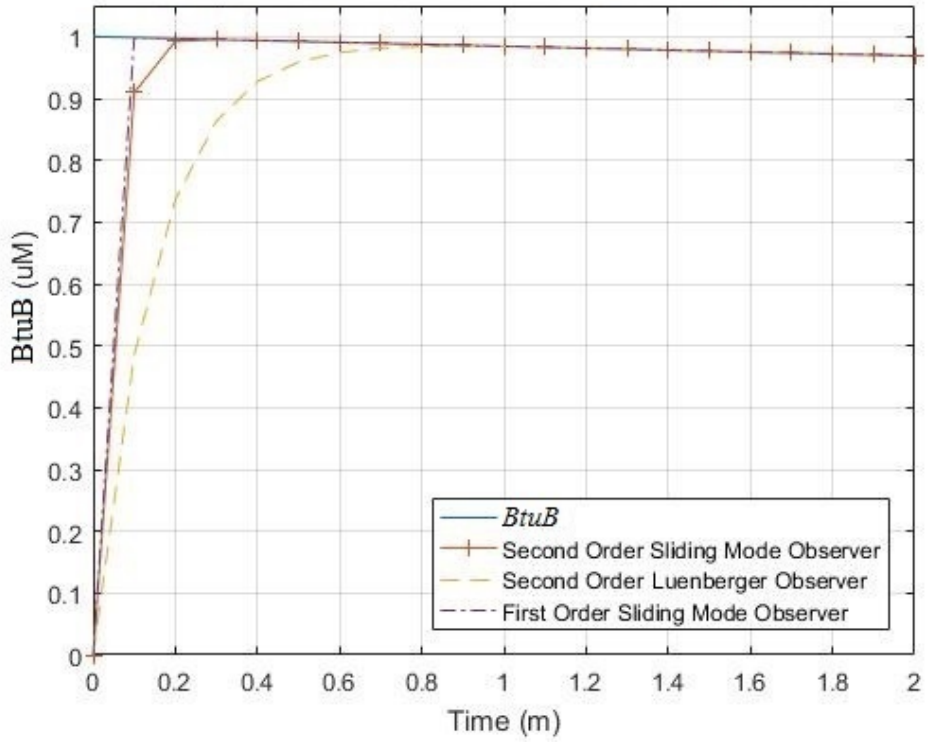

Figure 6.5: Comparison between the estimated and the actual value of *BtuB* when *btuB* degradation rate ξ changes between the system and observer from 0.016 to 0.008

observe the correct value of the *BtuB* concentration based only on knowledge of the concentration of vitamin B_{12} in less than 1 minute. The second test assumes that the parameters of the observer have been configured for a different bacteria than is present in the real system. This corresponds to changing all the parameters in equations (4.4) and (4.5). Previously, *E.coli* was used as a bacterial strain in the

system model. This test uses the parameters for *salmonella* in the system model presented in Chapter 4; the observers remain parametrised as for $E.coli$. In the system model the growth rate is 0.007 and thus $\delta = \xi = 0.007$; bacterial strain changes to $\varepsilon = 21.5$ based on the results which were found earlier in Chapter 4. In the observers the model parameters are as in Table 5.1. The corresponding observation

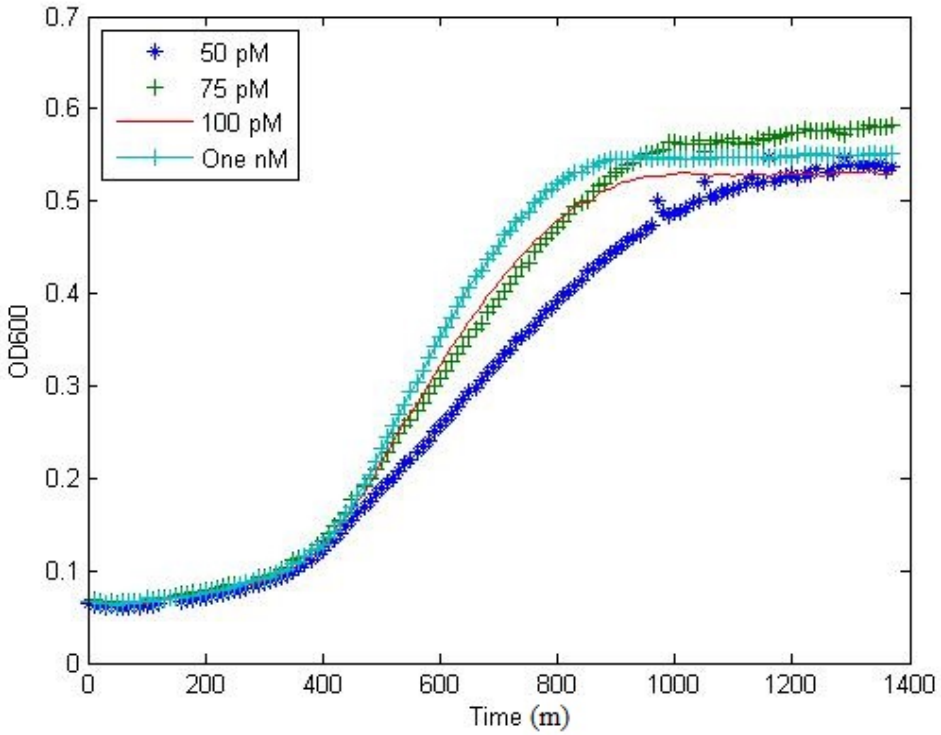

Figure 6.6: Experimentally measured *S.enterica* growth curves with varying vitamin B_{12} concentration ($50p$M to $1n$M)

results after changing the bacterial type are shown in Fig. 6.7-6.8.

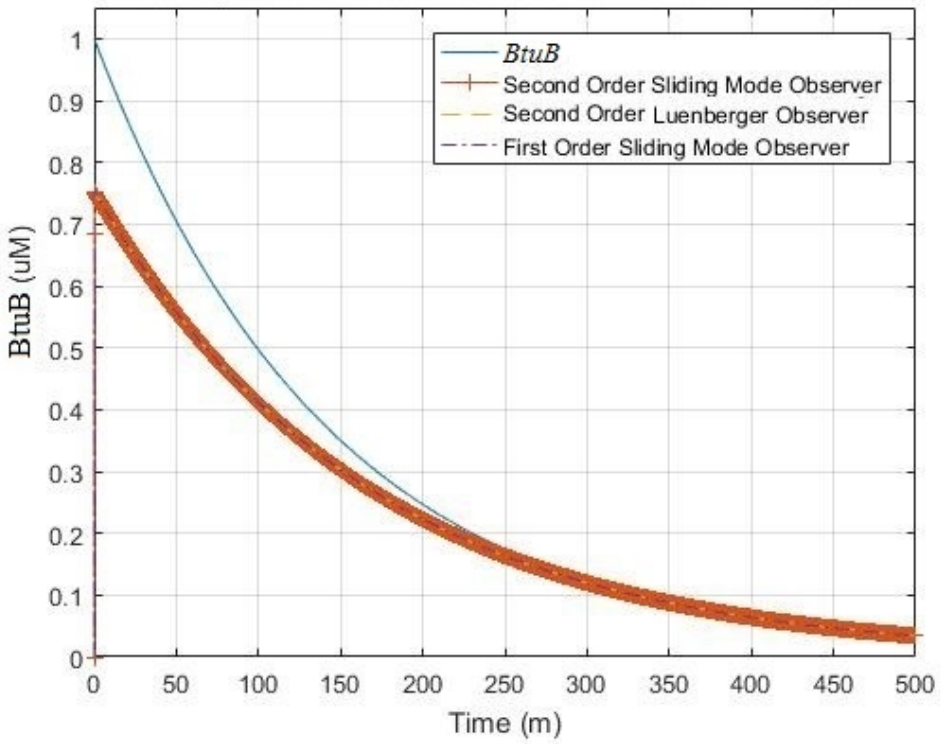

Figure 6.7: Comparison between the estimated and the actual value of *BtuB* when the bacteria changes between the system and observers - steady-state performance

It is seen from Fig. 6.7 that the steady-state performance is reasonable with the observers requiring around 200 minutes to track the *BtuB* signal from the system model. From Fig. 6.8 it is seen that the Utkin observer has a better transient performance that the Luenberger observer as has been observed in the nominal simulations.

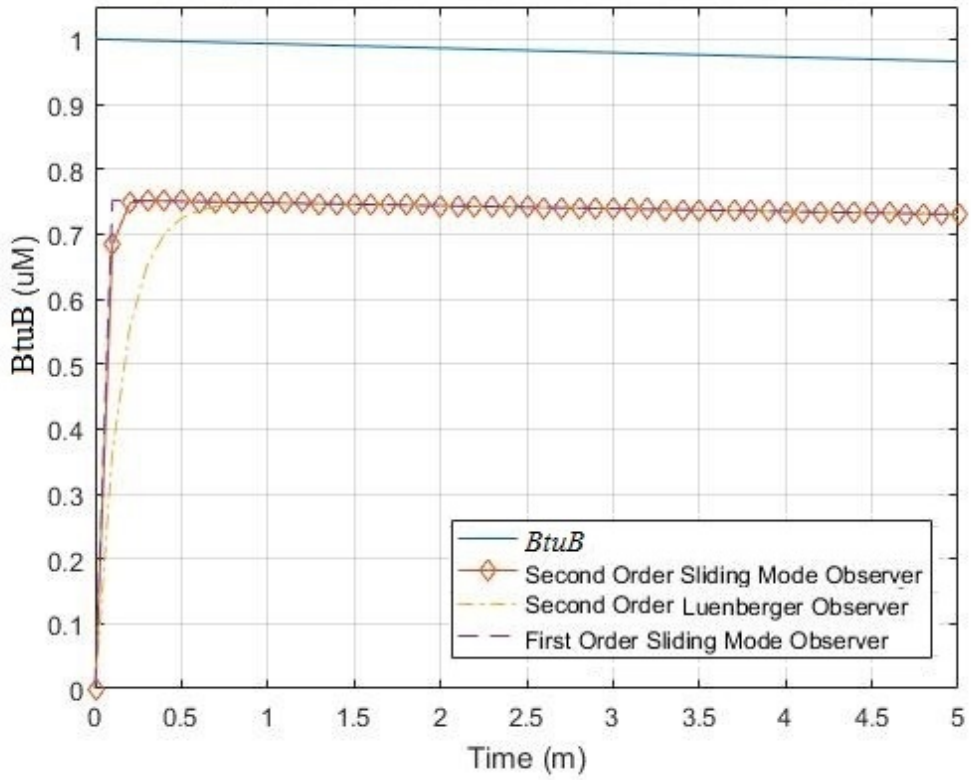

Figure 6.8: Comparison between the estimated and the actual value of *BtuB* when the bacteria changes between the system and observers- early transient

6.3 Experimental Validation of Observer Results

Observers have been presented for estimation of the concentration of *BtuB* from measurements of the concentration of vitamin B_{12}. The robustness and performance validation has thus far been based on results from experimentally validated mathematical models. Validation of the estimates of *BtuB* concentration obtained from

the observers against experimental measurements is desirable. It is, however, difficult to measure the concentration of *BtuB* directly experimentally. Fig. 6.9 shows a comparison of the variation in the concentration of vitamin B_{12} against the construction of a plasmid in which green fluorescent protein (*GFP*) production is controlled by a vitamin B_{12} riboswitch. This is an alternative way of viewing *BtuB* production experimentally. *GFP* is used because its levels can be readily detected after the reaction is completed by the use of anti-*GFP* antibodies and detection on a western blot. When this plasmid is subject to transcription/translation (in an *in vitro* protein synthesis kit), in the absence of B_{12}, *GFP* production will occur as usual. However, if B_{12} (the preferred riboswitch ligand being adenosylcobalamin) is present, it is thought that this will bind to the riboswitch and change its structure so that the ribosome can no longer bind and translation can no longer occur. Therefore, using this method, various B_{12} variants have been tested by adding them to the *in vitro* protein synthesis reactions, at increasing concentrations, to see the effect on the vitamin B_{12} riboswitch and in turn, on *GFP* production.

It is desirable to be able to directly compare the relationship between the evolution of the observed *BtuB* and the concentration of vitamin B_{12} and the relationship between *GFP* and the concentration of B_{12}. In particular, it is required to find the relationship between *GFP* production and *BtuB* production, as in the experiments, the *GFP* gene replaces the *BtuB* gene. It follows that the concentration of *GFP* should correlate with the concentration of *BtuB*. Certain factors will affect the absolute values of *GFP*. Figure 6.9 contains two curves, one obtained with adeno-

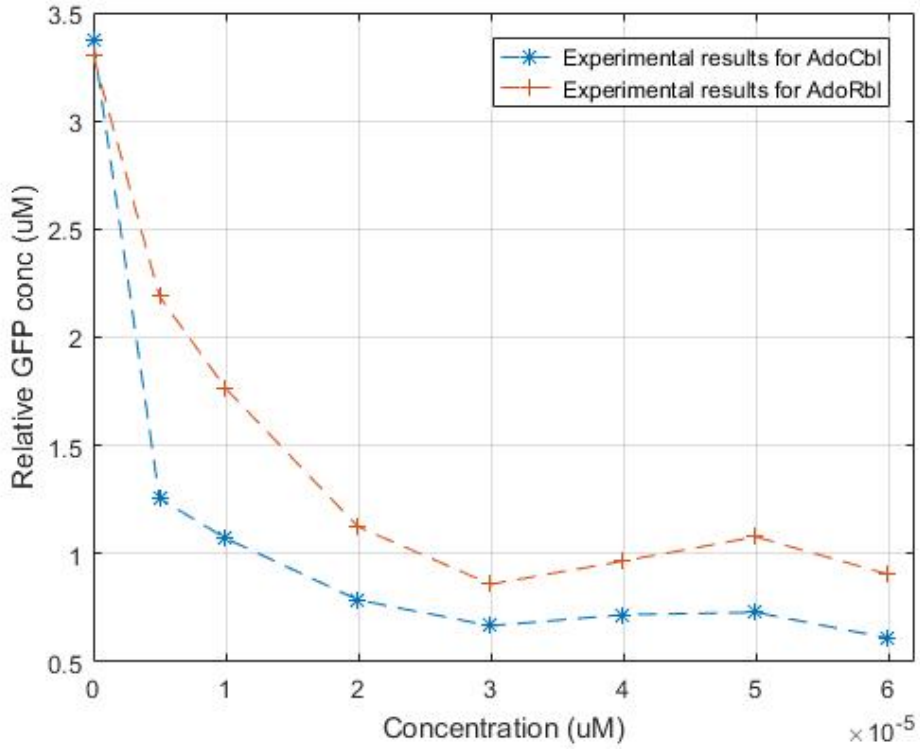

Figure 6.9: Experimental results to show the relation between GFP and vitamin B_{12} for $AdoCbl$, $AdoRbl$

sylcobalamin $AdoCbl$ and the other using adenosylrhodibalamin $AdoRbl$. The only difference between the variants is that in $AdoRbl$, the central cobalt ion is replaced with rhodium [101]. The plot shows that increasing vitamin B_{12} concentration will decrease the GFP concentration and changing B_{12} variants will affect the magnitude of the response. To validate the observer results experimentally, the observed concentration of $BtuB$, $\hat{e}(t)$ is plotted against the concentration of vitamin B_{12}, $p(t)$

for the case of the Utkin observer. The observer was parameterised using the strategy reported in [102] by considering the evolution of the concentration of vitamin B_{12} over time from the bacterial growth curve. A comparison between particular forms of vitamin B_{12} variants in [103] found that each vitamin B_{12} analogue has a specific degradation rate. In this case, each degradation rate will give a specific concentration of vitamin B_{12}. Fig. 6.10 shows the relation between the observed concentration of *BtuB* and the concentration of vitamin B_{12}. The simulation results were computed when δ in (4.5) was $\delta = 0.008$ for AdoRbl and $\delta = 0.0054$ for AdoCbl. The simulation results in Fig. 6.10 show that the *BtuB* concentration decreases when the concentration of vitamin B_{12} increases in line with the observations from the experimental results. The rate of decay is noted to be similar. The experimental set-up will impact the initial conditions for the experimental observations. The size of each protein will influence the experimental results. If one was $30kDa$ and another $15kDa$, then it may be expected that twice the amount of the smaller one may be produced because the RNA polymerase and protein translation apparatus can only work so fast. As both figures have the same dynamics, a factor λ has been introduced to adjust the magnitude observed in Fig. 6.10. Effectively it is assumed that a relationship $GFP = \lambda\, \hat{e}(t)$. Figure 6.11 shows a comparison between the simulation and experimental results when $\lambda = 2.5$. The comparison between the *BtuB* experimental results and the estimate of the concentration of *BtuB* obtained by the observer is reasonable. The experimental results further validate that the presented observer approach can estimate the concentration of *BtuB*.

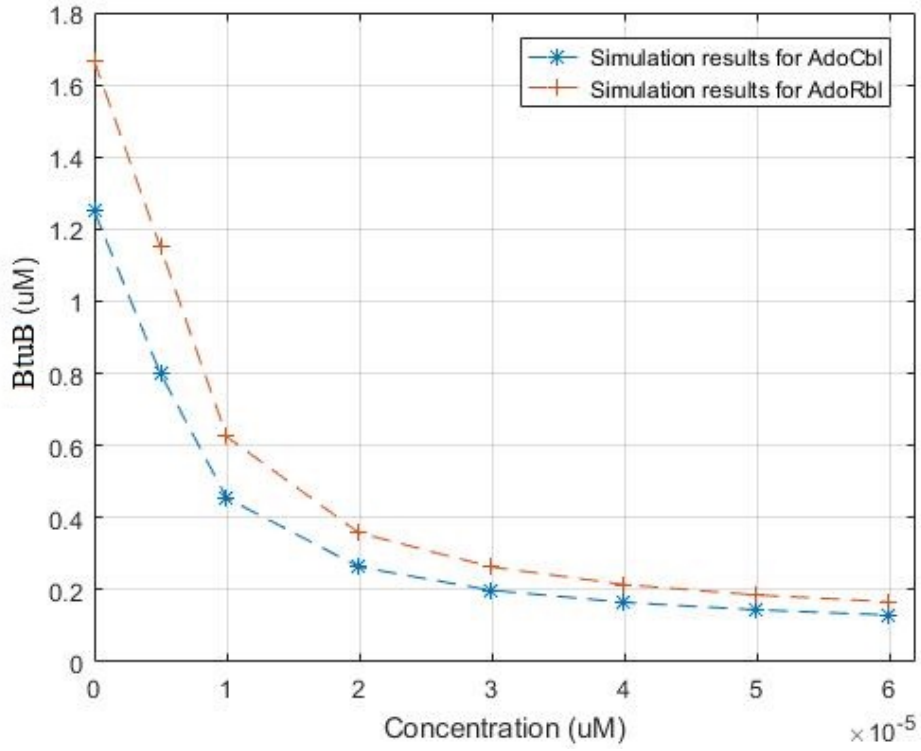

Figure 6.10: Simulation results to show the relation between *BtuB* and vitamin B_{12} for *AdoCbl* and *AdoRbl*

6.4 Conclusions

This chapter shows an example of using the observation method in a biological application, Luenburger and sliding mode observers are used to estimate the value of *BtuB* using a measured concentration of vitamin B_{12} concentration. A comparison is also shown between different observers, and it is shown that the sliding mode observer behaves the best to observe *BtuB* protein. The technique and the theory

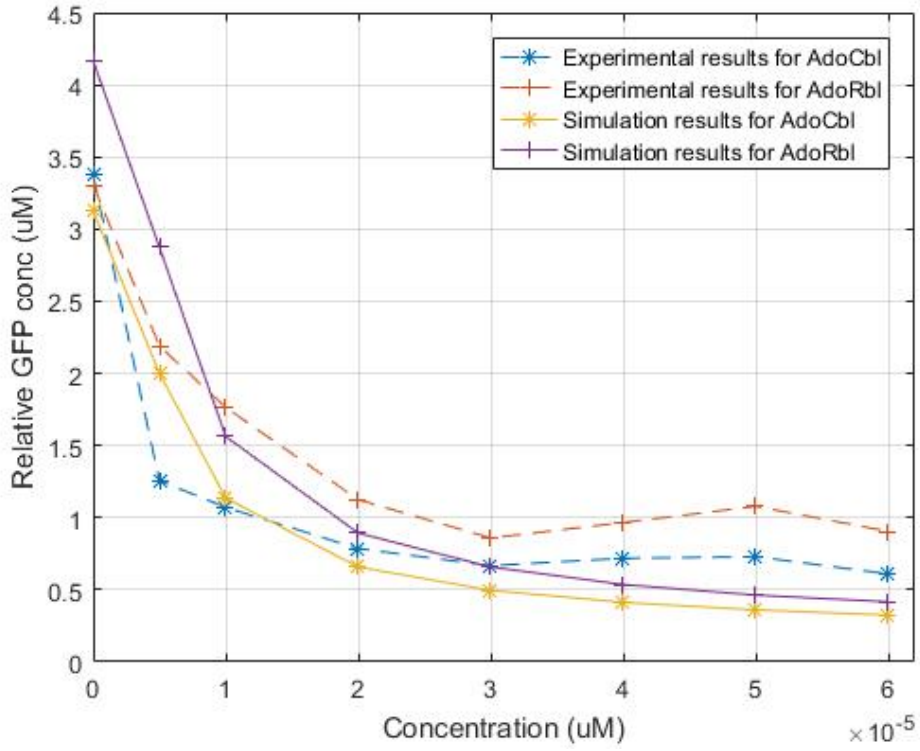

Figure 6.11: Comparison between the simulated and experimental *GFP* for *AdoCbl* and *AdoRbl*.

used in this chapter can also be used to estimate the gene *btuB* concentration, and this is set as one of the future work targets.

Chapter 7

General Conclusions and Future work

7.1 General Conclusions

As a general conclusion for this thesis, It has been proven from each chapter that using VSC is a novel and efficient means to study the control mechanism in bacterial growth. VSC is used to link the bacterial growth with the concentration of vitamin B_{12}, simulation results and experimental results proved that the switching mechanisms that happen inside the mRNA affect the bacterial levels, as when the switch is on, the bacterial growth be in the exponential phase and it goes to the saturation level when the riboswitch switches off. These results have been proven using simulation results and in *vivo* experiments using two types of bacterial strains. Both results using *E. coli* and *S. enterica* showed that the vitamin B_{12} controls the bacterial growth, and both reached the saturation level when the riboswitch turned

off.

Also, VSC is used in bacterial and algal co-culture, this was a moving step from a cellar to a population level, the reachability condition is used to find the saturation level of bacterial and algal growth by finding the reachability condition of each growth and using sliding mode control techniques. Linearisation methods are used to simplify the mathematical equations and to find real-time growth.

Robustness analysis is also performed in each chapter to check the effect of varying the parameters in each model, and it is found that all the systems are robust. The co-culture growth is studied before and after the add-back of nutrients, which are carbon and vitamin B_{12}. The analysis shows that vitamin B_{12} riboswitch saturates the growth.

Sliding mode observation methods are also used in this thesis to estimate the concentration of *BtuB* using the measured concentration of vitamin B_{12}. *BtuB* concentration is known to be hard to be measured experimentally and hence was the reason to use this method. Two first-order and two second-order observers, Luenberger observer and sliding mode observer, are used in this thesis to find and estimate *BtuB*. GFP production is used to validate the *BtuB* estimated by the observers, and the outcomes were promising. The simulation results show that the second-order sliding mode observer provides the best performance concerning robustness and accurate estimation.

This thesis provides an excellent tool to study the effect of vitamin B_{12} riboswitch in cell growth in general and can be used in several applications such as

controlling the growth of algae or in finding the carrying capacity of each growth. Also, the observation technique presented in this thesis will be used as a tool in bio-engineering to estimate variables that are hard to be estimated experimentally, for example, the concentration of *btuB* will be estimated using the same method shown in chapter six.

7.2 Future Work

This thesis brought to the attention that using VSC is efficient in understanding the dynamics of bacterial growth; the results were studied by analysing a mathematical model that represents the bacterial growth dynamics by linking it with the vitamin B_{12} riboswitch. One of the future work is to consider the system if it is inhibited by vitamin B_{12} analogues.

Vitamin B_{12} analogues are molecules which have a very similar chemical structure to that of vitamin B_{12}, but which should not be substituted for consumption. On the contrary, they are potentially harmful, since these molecules replace the important B_{12} transport molecules within the body, thus hindering the absorption of actual vitamin B_{12}.

During the initial research phase on vitamin B_{12}, it was difficult to differentiate between vitamin B_{12} analogues and real vitamin B_{12}, as the tests used were carried out using both forms. However, today, it is unequivocally possible to identify vitamin B_{12} analogues in many foods through the use of paper chromatography. This changes the idea for many foods which were previously thought to be rich in vitamin B_{12}, but in fact, have now been proven to contain nothing more than pseudo

vitamin B_{12}. Having a mathematical model that can distinguish between the active vitamin B_{12} and vitamin B_{12} analogues will provide an important tool in vitamin B_{12} deficiency and efficiency.

Observation techniques have proved to be useful in biological applications; previously, chapter 6 showed that using sliding mode observer or Luenburger observer can estimate the concentration of *BtuB*.

Equations (4.1) - (4.3) can be used in the future to build second-order observers to estimate and observe the concentration of *btub*. This will be helpful as it is hard to measure *btub* experimentally. Multiple observers will be used, and a comparison will be made to achieve the best observation.

Vitamin B_{12} riboswitch showed a play a role in the control mechanism of the algal growth; the mathematical model will be studied to analyse the effect of the riboswitch on algal growth and study the robustness of the system with different strains.

Appendix A

Defining Time Domain Equations and Differentiator

A.1 Time Domain Equations

To find the time evolution for $p(t)$ and $e(t)$, it is easier to deal with equations (4.4) - (4.5) when they are linearised using the linear approximations equation:

$$\frac{df(y,x)}{dt} = f(y_{ss},x_{ss}) + (y-y_{ss}).[\frac{\partial f}{\partial y}]_{y=y_{ss},x=x_{ss}} + (x-x_{ss}).[\frac{\partial f}{\partial x}]_{y=y_{ss},x=x_{ss}}$$

$f(y,x)$ is linearised by a Taylor series expansion, using only the first two terms. After applying the linear approximations for equations (A.6), (A.7), $p(t)$ and $e(t)$

will be:

$$e(t) = \frac{k}{k+1} + \frac{e^{-\xi t}}{k+1} \tag{A.1}$$

$$p(t) = \delta\varepsilon[\frac{\varepsilon k}{k+1}(1-e^{-\delta t}) + \frac{e^{-\beta t} - e^{-\delta t}}{(\delta-\xi)(k+1)}] \tag{A.2}$$

Equations (A.1), (A.2) show that the concentration of *BtuB* depends on the bacterial growth rate and the dissociation constant and the concentration of vitamin B_{12} depends on the dissociation consent, bacterial growth rate and the bacterial strain. The relation between $p(t)$ and $e(t)$ after solving equations (A.1), (A.2) is:

$$e(t) = \mid \frac{\delta\varepsilon^2 k}{\delta\varepsilon^2 k - p(t)} \mid \tag{A.3}$$

Equation (A.3) has a limitation when it was formed, which is $p(t) > \delta\varepsilon^2 k$, this means that the concentration of *BtuB* will not be affected unless the concentration of vitamin B_{12} become more than the multiplication of the bacterial growth rate and the dissociation constant and the constant that represents the bacterial strain that has been used. A new equation is created based on the dynamics of the bacterial growth as shown bellow:

$$\dot{a} = \alpha a\Big[1 - \Big(\frac{a}{P_{max}}\Big)\Big], \tag{A.4}$$

The output of this equation gives similar results as the experimental results.

P_{max} was found using linearisation and it is as shown bellow:

$$P_{max} = \frac{\varepsilon(P_{ext})}{k+1}(k + (\frac{\delta - \xi\, k + \delta\, k}{\xi})^{(\frac{\xi}{\xi-\delta})}) \tag{A.5}$$

A.2 Differentiator

The differentiator is a model that is used to find the derivative of the output signal and construct other signals from the system, this is another way to show that the system is observable. Recall:

$$\dot{e} = \xi \left[\phi(p)\, \theta(p) - e \right] \tag{A.6}$$

$$\dot{p} = \delta \left[\varepsilon(P_{ext})\, e - p \right] \tag{A.7}$$

Equation (A.7) shows that e can be constructed from p and its derivative as shown bellow:

$$e = \frac{\dot{p}}{\varepsilon(P_{ext})\, \delta} + \frac{p}{\varepsilon(P_{ext})} \tag{A.8}$$

Figure A.1 shows that the error goes to zero, this means that *Btub* can be estimated from the output and its derivative.

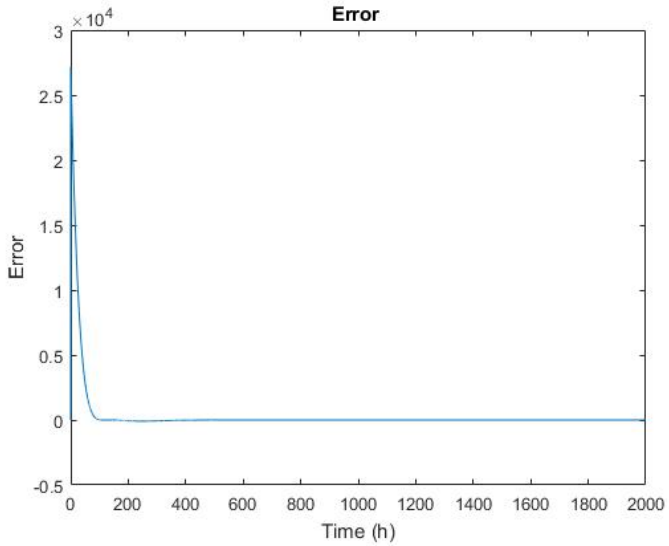

Figure A.1: *Btub* error between the model (4.4) and the differentiator (A.8)

Appendix B

Simulink models

In this appendix, all the models and the files that are used to create the observers are presented. Before simulating the model, the values of the parameters are calculated in MATLAB as:
$K = 2.25e-6, \alpha = 0.071, \xi = 0.008, \delta = 0.008, \varepsilon = 25, p_0 = 0, e_0 = 1.$
Figure B.1 shows the mathematical model (4.4) - (4.5).
Figure B.2 shows an unknown input approach to estimate $BtuB$ using sliding mode.

Figure B.3 shows a second order sliding mode observer to estimate $BtuB$.

Figure B.4 shows a second order luenberger observer to estimate $BtuB$.

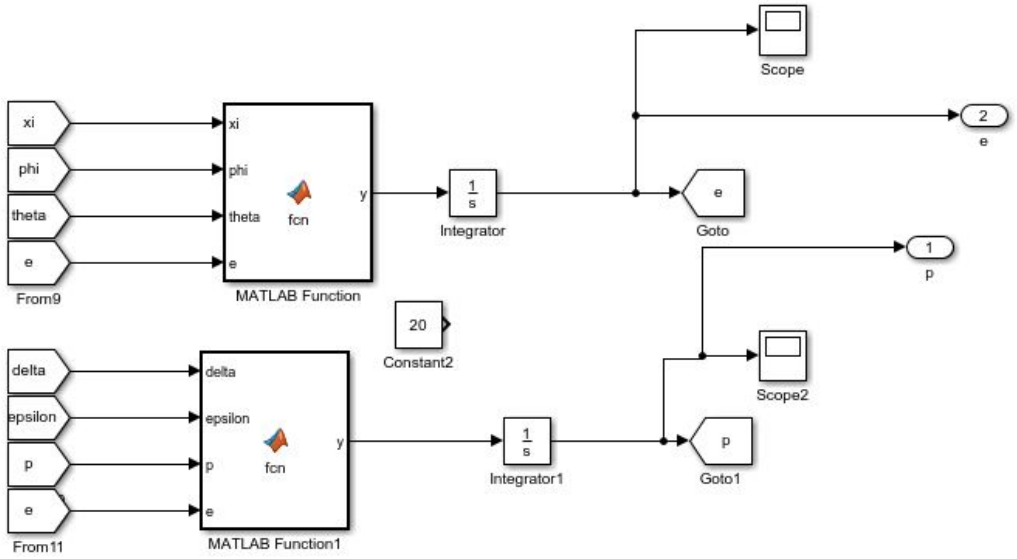

Figure B.1: Plant

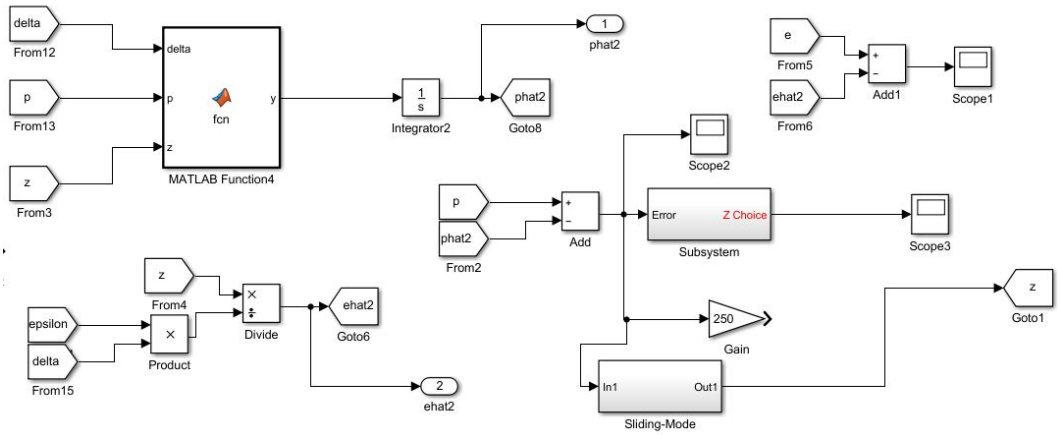

Figure B.2: Sliding mode observer using an unknown input approach

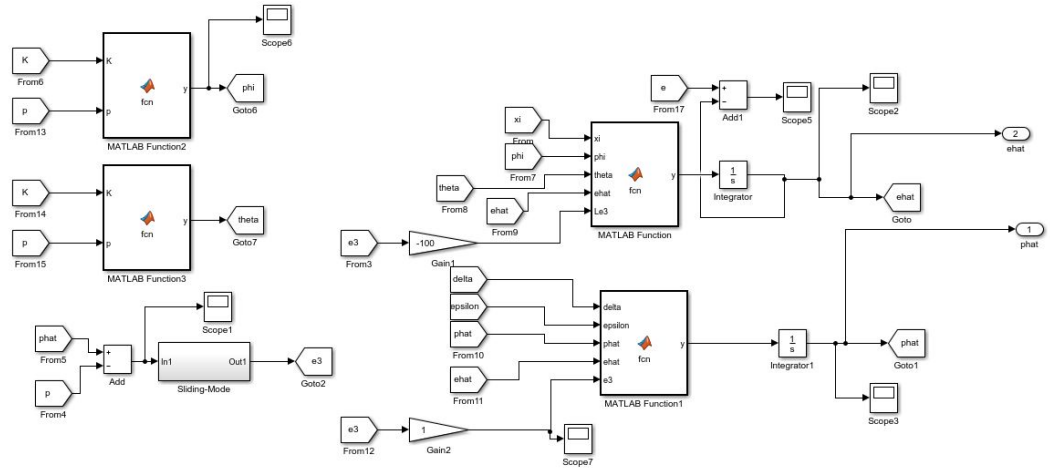

Figure B.3: Second order sliding mode observer

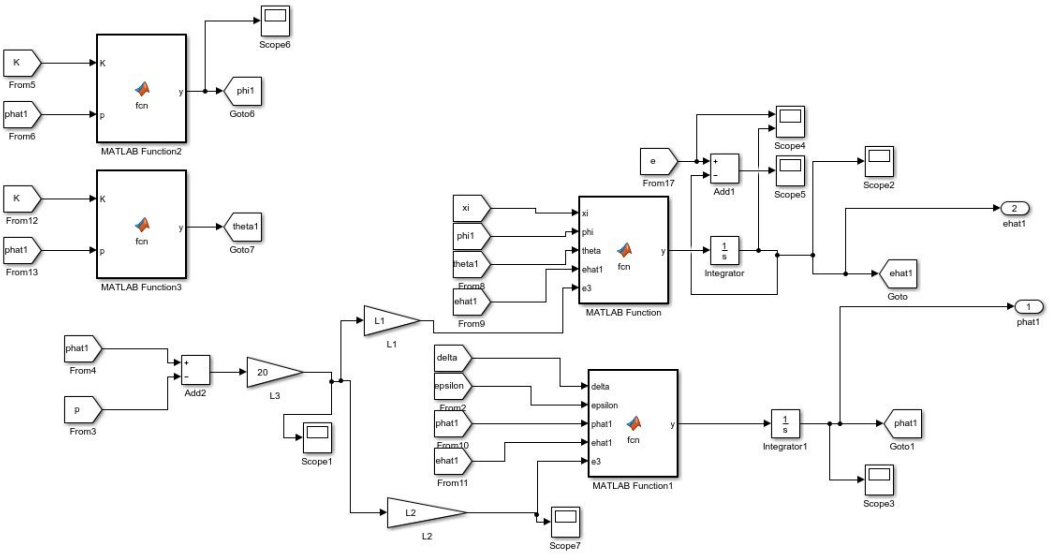

Figure B.4: Second order luenberger observer

Bibliography

[1] Lindsay H Allen. How common is vitamin b-12 deficiency? *The American journal of clinical nutrition*, 89(2):693S–696S, 2009.

[2] Patrick J Skerrett. Vitamin b12 deficiency can be sneaky, harmful. *Harvard Health Blog*, 2013.

[3] Gáspár Jékely. *Eukaryotic Membranes and Cytoskeleton: Origins and Evolution*, volume 607. Springer Science & Business Media, 2008.

[4] Chase L. Beisel and Christina D. Smolke. Design principles for riboswitch function. *PLOS Computational Biology*, 5(4):1–14, 04 2009.

[5] Andrea L Edwards and Robert T Batey. Riboswitches: A common rna regulatory element. *Nature Education*, 3(9):9, 2010.

[6] Moisés Santillán and Michael C Mackey. Dynamic behaviour of the b_{12} riboswitch. *Physical biology*, 2(1):29, 2005.

[7] Andrew D Garst, Andrea L Edwards, and Robert T Batey. Riboswitches: structures and mechanisms. *Cold Spring Harbor perspectives in biology*, 3(6):a003533, 2011.

[8] Ronald R Breaker. Riboswitches and the rna world. *Cold Spring Harbor perspectives in biology*, 4(2):a003566, 2012.

[9] Alexander Serganov and Evgeny Nudler. A decade of riboswitches. *Cell*, 152(1-2):17–24, 2013.

[10] Katherine E Deigan and Adrian R FerrÉ-DAmarÉ. Riboswitches: discovery of drugs that target bacterial gene-regulatory rnas. *Accounts of chemical research*, 44(12):1329–1338, 2011.

[11] Petra Dersch, Muna A Khan, Sabrina Mühlen, and Boris Görke. Roles of regulatory rnas for antibiotic resistance in bacteria and their potential value as novel drug targets. *Frontiers in microbiology*, 8:803, 2017.

[12] Ali Nahvi, Narasimhan Sudarsan, Margaret S Ebert, Xiang Zou, Kenneth L Brown, and Ronald R Breaker. Genetic control by a metabolite binding mrna. *Chemistry & biology*, 9(9):1043–1049, 2002.

[13] Sha Gong, Yanli Wang, Zhen Wang, and Wenbing Zhang. Computational methods for modeling aptamers and designing riboswitches. *International Journal of Molecular Sciences*, 18(11):2442, 2017.

[14] Manja Wachsmuth, Gesine Domin, Ronny Lorenz, Robert Serfling, Sven Findei, Peter F Stadler, and Mario Mrl. Design criteria for synthetic riboswitches acting on transcription. *RNA Biology*, 12(2):221–231, 2015.

[15] Fareed Aboul-ela, Wei Huang, Maaly Abd Elrahman, Vamsi Boyapati, and Pan Li. Linking aptamer-ligand binding and expression platform folding in riboswitches: prospects for mechanistic modeling and design. *Wiley Interdisciplinary Reviews: RNA*, 6(6):631–650, 2015.

[16] Chang C. Liu, Lei Qi, Julius B. Lucks, Thomas H. Segall-Shapiro, Denise Wang, Vivek K. Mutalik, and Adam P. Arkin. An adaptor from translational to transcriptional control enables predictable assembly of complex regulation. *Nature Methods*, 9(11):1088–1094, 11 2012.

[17] Atsushi Ogawa. *Artificial Riboswitches: Methods and Protocols*, volume 1111. 01 2014.

[18] Sven Findei, Maja Etzel, Sebastian Will, Mario Mrl, and Peter Stadler. Design of artificial riboswitches as biosensors. *Sensors*, 17:1990, 08 2017.

[19] Matthew AA Grant, Elena Kazamia, Pietro Cicuta, and Alison G Smith. Direct exchange of vitamin b 12 is demonstrated by modelling the growth dynamics of algal–bacterial cocultures. *The ISME journal*, 8(7):1418, 2014.

[20] David Keilin. *The history of cell respiration and cytochrome*. CUP Archive, 1966.

[21] Neil A Campbell, Brad Williamson, and Robin J Heyden. *Biology: exploring life*. Recording for the Blind & Dyslexic, 2006.

[22] Anthony JF Griffiths, Susan R Wessler, Richard C Lewontin, William M Gelbart, David T Suzuki, Jeffrey H Miller, et al. *An introduction to genetic analysis*. Macmillan, 2005.

[23] Chris A Kaiser, Monty Krieger, Harvey Lodish, and Arnold Berk. *Molecular cell biology.* WH Freeman, 2007.

[24] Andreas Wachter. Riboswitch-mediated control of gene expression in eukaryotes. *RNA biology*, 7(1):67–76, 2010.

[25] Sally P Stabler and Robert H Allen. Vitamin b_{12} deficiency as a worldwide problem. *Annu. Rev. Nutr.*, 24:299–326, 2004.

[26] Daniel C Baumgart and William J Sandborn. Crohn's disease. *The Lancet*, 380(9853):1590–1605, 2012.

[27] William R Best, Jack M Becktel, John W Singleton, and Fred Kern. Development of a crohn's disease activity index: National cooperative crohn's disease study. *Gastroenterology*, 70(3):439–444, 1976.

[28] Alexander Serganov and Dinshaw J Patel. Molecular recognition and function of riboswitches. *Current opinion in structural biology*, 22(3):279–286, 2012.

[29] Afsaneh Khani, Nicole Popp, Bernd Kreikemeyer, and Nadja Patenge. A glycine riboswitch in streptococcus pyogenes controls expression of a sodium: alanine symporter family protein gene. *Frontiers in microbiology*, 9:200, 2018.

[30] Hongguang Sun and Youli Zu. A highlight of recent advances in aptamer technology and its application. *Molecules*, 20(7):11959–11980, 2015.

[31] Kerry Hollands, Sergey Proshkin, Svetlana Sklyarova, Vitaly Epshtein, Alexander Mironov, Evgeny Nudler, and Eduardo A Groisman. Riboswitch control of rho-dependent transcription termination. *Proceedings of the National Academy of Sciences*, 109(14):5376–5381, 2012.

[32] Arthur L Koch, Joseph A Robinson, and George A Milliken. *Mathematical modeling in microbial ecology*. Springer Science & Business Media, 2012.

[33] Pierre-Francois Verhulst. Mathematical researches into the law of population growth increase. *Nouveaux Mémoires de lAcadémie Royale des Sciences et Belles-Lettres de Bruxelles*, 18:1–42, 1845.

[34] Willy Feller. On the logistic law of growth and its empirical verifications in biology. *Acta biotheoretica*, 5(2):51–66, 1940.

[35] SV Emelyanov. Variable structure control systems: Synthesis of scalar and vector systems by state and output feedback. *Computational Mathematics and Modeling*, 21(3):253–274, 2010.

[36] Uri Itkis. *Control systems of variable structure*. Wiley New York, 1976.

[37] Vadim Utkin. Variable structure systems with sliding modes. *IEEE Transactions on Automatic control*, 22(2):212–222, 1977.

[38] John Y Hung, Weibing Gao, and James C Hung. Variable structure control: A survey. *IEEE transactions on industrial electronics*, 40(1):2–22, 1993.

[39] Raymond A DeCarlo, Stanislaw H Zak, and Gregory P Matthews. Variable structure control of nonlinear multivariable systems: a tutorial. *Proceedings of the IEEE*, 76(3):212–232, 1988.

[40] Asif Sabanovic, Leonid M Fridman, Sarah Spurgeon, and Sarah K Spurgeon. *Variable structure systems: from principles to implementation*, volume 66. IET, 2004.

[41] Christopher Edwards and Sarah K Spurgeon. Sliding mode stabilization of uncertain systems using only output information. *International Journal of Control*, 62(5):1129–1144, 1995.

[42] A Ferrara and L Giacomini. Control of a class of mechanical systems with uncertainties via a constructive adaptive/second order vsc approach. *Journal of Dynamic Systems, Measurement, and Control*, 122(1):33–39, 2000.

[43] Alan SI Zinober. *Variable structure and Lyapunov control*, volume 193. Springer, 1994.

[44] Yury Stepanenko, Yong Cao, and Chun-Yi Su. Variable structure control of robotic manipulator with pid sliding surfaces. *International Journal of Robust and Nonlinear Control: IFAC-Affiliated Journal*, 8(1):79–90, 1998.

[45] Cezary Zieliński, Maciej Stefańczyk, Tomasz Kornuta, Maksym Figat, Wojciech Dudek, Wojciech Szynkiewicz, Włodzimierz Kasprzak, Jan Figat, Marcin Szlenk, Tomasz Winiarski, et al. Variable structure robot control systems: The rapp approach. *Robotics and Autonomous Systems*, 94:226–244, 2017.

[46] K-KD Young. A variable structure model following control design for robotics applications. *IEEE Journal on Robotics and Automation*, 4(5):556–561, 1988.

[47] R Morgan and Umit Ozguner. A decentralized variable structure control algorithm for robotic manipulators. *IEEE Journal on Robotics and Automation*, 1(1):57–65, 1985.

[48] Christopher Edwards and Sarah Spurgeon. *Sliding mode control: theory and applications*. Crc Press, 1998.

[49] Thierry Floquet, Chris Edwards, and Sarah K Spurgeon. On sliding mode observers for systems with unknown inputs. *International Journal of Adaptive Control and Signal Processing*, 21(8-9):638–656, 2007.

[50] Jamal Daafouz, Pierre Riedinger, and Claude Iung. Stability analysis and control synthesis for switched systems: a switched lyapunov function approach. *IEEE transactions on automatic control*, 47(11):1883–1887, 2002.

[51] Mohammad Abbadi and Sarah Spurgeon. Growth dynamics of algal-bacterial cocultures: A control engineering perspective. In *2018 European Control Conference (ECC)*, pages 2344–2349. IEEE, 2018.

[52] Vadim Utkin, Jürgen Guldner, and Jingxin Shi. *Sliding mode control in electro-mechanical systems*. CRC press, 2009.

[53] Guido Herrmann, Sarah K Spurgeon, and Christopher Edwards. A model-based sliding mode control methodology applied to the hda-plant. *Journal of Process Control*, 13(2):129–138, 2003.

[54] Sarah K Spurgeon. Sliding mode observers: a survey. *International Journal of Systems Science*, 39(8):751–764, 2008.

[55] Shailaja Kurode, Sarah K Spurgeon, Bijnan Bandyopadhyay, and PS Gandhi. Sliding mode control for slosh-free motion using a nonlinear sliding surface. *IEEE/ASME Transactions on Mechatronics*, 18(2):714–724, 2012.

[56] Christopher Edwards, Sarah K Spurgeon, and Roderick G Hebden. On the design of sliding mode output feedback controllers. *International Journal of Control*, 76(9-10):893–905, 2003.

[57] Xiao-Yun Lu and Sarah K Spurgeon. Robust sliding mode control of uncertain nonlinear systems. *Systems & control letters*, 32(2):75–90, 1997.

[58] Christopher Edwards, Ashu Akoachere, and Sarah K Spurgeon. Sliding-mode output feedback controller design using linear matrix inequalities. *IEEE Transactions on Automatic Control*, 46(1):115–119, 2001.

[59] Gamal El-Ghazaly, Marc Gouttefarde, and Vincent Creuze. Adaptive terminal sliding mode control of a redundantly-actuated cable-driven parallel manipulator: cogiro. In *Cable-Driven Parallel Robots*, pages 179–200. Springer, 2015.

[60] Jon H Davis. *Foundations of deterministic and stochastic control*. Springer Science & Business Media, 2002.

[61] Rudolf E Kalman. On the general theory of control systems. In *Proceedings First International Conference on Automatic Control, Moscow, USSR*, 1960.

[62] KC Veluvolu, YC Soh, and W Cao. Robust observer with sliding mode estimation for nonlinear uncertain systems. *IET Control Theory & Applications*, 1(5):1533–1540, 2007.

[63] Thierry Floquet and Jean-Pierre Barbot. A canonical form for the design of unknown input sliding mode observers. In *Advances in variable structure and sliding mode control*, pages 271–292. Springer, 2006.

[64] Christopher Edwards, Sarah K Spurgeon, and Chee Pin Tan. On the development and application of sliding mode observers. In *Variable structure systems: Towards the 21st century*, pages 253–282. Springer, 2002.

[65] Christopher Edwards, Sarah K Spurgeon, and Ron J Patton. Sliding mode observers for fault detection and isolation. *Automatica*, 36(4):541–553, 2000.

[66] Sergey Drakunov and Vadim Utkin. Sliding mode observers. tutorial. In *Proceedings of 1995 34th IEEE Conference on Decision and Control*, volume 4, pages 3376–3378. IEEE, 1995.

[67] Ali Nahvi, Jeffrey E Barrick, and Ronald R Breaker. Coenzyme b12 riboswitches are widespread genetic control elements in prokaryotes. *Nucleic acids research*, 32(1):143–150, 2004.

[68] Yingying Cai, Miaomiao Xia, Huina Dong, Yuan Qian, Tongcun Zhang, Beiwei Zhu, Jinchuan Wu, and Dawei Zhang. Engineering a vitamin b 12 high-throughput screening system by riboswitch sensor in sinorhizobium meliloti. *BMC biotechnology*, 18(1):27, 2018.

[69] Digby F Warner, Suzana Savvi, Valerie Mizrahi, and Stephanie S Dawes. A riboswitch regulates expression of the coenzyme b12-independent methionine synthase in mycobacterium tuberculosis: implications for differential methionine synthase function in strains h37rv and cdc1551. *Journal of bacteriology*, 189(9):3655–3659, 2007.

[70] ALEXEY G VITRESCHAK, DMITRY A RODIONOV, ANDREY A MIRONOV, and MIKHAIL S GELFAND. Regulation of the vitamin b12 metabolism and transport in bacteria by a conserved rna structural element. *Rna*, 9(9):1084–1097, 2003.

[71] Dmitry A Rodionov, Alexey G Vitreschak, Andrey A Mironov, and Mikhail S Gelfand. Comparative genomics of thiamin biosynthesis in procaryotes new genes and regulatory mechanisms. *Journal of Biological chemistry*, 277(50):48949–48959, 2002.

[72] JM Berg, JL Tymoczko, and L Stryer. Eukaryotic transcription and translation are separated in space and time. *Biochemistry. 5th ed. New York, NY: WH Freeman*, 2002.

[73] James A Stapleton, Kei Endo, Yoshihiko Fujita, Karin Hayashi, Masahiro Takinoue, Hirohide Saito, and Tan Inoue. Feedback control of protein expression in mammalian cells by tunable synthetic translational inhibition. *ACS synthetic biology*, 1(3):83–88, 2011.

[74] A Gudmundsdottir, C Bradbeer, and RJ Kadner. Altered binding and transport of vitamin b_{12} resulting from insertion mutations in the escherichia coli btub gene. *Journal of Biological Chemistry*, 263(28):14224–14230, 1988.

[75] SA Amin, LR Hmelo, HM Van Tol, BP Durham, LT Carlson, KR Heal, RL Morales, CT Berthiaume, MS Parker, B Djunaedi, et al. Interaction and

signalling between a cosmopolitan phytoplankton and associated bacteria. *Nature*, 522(7554):98, 2015.

[76] Martin T Croft, Andrew D Lawrence, Evelyne Raux-Deery, Martin J Warren, and Alison G Smith. Algae acquire vitamin b 12 through a symbiotic relationship with bacteria. *Nature*, 438(7064):90, 2005.

[77] G-Yull Rhee. Competition between an alga and an aquatic bacterium for phosphate 1. *Limnology and Oceanography*, 17(4):505–514, 1972.

[78] Kenneth C Haines and Robert RL Guillard. Growth of vitamin b_{12}-requiring marine diatoms in mixed laboratory cultures with vitamin b_{12}-producing marine bacteria 1 2. *Journal of Phycology*, 10(3):245–252, 1974.

[79] Patrick Lavens, Patrick Sorgeloos, et al. *Manual on the production and use of live food for aquaculture.* Number 361. Food and Agriculture Organization (FAO)., 1996.

[80] Hao Wang, Hal L Smith, Yang Kuang, and James J Elser. Dynamics of stoichiometric bacteria-algae interactions in the epilimnion. *SIAM Journal on Applied Mathematics*, 68(2):503–522, 2007.

[81] A Agung Julius, Ádám Halász, M Selman Sakar, Harvey Rubin, Vijay Kumar, and George J Pappas. Stochastic modeling and control of biological systems: the lactose regulation system of escherichia coli. *IEEE Transactions on Automatic Control*, 53(Special Issue):51–65, 2008.

[82] Rishiram Ramanan, Byung-Hyuk Kim, Dae-Hyun Cho, Hee-Mock Oh, and Hee-Sik Kim. Algae–bacteria interactions: evolution, ecology and emerging applications. *Biotechnology advances*, 34(1):14–29, 2016.

[83] Jimin Zhang, Junping Shi, and Xiaoyuan Chang. A mathematical model of algae growth in a pelagic–benthic coupled shallow aquatic ecosystem. *Journal of Mathematical Biology*, 76(5):1159–1193, Apr 2018.

[84] Joana Correia Prata, João P da Costa, Isabel Lopes, Armando C Duarte, and Teresa Rocha-Santos. Effects of microplastics on microalgae populations: A critical review. *Science of the Total Environment*, 2019.

[85] M. H. Zwietering, I. Jongenburger, F. M. Rombouts, and K. van 't Riet. Modeling of the bacterial growth curve. *Applied and Environmental Microbiology*, 56(6):1875–1881, 1990.

[86] DE Contois. Kinetics of bacterial growth: relationship between population density and specific growth rate of continuous cultures. *Microbiology*, 21(1):40–50, 1959.

[87] RC McKellar. A heterogeneous population model for the analysis of bacterial growth kinetics. *International Journal of Food Microbiology*, 36(2-3):179–186, 1997.

[88] Byung-Hyuk Kim, Rishiram Ramanan, Dae-Hyun Cho, Hee-Mock Oh, and Hee-Sik Kim. Role of rhizobium, a plant growth promoting bacterium, in en-

hancing algal biomass through mutualistic interaction. *Biomass and Bioenergy*, 69:95–105, 2014.

[89] Elena Kazamia, Hjrdis Czesnick, Thi Thanh Van Nguyen, Martin Tom Croft, Emma Sherwood, Severin Sasso, Sarah James Hodson, Martin James Warren, and Alison Gail Smith. Mutualistic interactions between vitamin b_{12}-dependent algae and heterotrophic bacteria exhibit regulation. *Environmental Microbiology*, 14(6):1466–1476, 2012.

[90] Elizabeth H Harris. Chlamydomonas as a model organism. *Annual Review of Plant Physiology and Plant Molecular Biology*, 52(1):363–406, 2001.

[91] Thake B. Fogg GE. *Algal cultures and phytoplankton ecology*. University of Wisconsin Press, third edition, 1987.

[92] Anet J. N. Anelone and Sarah K. Spurgeon. Modelling and simulation of the dynamics of the antigen-specific t cell response using variable structure control theory. *PLOS ONE*, 11:1–22, 11 2016.

[93] M. M. Mason. A comparison of the maximal growth rates of various bacteria under optimal conditions. *Journal of Bacteriology*, 29(2):103–110, 1935.

[94] Cole JJ. Interactions between bacteria and algae in aquatic ecosystems. 13(1):291–314, 1982.

[95] Jinghao Li, Qingling Zhang, Xing-Gang Yan, and Sarah K Spurgeon. Observer-based fuzzy integral sliding mode control for nonlinear descriptor systems. *IEEE Transactions on Fuzzy Systems*, 26(5):2818–2832, 2018.

[96] J Gonzalez, G Fernandez, R Aguilar, M Barron, and J Alvarez-Ramirez. Sliding mode observer-based control for a class of bioreactors. *Chemical Engineering Journal*, 83(1):25–32, 2001.

[97] L. STRYER. Eukaryotic transcription and translation are separated in space and time. *Biochemistry*, pages 792–797, 2003.

[98] James A. Stapleton, Kei Endo, Yoshihiko Fujita, Karin Hayashi, Masahiro Takinoue, Hirohide Saito, and Tan Inoue. Feedback control of protein expression in mammalian cells by tunable synthetic translational inhibition. *ACS Synthetic Biology*, 1(3):83–88, 2012.

[99] Lacramioara Bintu, Nicolas E Buchler, Hernan G Garcia, Ulrich Gerland, Terence Hwa, Jan Kondev, Thomas Kuhlman, and Rob Phillips. Transcriptional regulation by the numbers: applications. *Current Opinion in Genetics and Development*, 15(2):125 – 135, 2005. Chromosomes and expression mechanisms.

[100] Davis JH. *Foundations of deterministic and stochastic control*. Springer Science and Business Media, 2002.

[101] Florian J. Widner, Andrew D. Lawrence, Evelyne Deery, Dana Heldt, Stefanie Frank, Karl Gruber, Klaus Wurst, Martin J. Warren, and Bernhard Krutler. Total synthesis, structure, and biological activity of adenosylrhodibalamin, the non-natural rhodium homologue of coenzyme b_{12}. *Angewandte Chemie International Edition*, 55(37):11281–11286, 2016.

[102] Mohammad Abbadi, Sarah K. Spurgeon, Naziyat Khan, and Martin J Warren. Understanding the control of a vitamin b_{12} riboswitch. *2018 UKACC 12th International Conference on Control (CONTROL)*, pages 474–479, 2018.

[103] Cristiana Paul and David Michael Brady. Comparative bioavailability and utilization of particular forms of b_{12} supplements with potential to mitigate b_{12}-related genetic polymorphisms. *Integrative medicine*, 16 1:42–49, 2017.